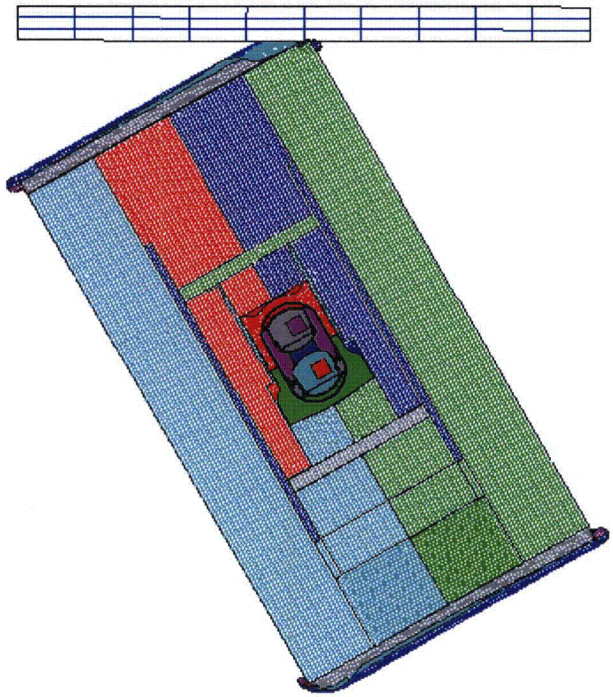

Figure 2-391. Finite Element Mesh for HAC Run 5, SC-2, CGOC Impact, Support Structure 45° - Final Displacement

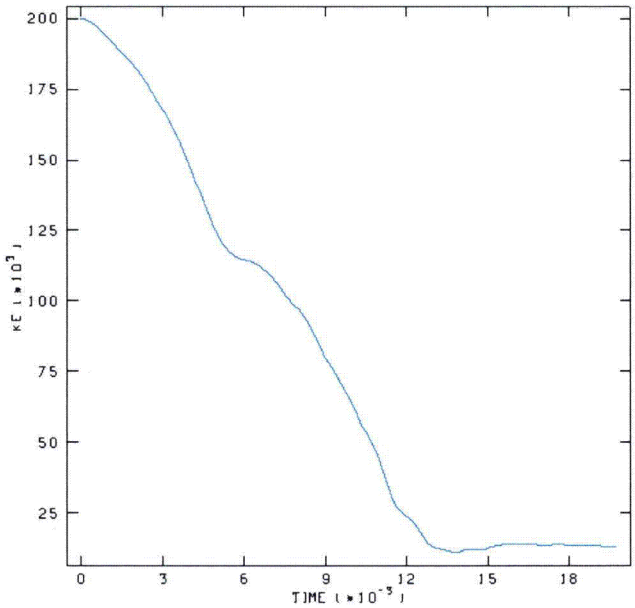

Figure 2-392. Kinetic Energy Time History for HAC Run 5, SC-2, CGOC Impact, Support Structure 45°

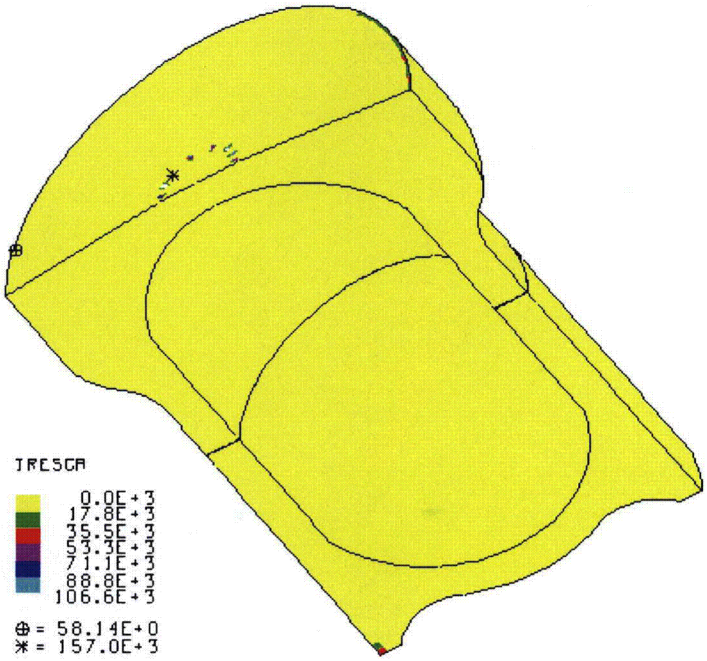

Figure 2-393. Plot of Tresca Stress in the TB-1 for HAC Run 5, SC-2, CGOC Impact, Support Structure 45° when Stress is a Maximum

2.12.5.6.6 HAC- Run 6, SC-1, End Impact

The dynamic crush end impact HAC analysis run for the SC-1 sample container with its support structure rotated 0° uses the same model as that used for the 4-ft-drop, but the flange is added to both ends so that it available to deform where impacted by the plate and the rigid surface upon which it is resting. The finite element mesh and initial position of the model are shown in Figure 2-394. The Pu contents and support structure within the T-Ampoule are positioned at the bottom of the model because it was considered to be at rest at the time of impact.

The post-impact deformation is shown in Figure 2-395 and its kinetic energy history in Figure 2-396. The flanges on the overpack deform, and the contents bounce due to the impact of the plate. There was zero EQPS in the TB-1, and zero elements extended beyond the tested Bao-Wierzbicki strain locus. The maximum Tearing Parameter was 3.03e-5 in the T-Ampoule, and is below the critical Tearing Parameter value of 1.012 for Ti-6Al-4V, thus T-Ampoule integrity is maintained. Figure 2-397 is a plot of the Tresca stresses within the TB-1. The maximum Tresca stress in the TB-1 is 127.1 ksi, but there are no through thickness stresses exceeding the limit of 106.6 ksi, which can be seen clearly in the figures. Figure 2-398 is a plot of the Tresca stresses at the time when all of the kinetic energy of the plate has been transferred to the package, just as the plate begins to rebound. The maximum through thickness stress at this time is below 8.33 ksi, below the allowable through thickness stress of 106.6 ksi, as seen in the figure.

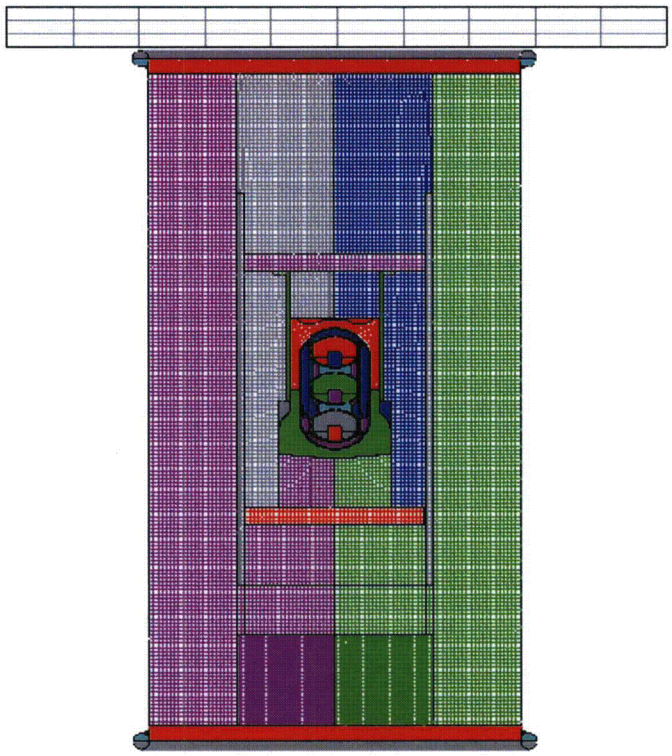

Figure 2-394. Finite Element Mesh for HAC Run 6, SC-1, End Impact, Support Structure 0°

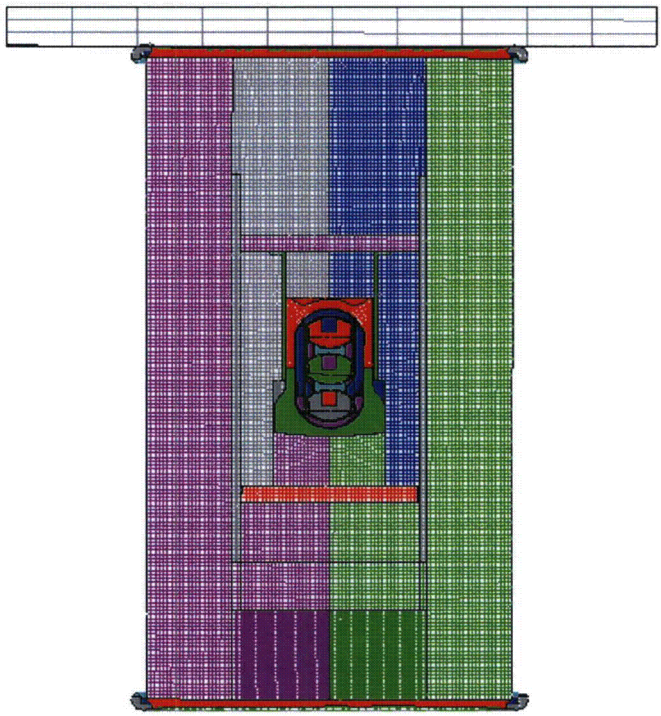

Figure 2-395. Finite Element Mesh for HAC Run 6, SC-1, End Impact, Support Structure 0° - Final Displacement

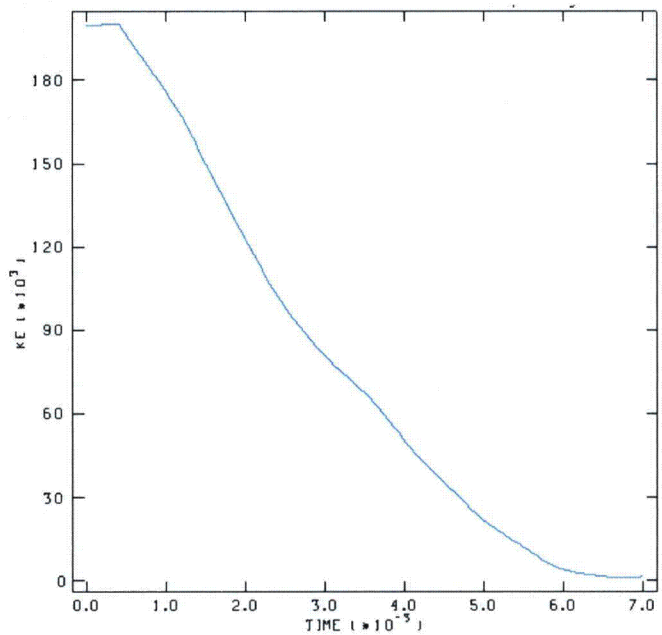

Figure 2-396. Kinetic Energy Time History for HAC Run 6, SC-1, End Impact, Support Structure 0°

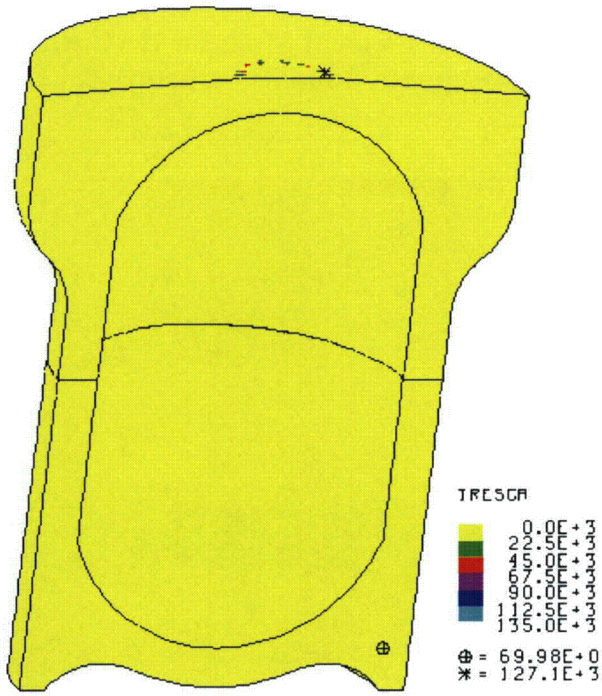

Figure 2-397. Plot of Tesca Stress in the TB-1 for HAC Run 6, SC-1, End Impact, Support Structure 0°

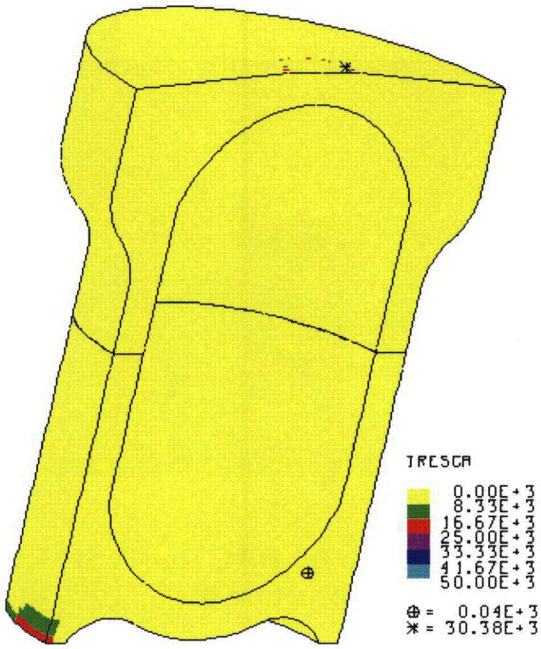

Figure 2-398. Plot of Tresca Stress in the TB-1 for HAC Run 6, SC-1, End Impact, Support Structure 0° when Plate Velocity Reaches Zero

2.12.5.6.7 HAC- Run 7, SC-1, Side Impact, Support Structure 0°

The dynamic crush side impact HAC analysis run for the SC-1 sample containers with its support structure rotated 45° uses the same model as that used for the 4-ft-drop, but the flange is added to both ends so that it available to deform where impacted by the plate and the rigid surface upon which it is resting. The finite element mesh and initial position of the model are shown in Figure 2-399. The Pu contents and support structure within the T-Ampoule are positioned at the bottom of the model because it was considered to be at rest at the time of impact. The plate was positioned between the flanges to be most damaging to the TB-1 and contents by preventing the flanges from absorbing energy and slowing down the plate before it hits the overpack.

The post-impact deformation is shown in Figure 2-400 and its kinetic energy history in Figure 2-401. The flanges on the overpack deform, and the contents bounce due to the impact of the plate. Zero elements extended beyond the tested Bao-Wierzbicki strain locus. The maximum Tearing Parameter value for this analysis was 3.03e-5, and is below the critical Tearing Parameter value of 1.012 for Ti-6Al-4V, thus T-Ampoule integrity is maintained.

Peak EQPS in the TB-1 vessel is shown in Figure 2-402 to be 27.67e-3, and is localized in the outer contact regions with the redwood overpack. Figure 2-403 is a plot of the Tresca stresses within the TB-1. The maximum Tresca stress in the TB-1 is 172.3 ksi, but there are no through thickness stresses exceeding the limit of 106.6 ksi, which can be seen clearly in the figure. Figure 2-404 is a plot of the Tresca stresses at the time when all of the kinetic energy of the plate has been transferred to the package, just as the plate begins to rebound. The maximum through thickness stress at this time is below 25.0 ksi, below the allowable through thickness stress of 106.6 ksi, as seen in the figure.

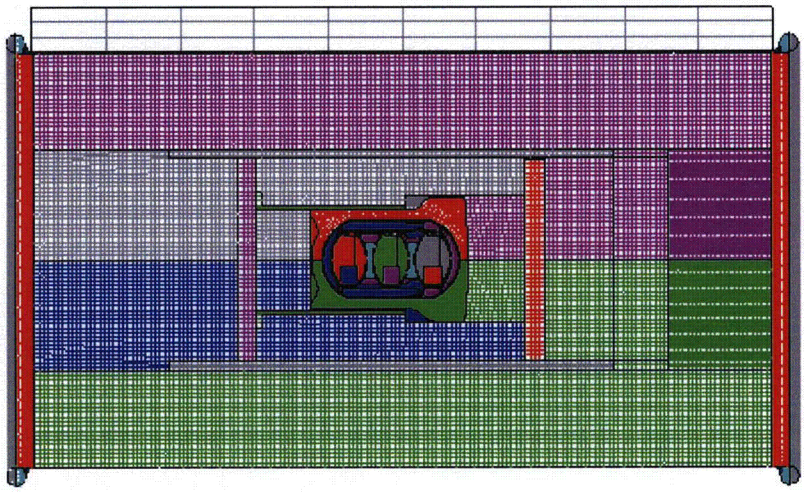

Figure 2-399. Finite Element Mesh for HAC Run 7, SC-1, Side Impact, Support Structure 0°

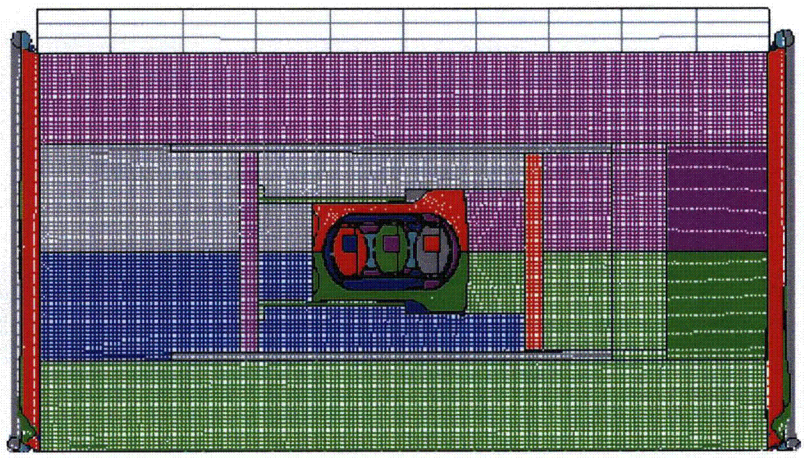

Figure 2-400. Finite Element Mesh for HAC Run 7, SC-1, Side Impact, Support Structure 0° - Final Displacement

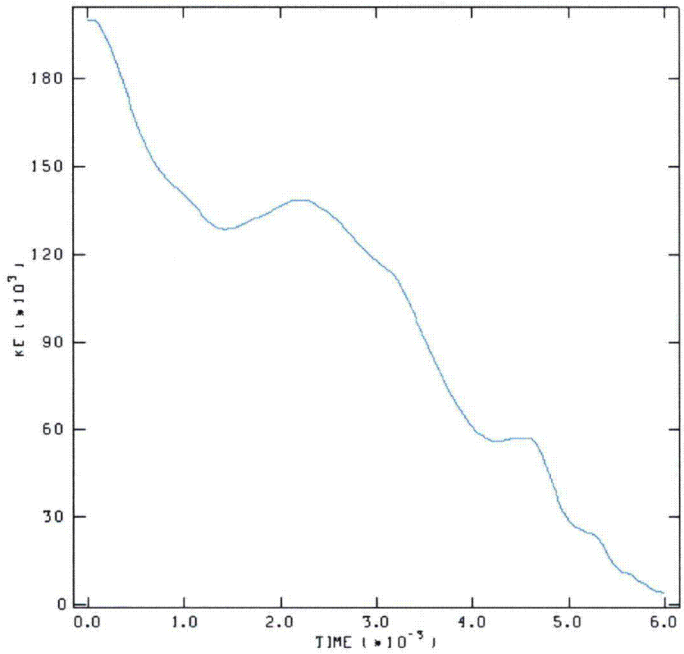

Figure 2-401. Kinetic Energy Time History for HAC Run 7, SC-1, Side Impact, Support Structure 0°

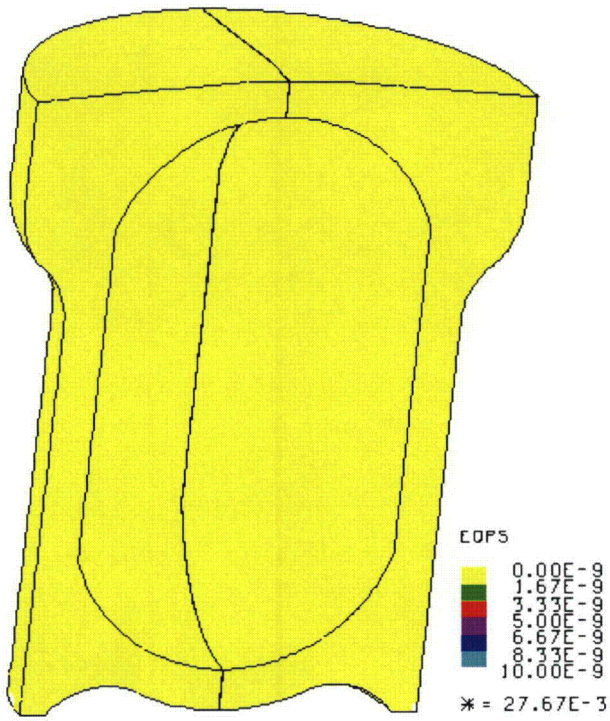

Figure 2-402. Plot of EQPS in TB-1 for HAC Run 7, SC-1, Side Impact, Support Structure 0°

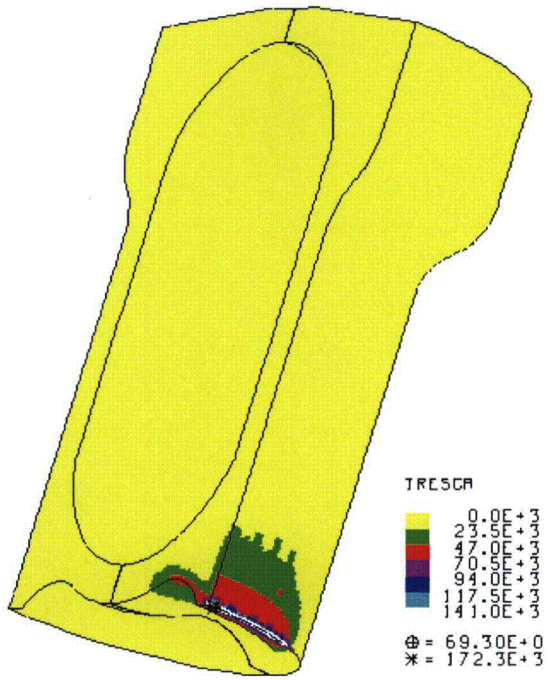

Figure 2-403. Plot of Tresca Stress in the TB-1 for HAC Run 7, SC-1, Side Impact, Support Structure 0°

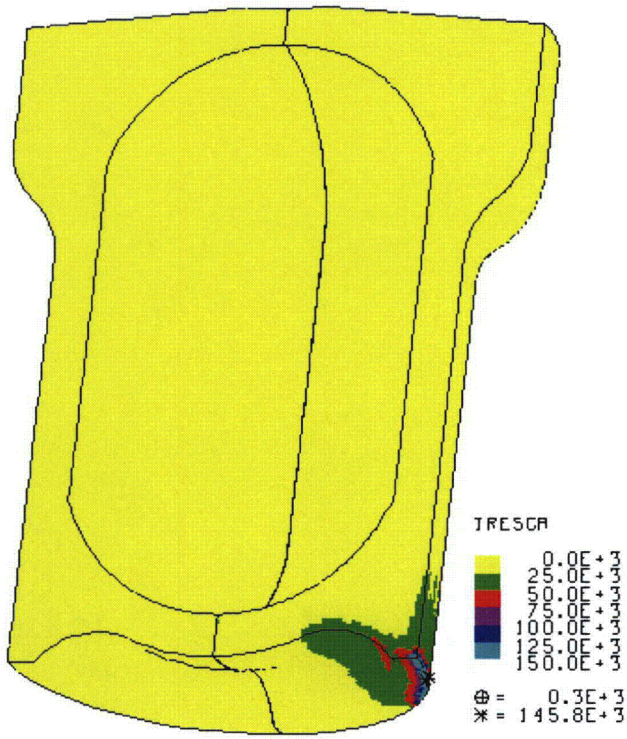

Figure 2-404. Plot of Tresca Stress in the TB-1 for HAC Run 7, SC-1, Side Impact, Support Structure 0° when Plate Velocity Reaches Zero

2.12.5.6.8 HAC- Run 8, SC-1, Side Impact, Support Structure 45°

The dynamic crush side impact HAC analysis run for the SC-1 sample container with its support structure rotated 45° uses the same model as that used for the 4-ft-drop, but the flange is added to both ends so that it available to deform where impacted by the plate and the rigid surface upon which it is resting. The finite element mesh and initial position of the model are shown in Figure 2-405. The Pu contents and support structure within the T-Ampoule are positioned at the bottom of the model because it was considered to be at rest at the time of impact. The plate was positioned between the flanges to be most damaging to the TB-1 and contents by preventing the flanges from absorbing energy and slowing down the plate before it hits the overpack.

The post-impact deformation is shown in Figure 2-406 and its kinetic energy history in Figure 2-407. The flanges on the overpack deform, and the contents bounce due to the impact of the plate. Zero elements extended beyond the tested Bao-Wierzbicki strain locus. The maximum Tearing Parameter value for this analysis was 1.6e-2, and is below the critical Tearing Parameter value of 1.012 for Ti-6Al-4V, thus T-Ampoule integrity is maintained.

Peak EQPS in the TB-1 vessel is shown in Figure 2-408 to be 0.1829, and is localized in the outer contact regions with the redwood overpack. Figures 2-409 and 2-410 are plots of the Tresca stresses within the TB-1. The maximum Tresca stress in the TB-1 is 225.9 ksi (contact modeling artifact), but there are no through thickness stresses exceeding the limit of 106.6 ksi, which can be seen clearly in the figures. Figure 2-411 is a plot of the Tresca stresses at the time when all of the kinetic energy of the plate has been transferred to the package, just as the plate begins to rebound. The maximum through thickness stress at this time is below 33.3 ksi, below the allowable through thickness stress of 106.6 ksi, as seen in the figure.

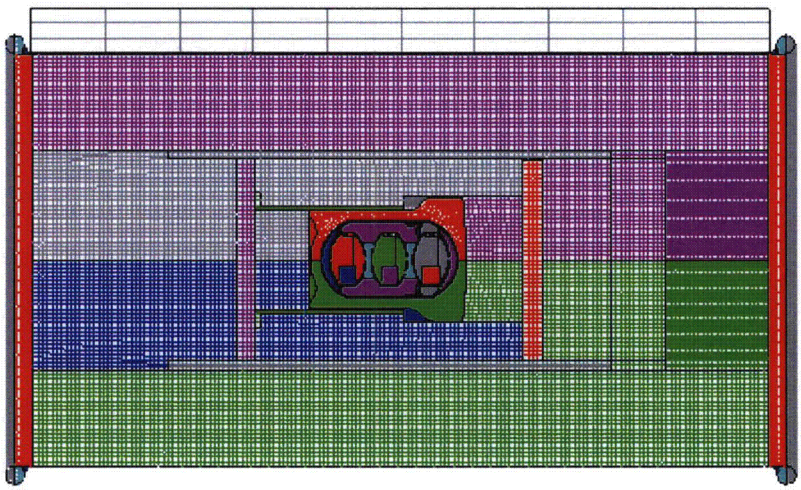

Figure 2-405. Finite Element Mesh for HAC Run 8, SC-1, Side Impact, Support Structure 45°

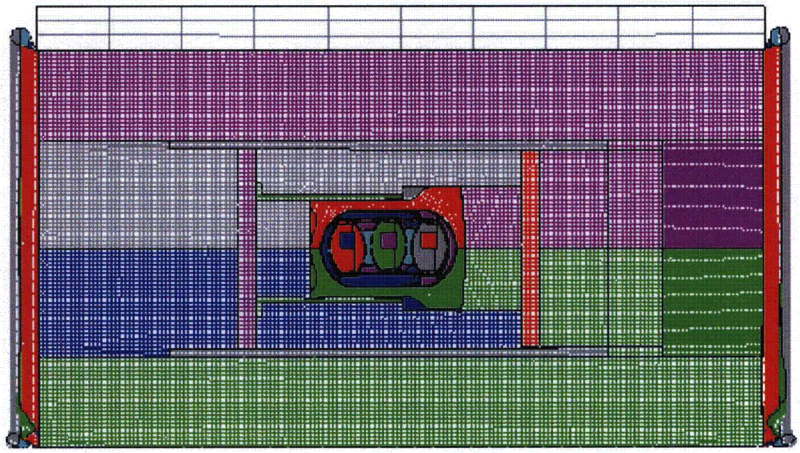

Figure 2-406. Finite Element Mesh for HAC Run 8, SC-1, Side Impact, Support Structure 45° - Final Displacement

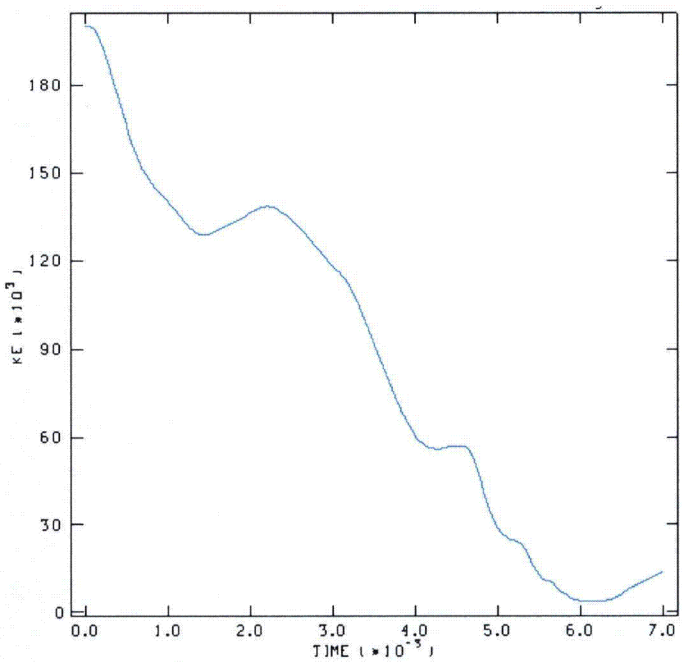

Figure 2-407. Kinetic Energy Time History for HAC Run 8, SC-1, Side Impact, Support Structure 45°

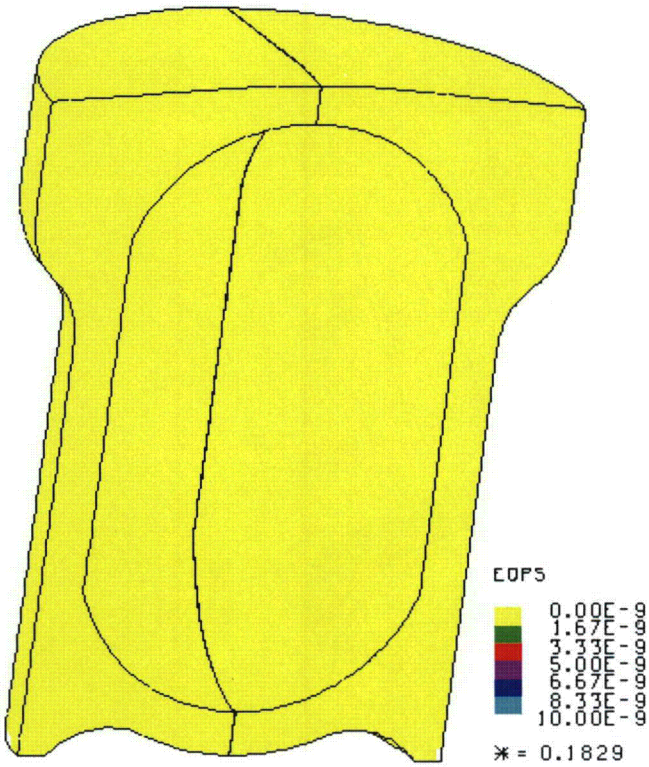

Figure 2-408. Plot of EQPS in TB-1 for HAC Run 8, SC-1, Side Impact, Support Structure 45°

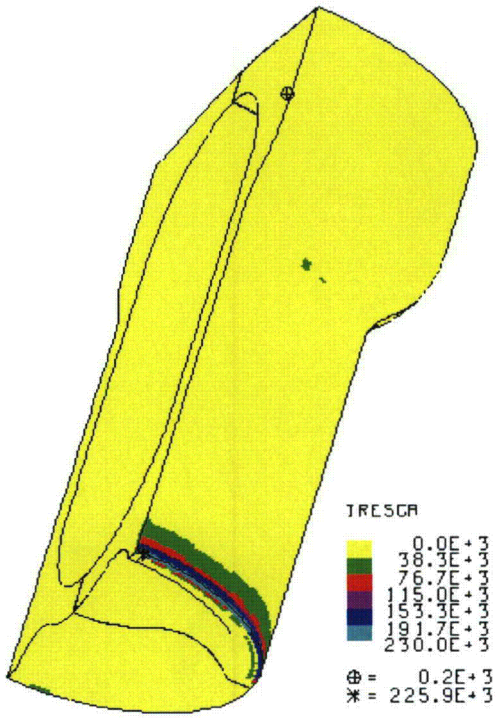

Figure 2-409. Plot of Tresca Stress in TB-1 for HAC Run 8, SC-1, Side Impact, Support Structure 45°

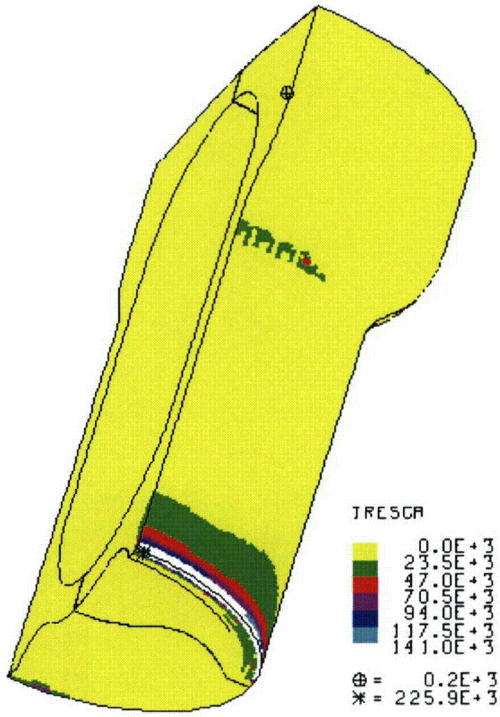

Figure 2-410. Plot of Tresca Stress in TB-1 for HAC Run 8, SC-1, Side Impact, Support Structure 45°

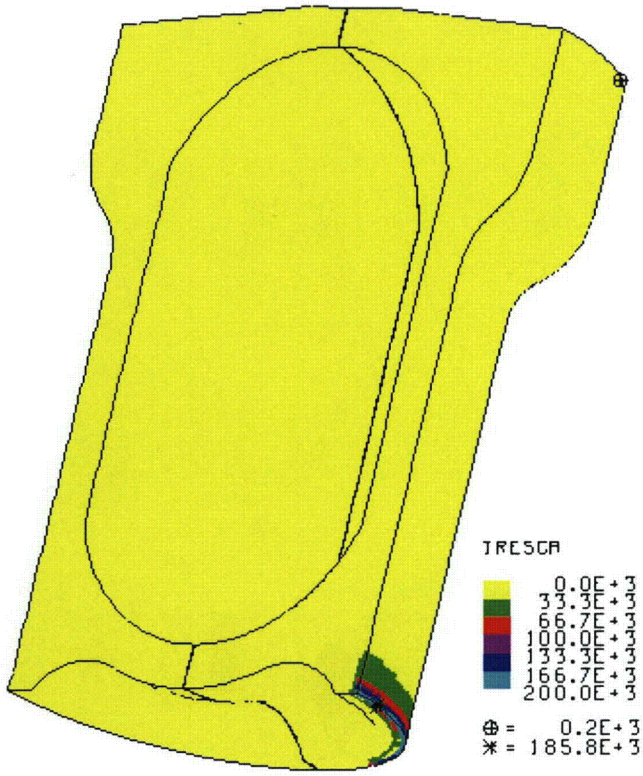

Figure 2-411. Plot of Tresca Stress in TB-1 for HAC Run 8, SC-1, Side Impact, Support Structure 45° when Plate Velocity Reaches Zero

2.12.5.6.9 HAC- Run 9, SC-1, CGOC Impact, Support Structure 0°

The dynamic crush CGOC impact HAC analysis for the SC-1 sample container run uses the same overpack model as those used in HAC runs 1 through 8. The finite element mesh and initial position of the model are shown in Figure 2-412. The Pu contents and support structure within the T-Ampoule are positioned at the bottom of the model because it was considered to be at rest.

The post-impact deformation is shown in Figure 2-413 and its kinetic energy history in Figure 2-414. The flanges on the overpack deform, and the contents bounce due to the impact of the plate. The kinetic energy does not drop completely to zero because the plate is still vibrating and internal contents are still in motion. The plutonium cylinders have bounced off of the top and bottom surface of the sample containers, and the plate is now rebounding slowly with the package, ensuring that the highest containment vessel and contents loadings have occurred.

There was zero EQPS in the T-Ampoule and the TB-1, and the maximum Tearing Parameter was 0. Figure 2-415 is a plot of the Tresca stresses within the TB-1. The maximum Tresca stress in the TB-1 is 146.5 Ksi, but there are no through thickness stresses exceeding the limit of 106.6 ksi, which can be seen clearly in the figure. Figure 2-416 is a plot of the Tresca stresses at the time when all of the kinetic energy of the plate has been transferred to the package, just as the plate begins to rebound. The maximum through thickness stress at this time is below 8.33 ksi, below the allowable through thickness stress of 106.6 ksi, as seen in the figure.

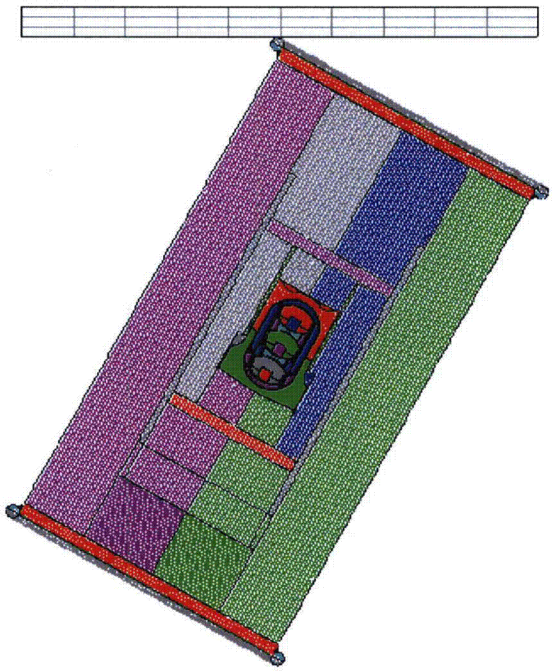

Figure 2-412. Finite Element Mesh for HAC Run 9, SC-1, CGOC Impact, Support Structure 0°

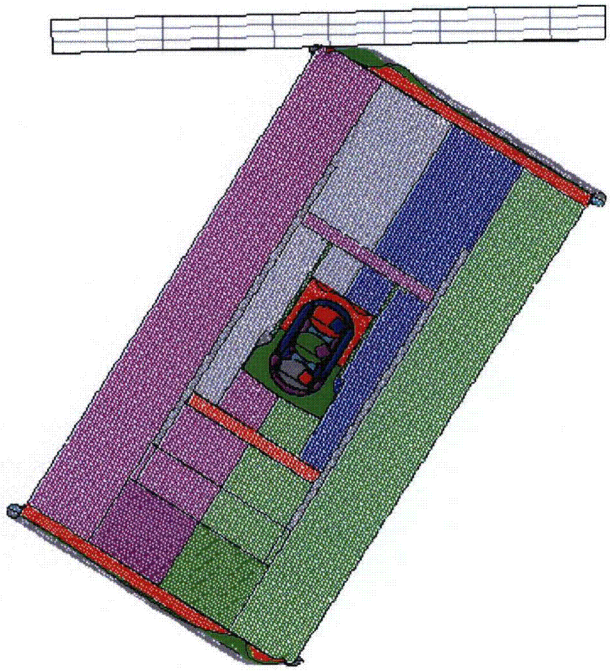

Figure 2-413. Finite Element Mesh for HAC Run 9, SC-1, CGOC Impact, Support Structure 0° - Final Displacement

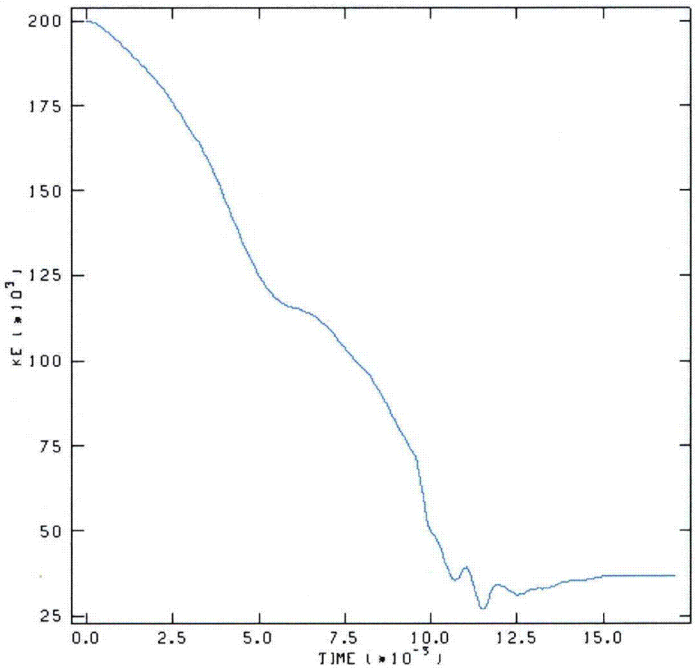

Figure 2-414. Kinetic Energy Time History for HAC Run 9, SC-1, CGOC Impact, Support Structure 0°

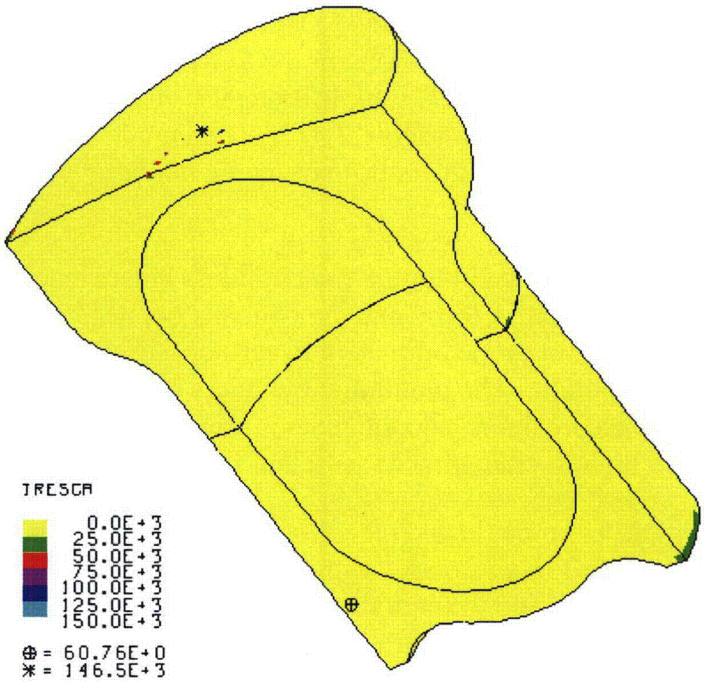

Figure 2-415. Tresca Stress for HAC Run 9, SC-1, CGOC Impact, Support Structure 0°

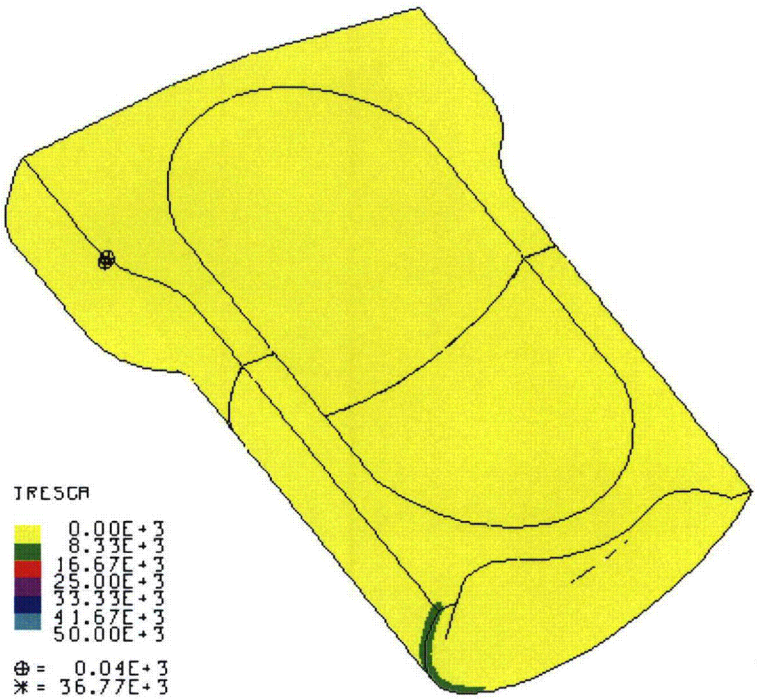

Figure 2-416. Plot of Tresca Stress in the TB-1 for HAC Run 9, SC-1, CGOC Impact, Support Structure 0° when Plate Velocity Reaches Zero

2.12.5.6.10 HAC- Run 10, SC-1, CGOC Impact, Support Structure 45°

The dynamic crush CGOC impact HAC analysis for the SC-1 sample container run uses the same overpack model as those used in HAC runs 1 through 9. The finite element mesh and initial position of the model are shown in Figure 2-417. The Pu contents and support structure within the T-Ampoule are positioned at the bottom of the model because it was considered to be at rest.

The post-impact deformation is shown in Figure 2-418 and its kinetic energy history in Figure 2-419. The flanges on the overpack deform, and the contents bounce due to the impact of the plate. The kinetic energy does not drop completely to zero because the plate is still vibrating and internal contents are still in motion. The plutonium cylinders have bounced off of the top and bottom surface of the sample containers, and the plate is now rebounding slowly with the package, ensuring that the highest containment vessel and contents loadings have occurred.

There was zero EQPS in the T-Ampoule and the TB-1, and the maximum Tearing Parameter was 0. Figure 2-420 is a plot of the Tresca stresses within the TB-1. The maximum Tresca stress in the TB-1 is 158.8 ksi, but there are no through thickness stresses exceeding the limit of 106.6 ksi, which can be seen clearly in the figure. Figure 2-421 is a plot of the Tresca stresses at the time when all of the kinetic energy of the plate has been transferred to the package, just as the plate begins to rebound. The maximum through thickness stress at this time is below 16.7 ksi, below the allowable through thickness stress of 106.6 ksi, as seen in the figure.

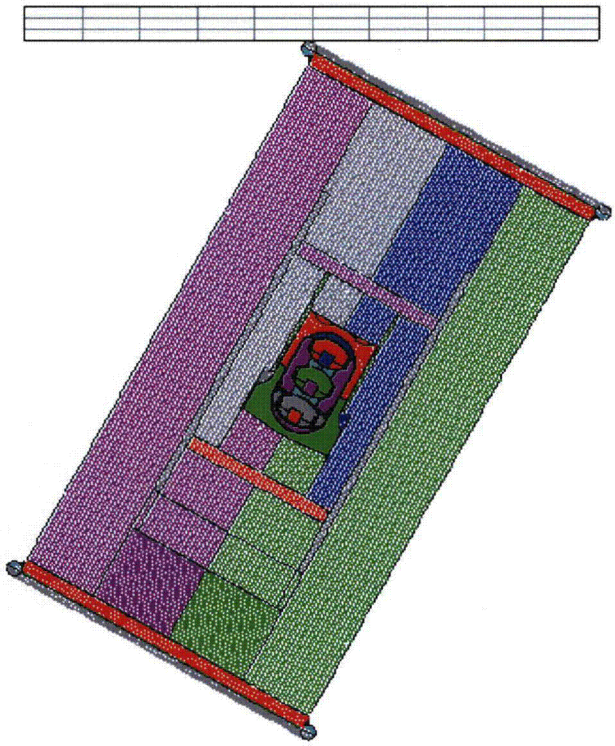

Figure 2-417. Finite Element Mesh for HAC Run 10, SC-1, CGOC Impact, Support Structure 45°

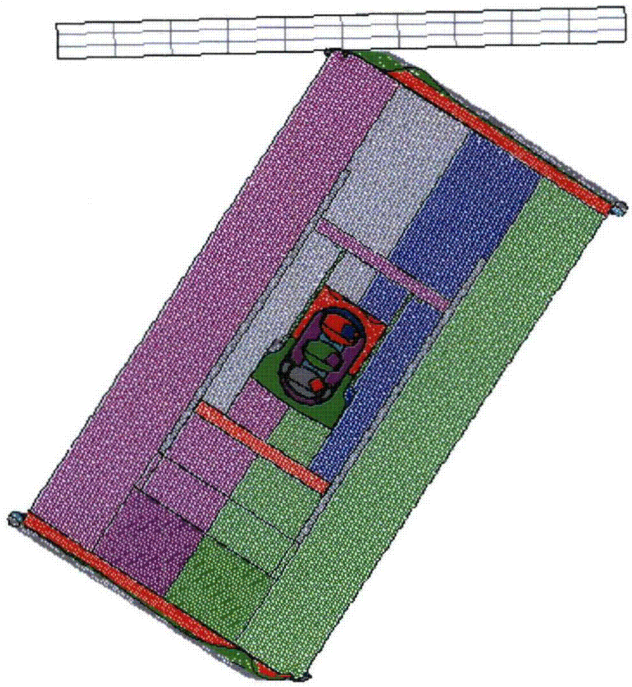

Figure 2-418. Finite Element Mesh for HAC Run 10, SC-1, CGOC Impact, Support Structure 45° - Final Displacement

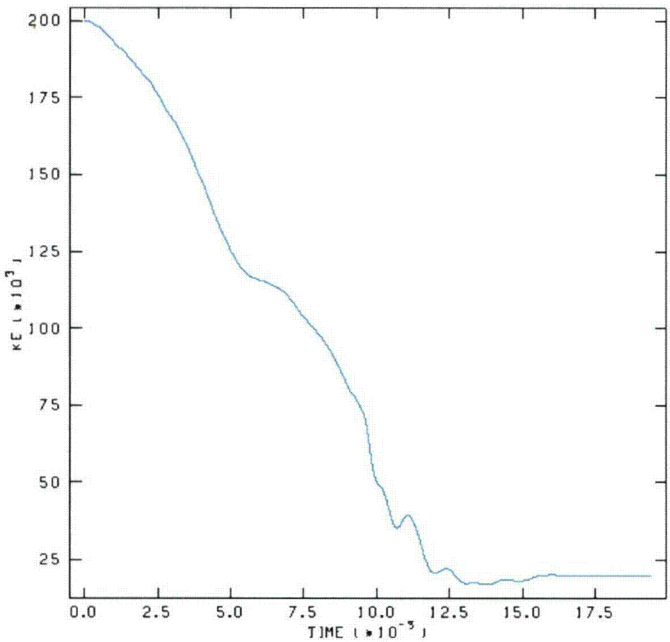

Figure 2-419. Kinetic Energy Time History for HAC Run 10, SC-1, CGOC Impact, Support Structure 45°

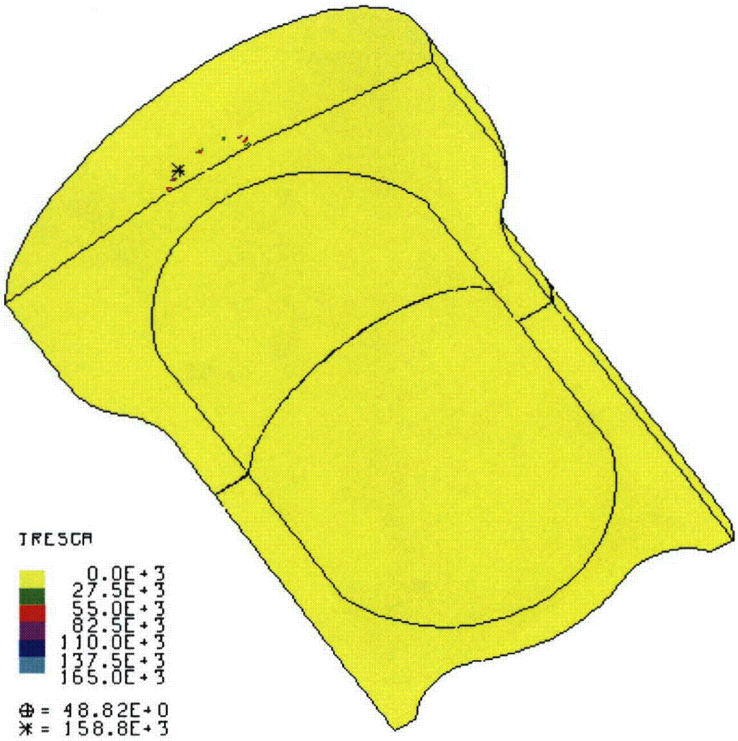

Figure 2-420. Plot of Tresca Stress in the TB-1 for HAC Run 10, SC-1, CGOC Impact, Support Structure 45°

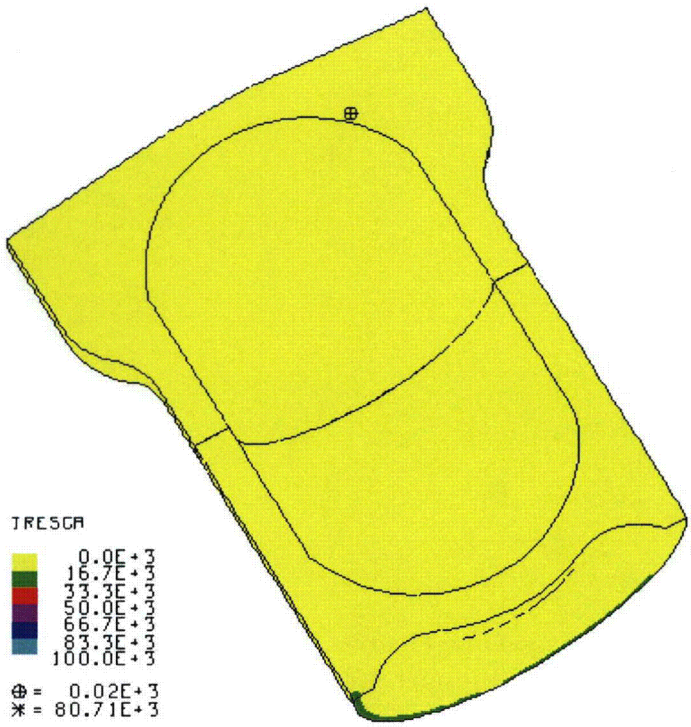

Figure 2-421. Plot of Tresca Stress in the TB-1 for HAC Run 10, SC-1, CGOC Impact, Support Structure 45° when Plate Velocity Reaches Zero

2.12.5.6.11 HAC- Run 11, 831 g Plutonium Metal Hollow Cylinder, End Impact

The dynamic crush end impact HAC analysis run for the 831 g plutonium metal hollow cylinder uses the same model for the overpack as the one used in the previous 10 runs. The TB-1, T-Ampoule, and plutonium metal hollow cylinder are the same model as that used in the aircraft analysis. The finite element mesh and initial position of the model are shown in Figure 2-422. The plutonium metal hollow cylinder within the T-Ampoule is positioned at the bottom of the model because it was considered to be at rest at the time of impact.

The post-impact deformation is shown in Figure 2-423 and its kinetic energy history in Figure 2-424. The flanges on the overpack deform, and the cylinder bounces due to the impact of the plate. Zero elements extended beyond the tested Bao-Wierzbicki strain locus. The maximum Tearing Parameter value for this analysis was 0.

Peak EQPS in the TB-1 vessel is shown in Figure 2-425 to be 2.68e-3, and is localized in the outer contact regions with the redwood overpack. Figure 2-426 plots the Tresca stresses within the TB-1. The maximum Tresca stress in the TB-1 is 156.7 ksi, but there are no through thickness stresses exceeding the limit of 106.6 ksi, which can be seen clearly in the figure. Figure 2-427 is a plot of the Tresca stresses at the time when all of the kinetic energy of the plate has been transferred to the package, just as the plate begins to rebound. The maximum through thickness stress at this time is below 25.0 ksi, below the allowable through thickness stress of 106.6 ksi, as seen in the figure.

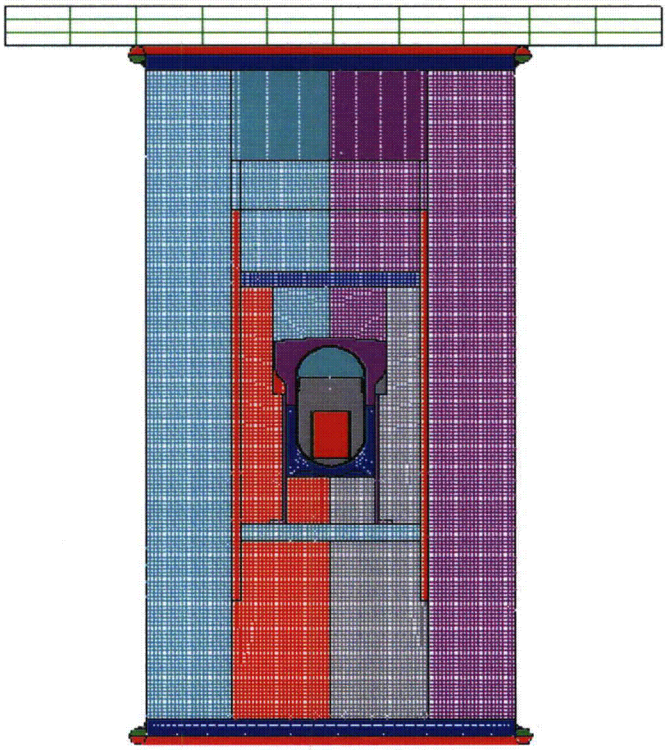

Figure 2-422. Finite Element Mesh for HAC Run 11, 831 g Plutonium Metal Hollow Cylinder, End Impact

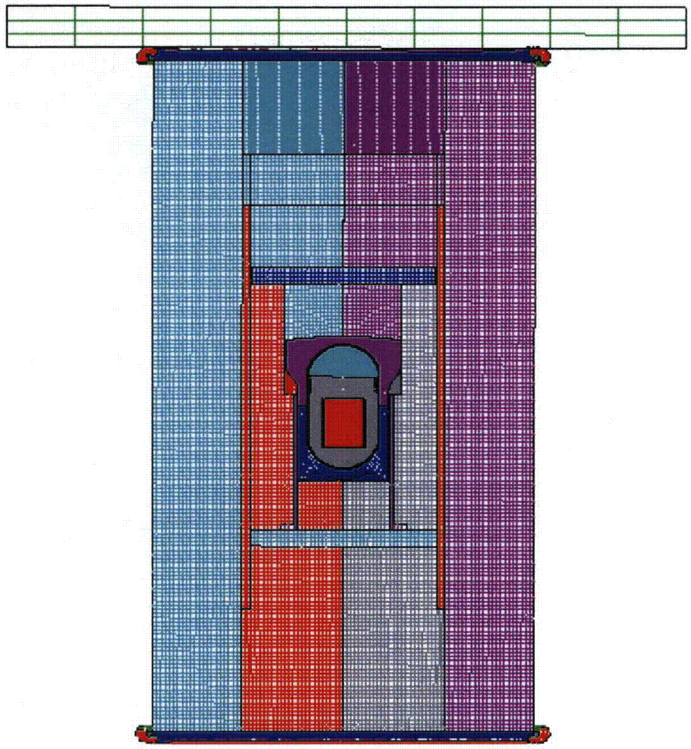

Figure 2-423. Finite Element Mesh for HAC Run 11, 831 g, Plutonium Metal Hollow Cylinder, End Impact – Final Displacement

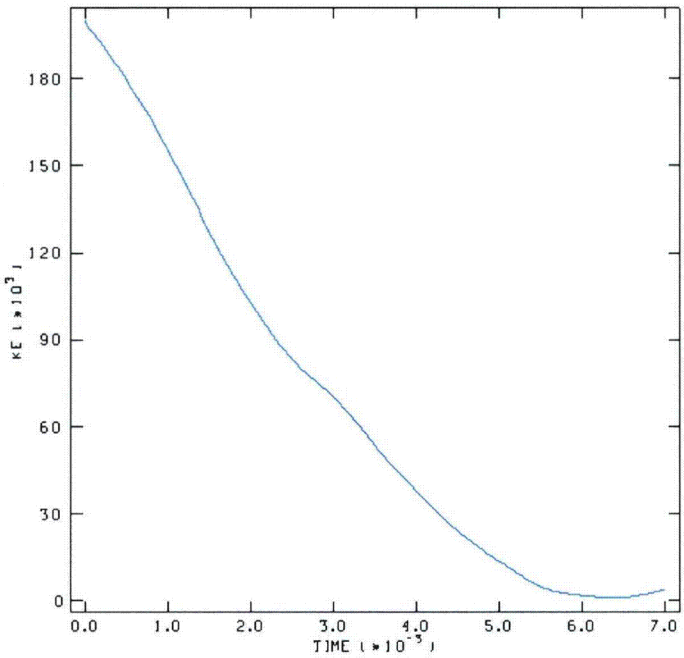

Figure 2-424. Kinetic Energy Time History for HAC Run 11, 831 g, Plutonium Metal Hollow Cylinder, End Impact

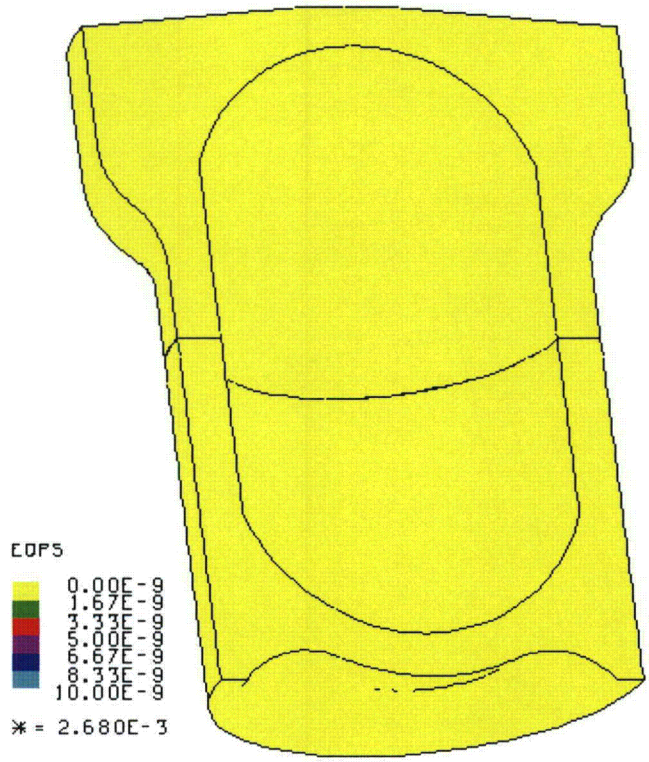

Figure 2-425. Plot of EQPS in the TB-1 for HAC Run 11, 831 g, Plutonium Metal Hollow Cylinder, End Impact

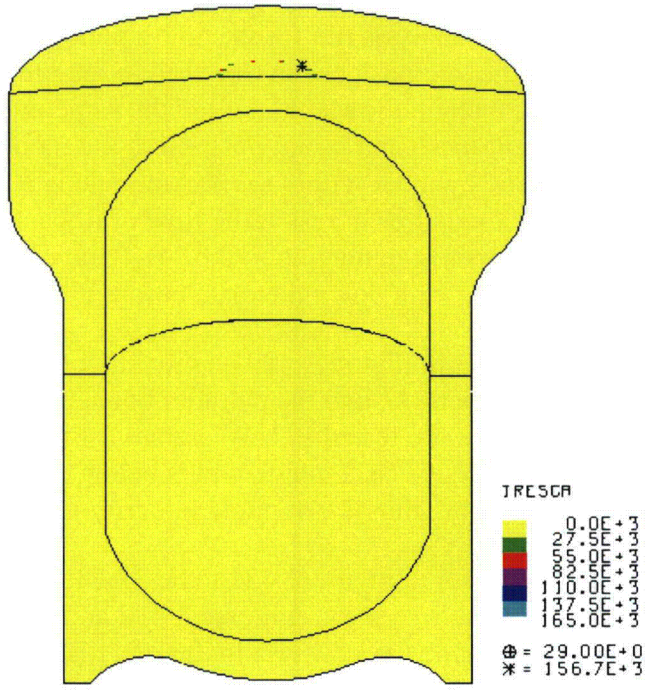

Figure 2-426. Plot of Tresca Stress in the TB-1 for HAC Run 11, 831 g, Plutonium Metal Hollow Cylinder, End Impact

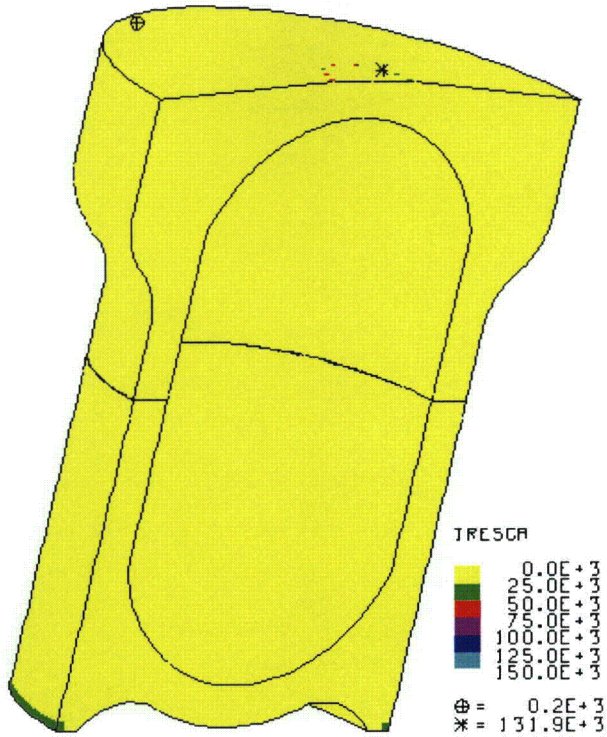

Figure 2-427. Plot of Tresca Stress in the TB-1 for HAC Run 11, 831 g Plutonium Metal Hollow Cylinder, End Impact when Plate Velocity Reaches Zero

2.12.5.6.12 HAC- Run 12, 831 g Plutonium Metal Hollow Cylinder, Side Impact

The dynamic crush side impact HAC analysis run for the 831 g plutonium metal hollow cylinder uses the same model for the overpack as the one used in the previous 11 runs. The TB-1, T-Ampoule, and plutonium metal hollow cylinder are the same model as that used in the aircraft analysis. The finite element mesh and initial position of the model are shown in Figure 2-428. The plutonium metal hollow cylinder within the T-Ampoule is positioned at the bottom of the model because it was considered to be at rest at the time of impact. The plate was positioned between the flanges to be most damaging to the TB-1 and contents by preventing the flanges from absorbing energy and slowing down the plate before it hits the overpack.

The post-impact deformation is shown in Figure 2-429 and its kinetic energy history in Figure 2-430. The flanges on the overpack deform, and the cylinder bounces due to the impact of the plate. Zero elements extended beyond the tested Bao-Wierzbicki strain locus. The maximum Tearing Parameter value for this analysis was 2.94e-6, and is below the critical Tearing Parameter value of 1.012 for Ti-6Al-4V, thus T-Ampoule integrity is maintained.

Peak EQPS in the TB-1 vessel is shown in Figure 2-431 to be 32.78e-3, and is localized in the outer contact regions with the redwood overpack. Figures 2-432 and 2-433 plot the Tresca stresses within the TB-1. The maximum Tresca stress in the TB-1 is 173.8 ksi, but there are no through thickness stresses exceeding the limit of 106.6 ksi, which can be seen clearly in the figure. Figure 2-434 is a plot of the Tresca stresses at the time when all of the kinetic energy of the plate has been transferred to the package, just as the plate begins to rebound. The maximum

through thickness stress at this time is below 20.8 ksi, below the allowable through thickness stress of 106.6 ksi, as seen in the figure.

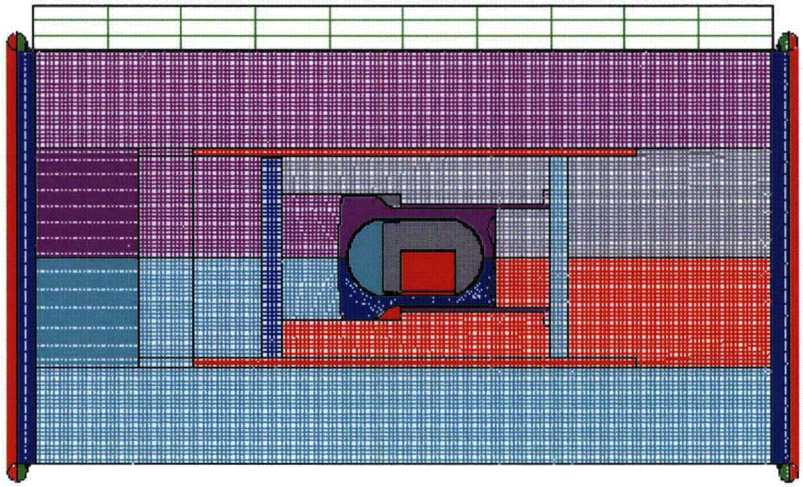

Figure 2-428. Finite Element Mesh for HAC Run 12, 831 g, Plutonium Metal Hollow Cylinder, Side Impact

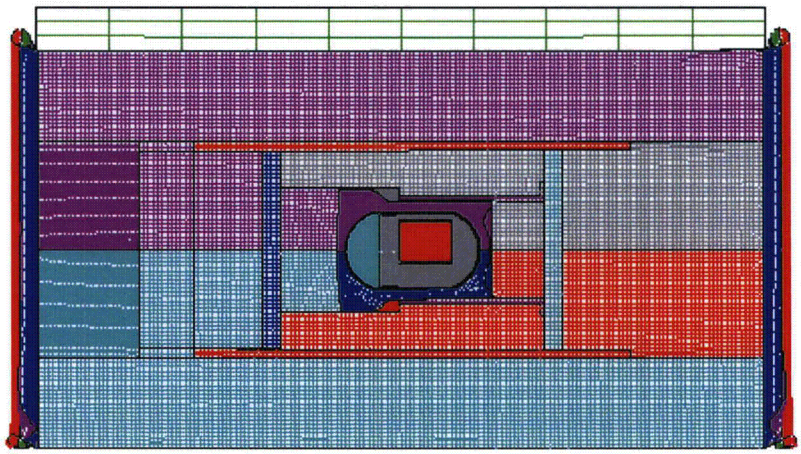

Figure 2-429. Finite Element Mesh for HAC Run 12, 831 g, Plutonium Metal Hollow Cylinder, Side Impact – Final Displacement

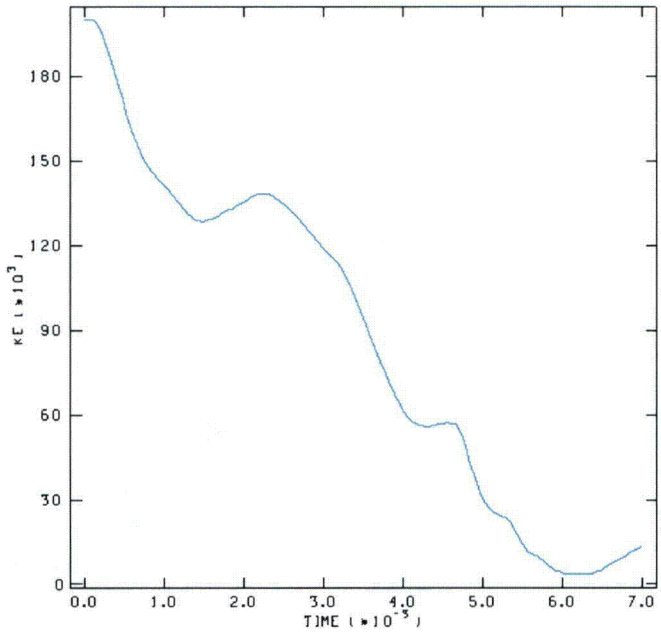

Figure 2-430. Kinetic Energy Time History for HAC Run 12, 831 g, Plutonium Metal Hollow Cylinder, Side Impact

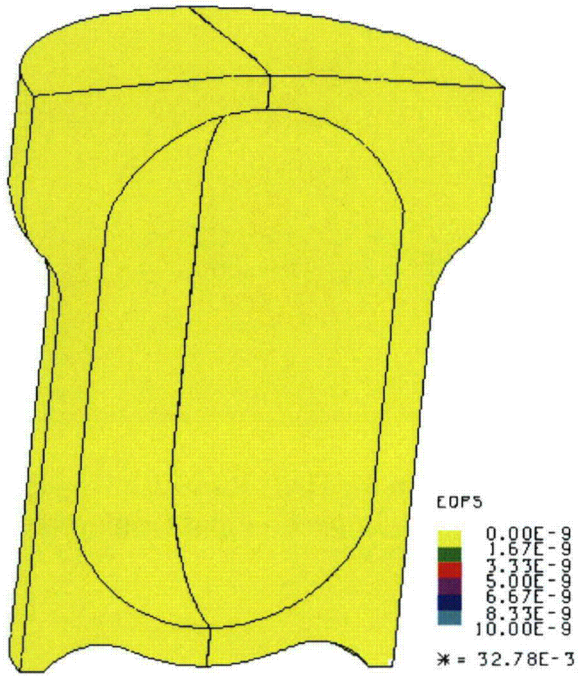

Figure 2-431. Plot of EQPS in the TB-1 for HAC Run 12, 831 g, Plutonium Metal Hollow Cylinder, Side Impact

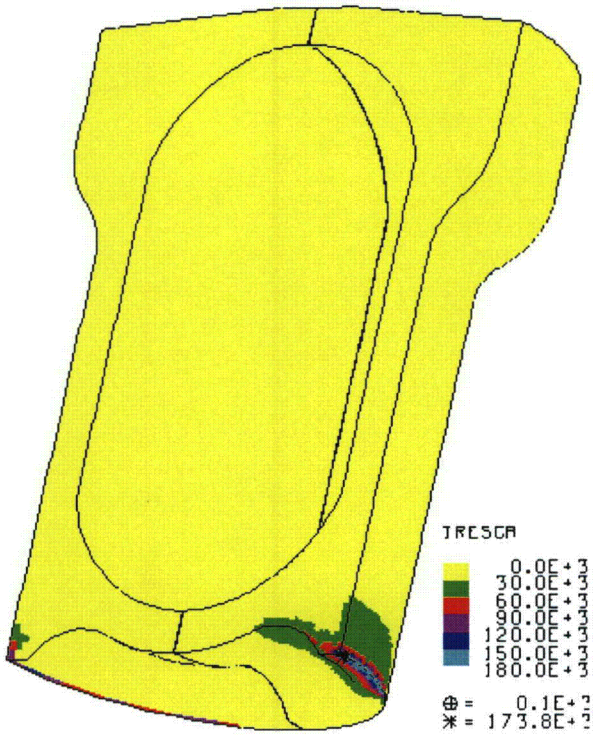

Figure 2-432. Plot of Tresca Stress in the TB-1 for HAC Run 12, 831 g Plutonium Metal Hollow Cylinder, Side Impact

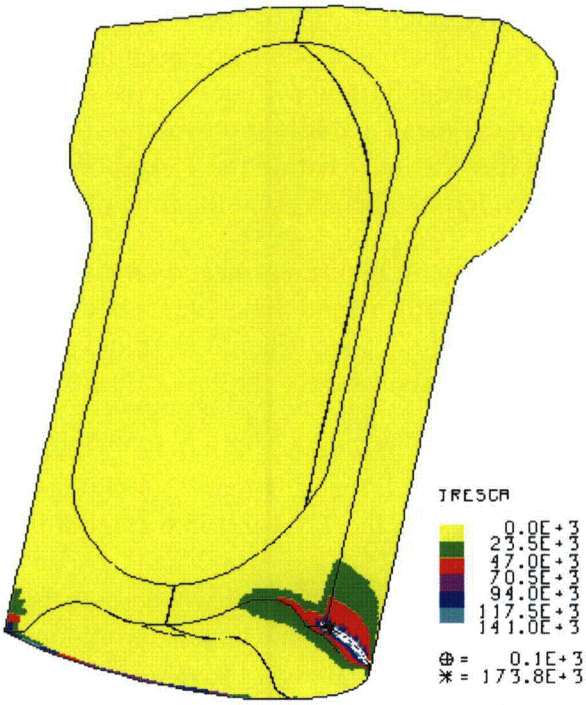

Figure 2-433. Plot of Tresca Stress for HAC Run 12, 831 g Plutonium Metal Hollow Cylinder, Side Impact

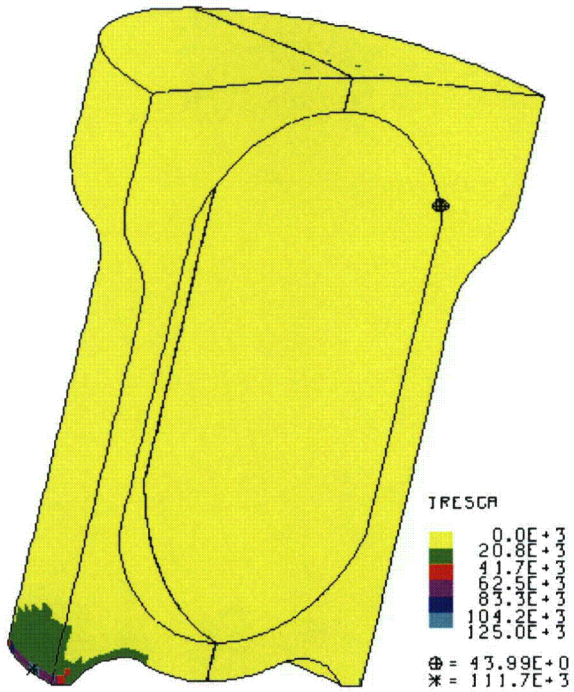

Figure 2-434. Plot of Tresca Stress for HAC Run 12, 831 g Plutonium Metal Hollow Cylinder, Side Impact when Plate Velocity Reaches Zero

2.12.5.6.13 HAC- Run 13, 831 g Angled Plutonium Metal Hollow Cylinder, End Impact

The dynamic crush end impact HAC analysis run for the 831 g angled plutonium metal hollow cylinder uses the same model for the overpack as the one used in the previous 12 runs. The TB-1, T-Ampoule, and plutonium metal hollow cylinder are the same model as that used in the aircraft analysis. The finite element mesh and initial position of the model are shown in Figure 2-435. The plutonium metal hollow cylinder within the T-Ampoule is positioned at the bottom of the model because it was considered to be at rest at the time of impact.

The post-impact deformation is shown in Figure 2-436 and its kinetic energy history in Figure 2-437. The flanges on the overpack deform, and the contents bounce due to the impact of the plate. Zero elements extended beyond the tested Bao-Wierzbicki strain locus. The maximum Tearing Parameter value for this analysis was 0.

Peak EQPS in the TB-1 vessel is shown in Figure 2-438 to be 2.389e-3, and is localized in the outer contact regions with the redwood overpack. Figure 2-439 plots the Tresca stresses within the TB-1. The maximum Tresca stress in the TB-1 is 155.6 ksi, but there are no through thickness stresses exceeding the limit of 106.6 ksi, which can be seen clearly in the figure. Figure 2-440 is a plot of the Tresca stresses at the time when all of the kinetic energy of the plate has been transferred to the package, just as the plate begins to rebound. The maximum through thickness stress at this time is below 25.0 ksi, below the allowable through thickness stress of 106.6 ksi, as seen in the figure.

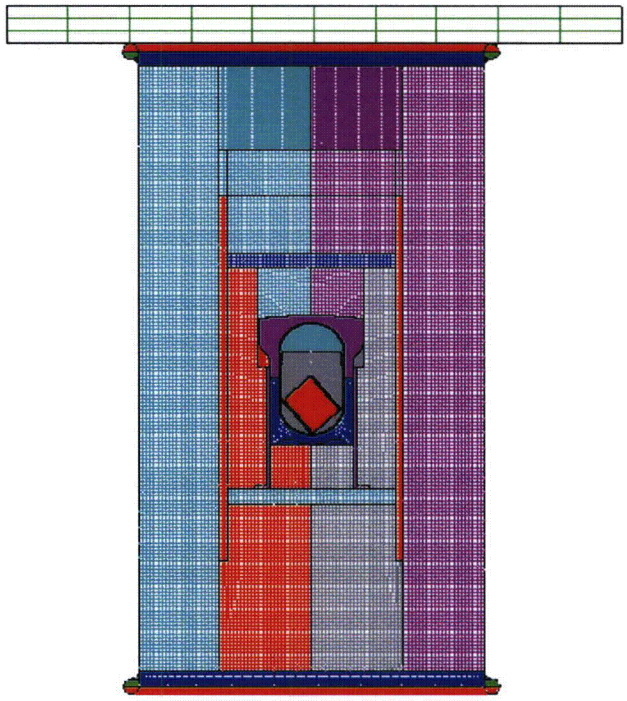

Figure 2-435. Finite Element Mesh for HAC Run 13, 831 g, Angled, Plutonium Metal Hollow Cylinder, End Impact

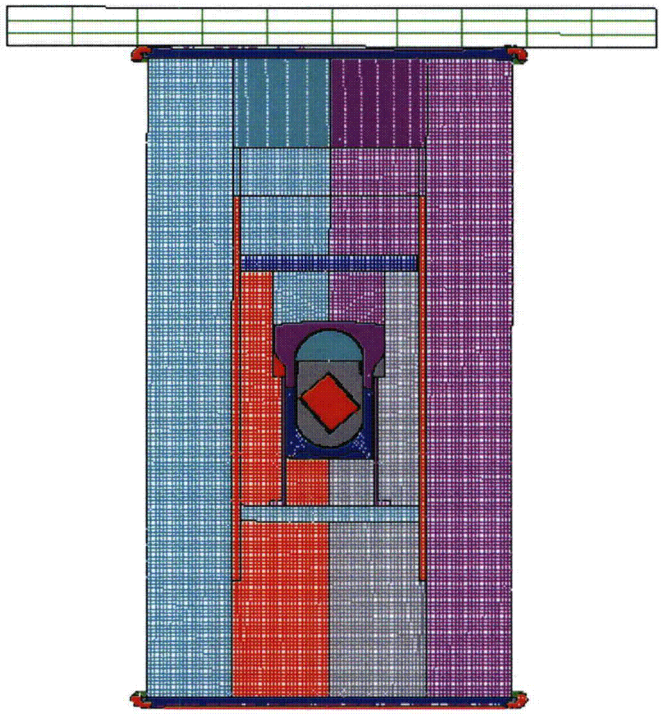

Figure 2-436. Finite Element Mesh for HAC Run 13, 831 g, Angled, Plutonium Metal Hollow Cylinder, End Impact – Final Displacement

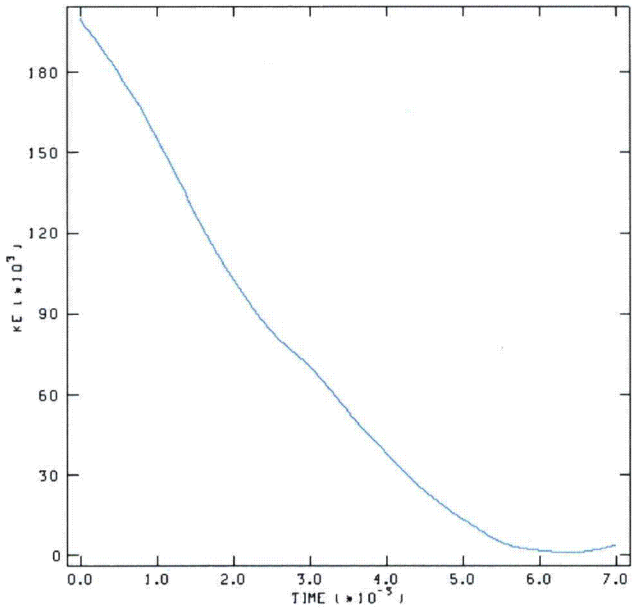

Figure 2-437. Kinetic Energy Time History for HAC Run 13, 831 g, Angled, Plutonium Metal Hollow Cylinder, End Impact

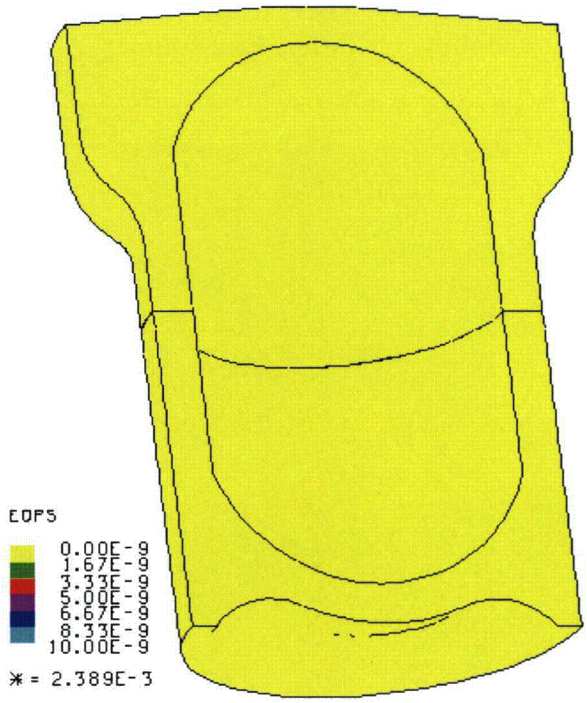

Figure 2-438. Plot of EQPS in the TB-1 for HAC Run 13, 831 g, Angled, Plutonium Metal Hollow Cylinder, End Impact

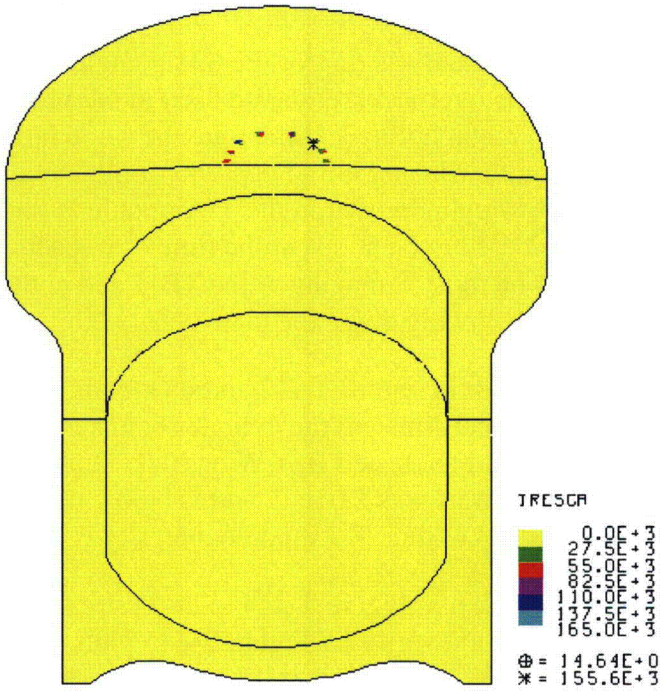

Figure 2-439. Plot of Tresca Stress in the TB-1 for HAC Run 13, 831 g, Angled, Plutonium Metal Hollow Cylinder, End Impact

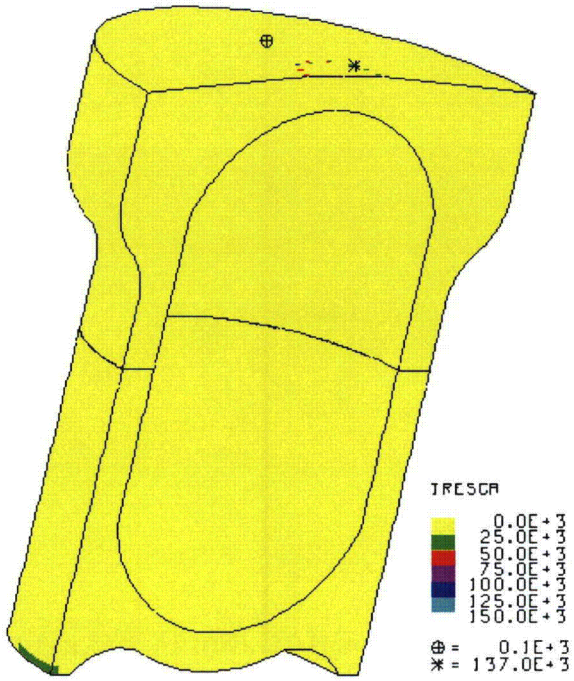

Figure 2-440. Plot of Tresca Stress in the TB-1 for HAC Run 13, 831 g Angled Plutonium Metal Hollow Cylinder, End Impact when Plate Velocity Reaches Zero

2.12.5.6.14 HAC- Run 14, 831 g Angled Plutonium Metal Hollow Cylinder, Side Impact

The dynamic crush side impact HAC analysis run for the 831 g angled plutonium metal hollow cylinder uses the same model for the overpack as the one used in the previous 13 runs. The TB-1, T-Ampoule, and plutonium metal hollow cylinder are the same model as that used in the aircraft analysis. The finite element mesh and initial position of the model are shown in Figure 2-441. The plutonium metal hollow cylinder within the T-Ampoule is positioned at the bottom of the model because it was considered to be at rest at the time of impact. The plate was positioned between the flanges to be most damaging to the TB-1 and contents by preventing the flanges from absorbing energy and slowing down the plate before it hits the overpack.

The post-impact deformation is shown in Figure 2-442 and its kinetic energy history in Figure 2-443. The flanges on the overpack deform, and the cylinder bounces due to the impact of the plate. Zero elements extended beyond the tested Bao-Wierzbicki strain locus. The maximum Tearing Parameter value for this analysis was 2.01e-2, and is below the critical Tearing Parameter value of 1.012 for Ti-6Al-4V, thus T-Ampoule integrity is maintained.

Peak EQPS in the TB-1 vessel is shown in Figure 2-444 to be 31.46e-3, and is localized in the outer contact regions with the redwood overpack. Figure 2-445 plots the Tresca stresses within the TB-1. The maximum Tresca stress in the TB-1 is 172.5 ksi, but there are no through thickness stresses exceeding the limit of 106.6 ksi, which can be seen clearly in the figure. Figure 2-446 is a plot of the Tresca stresses at the time when all of the kinetic energy of the plate has been transferred to the package, just as the plate begins to rebound. The maximum through thickness stress at this time is below 25.0 ksi, below the allowable through thickness stress of 106.6 ksi, as seen in the figure.

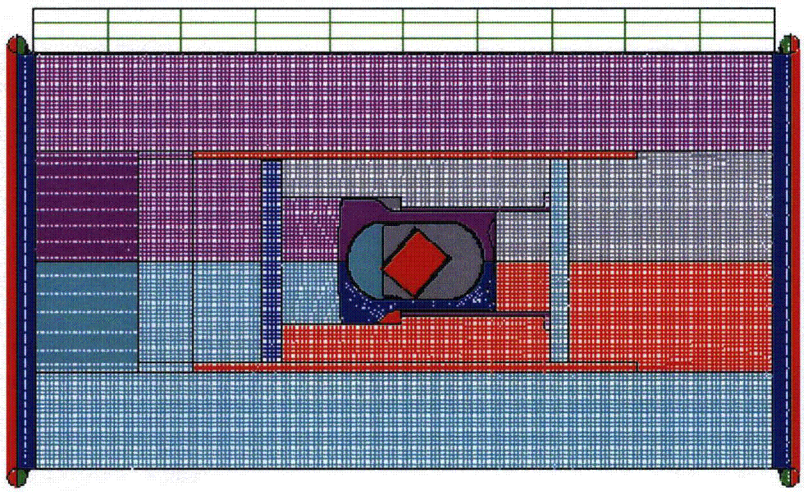

Figure 2-441. Finite Element Mesh for HAC Run 14, 831 g Angled Plutonium Metal Hollow Cylinder, Side Impact

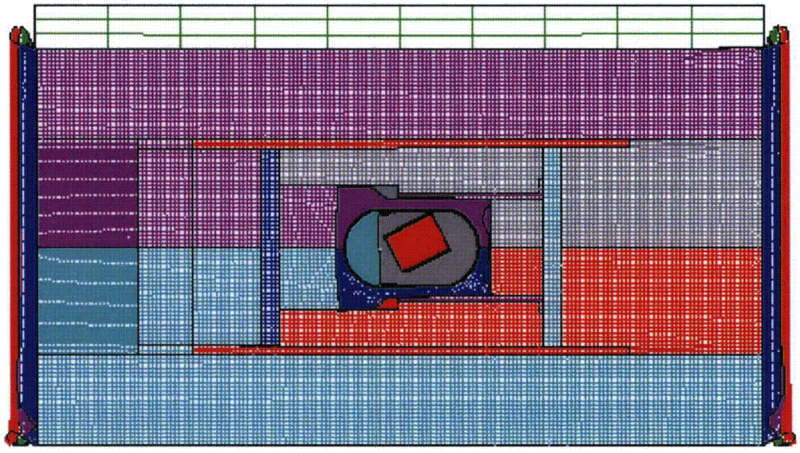

Figure 2-442. Finite Element Mesh for HAC Run 14, 831 g Angled Plutonium Metal Hollow Cylinder, Side Impact – Final Displacement

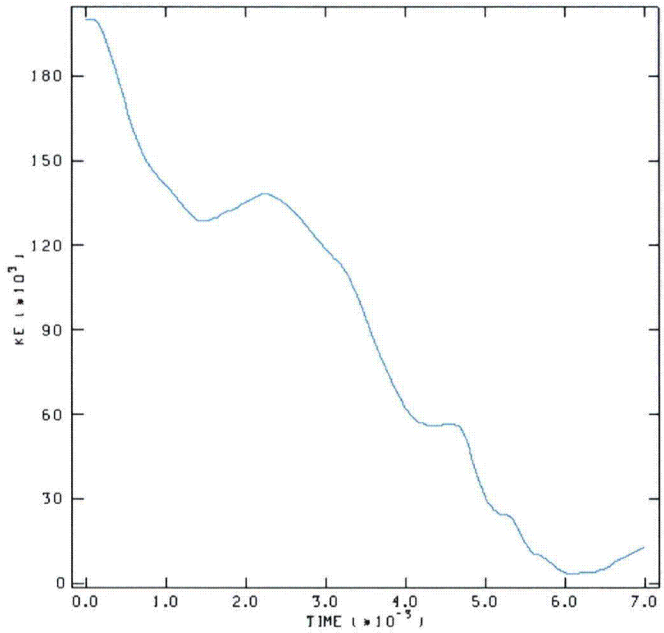

Figure 2-443. Kinetic Energy Time History for HAC Run 14, 831 g Angled Plutonium Metal Hollow Cylinder, Side Impact

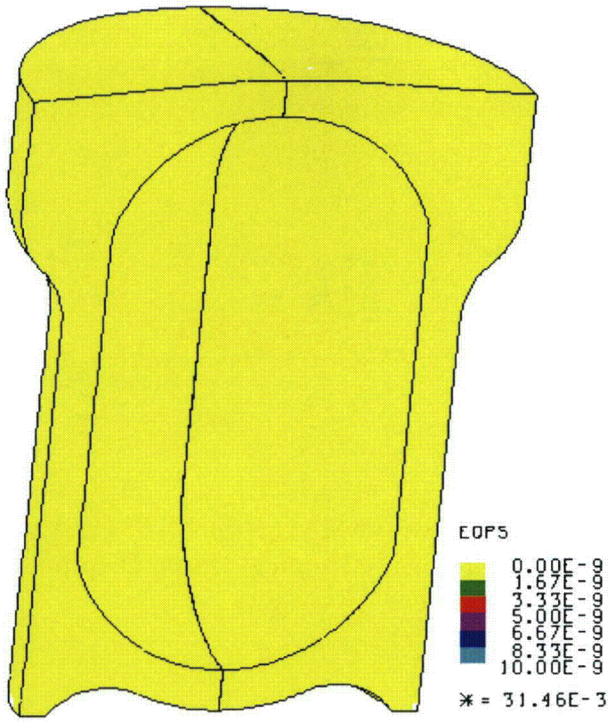

Figure 2-444. Plot of EQPS in the TB-1 for HAC Run 14, 831 g Angled Plutonium Metal Hollow Cylinder, Side Impact

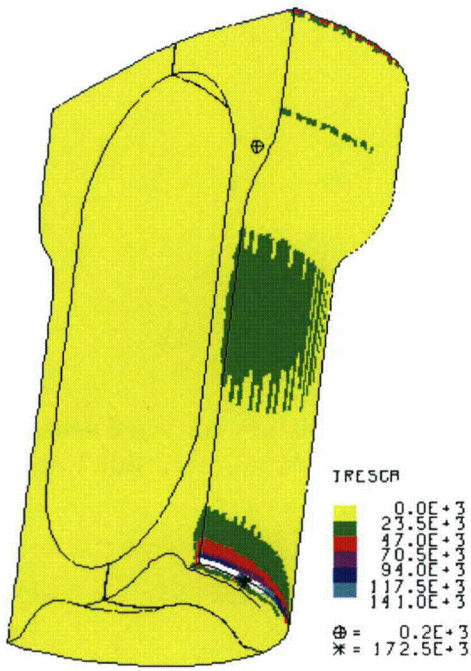

Figure 2-445. Plot of Tresca Stress in the TB-1 for HAC Run 14, 831 g Angled, Plutonium Metal Hollow Cylinder, Side Impact

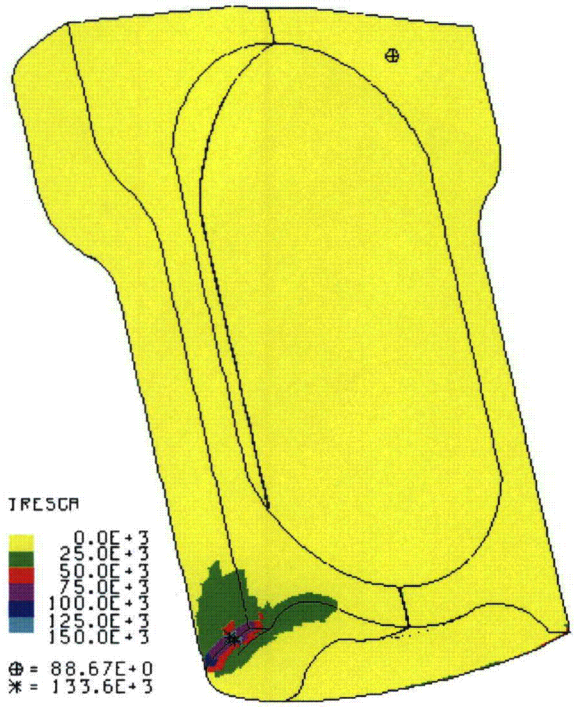

Figure 2-446. Plot of Tresca Stress in the TB-1 for HAC Run 14, 831 g Angled Plutonium Metal Hollow Cylinder, Side Impact when Plate Velocity Reaches Zero

2.12.5.6.15 HAC- Run 15, 831 g Angled Plutonium Metal Hollow Cylinder, CGOC Impact

The dynamic crush CGOC impact HAC analysis run for the 831 g angled plutonium metal hollow cylinder uses the same overpack model as those used in HAC runs 1 through 14. The finite element mesh and initial position of the model are shown in Figure 2-447. The plutonium metal hollow cylinder within the T-Ampoule is positioned at the bottom of the model because it was considered to be at rest.

The post-impact deformation is shown in Figure 2-448 and its kinetic energy history in Figure 2-449. The flanges on the overpack deform, and the cylinder bounces due to the impact of the plate. The kinetic energy does not drop completely to zero because the plate is still vibrating and internal contents are still in motion. The plutonium metal hollow cylinder has bounced off of the top and bottom surface of the T-Ampoule, and the plate is now rebounding slowly with the package, ensuring that the highest containment vessel and contents loadings have occurred.

There was zero EQPS in the T-Ampoule and the TB-1, and the maximum Tearing Parameter was 0. Figure 2-450 is a plot of the Tresca stresses within the TB-1. The maximum Tresca stress in the TB-1 is 147.1 ksi, but there are no through thickness stresses exceeding the limit of 106.6 ksi, which can be seen clearly in the figure. Figure 2-451 is a plot of the Tresca stresses at the time when all of the kinetic energy of the plate has been transferred to the package, just as the plate begins to rebound. The maximum through thickness stress at this time is below 16.7 ksi, below the allowable through thickness stress of 106.6 ksi, as seen in the figure.

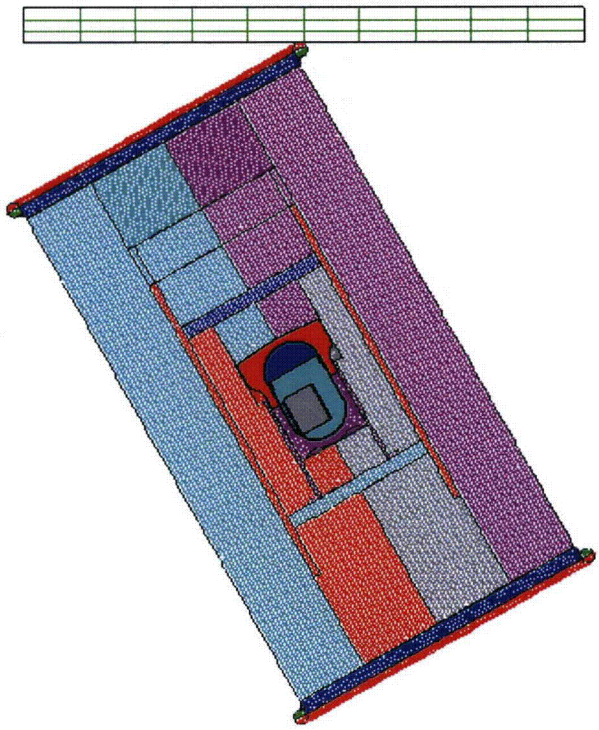

Figure 2-447. Finite Element Mesh for HAC Run 15, 831 g Angled Plutonium Metal Hollow Cylinder, CGOC Impact

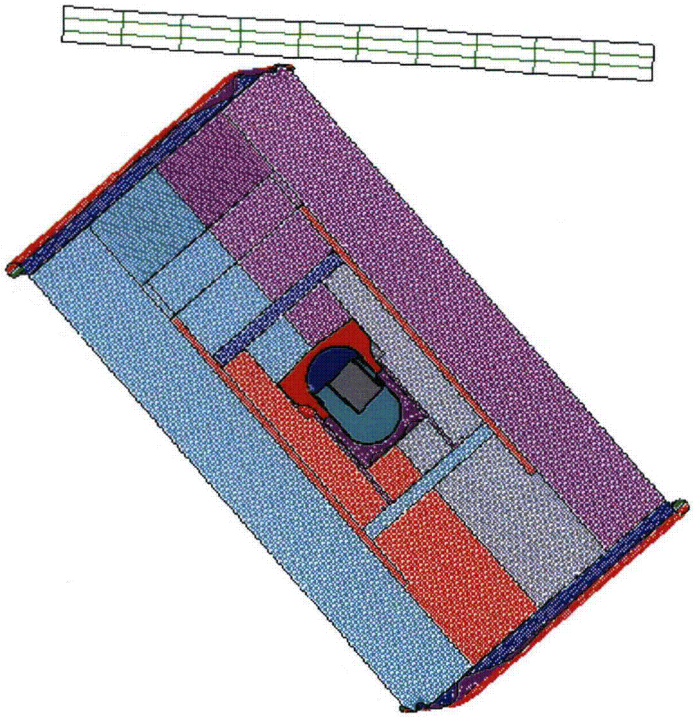

Figure 2-448. Finite Element Mesh for HAC Run 15, 831 g Angled Plutonium Metal Hollow Cylinder, CGOC Impact – Final Displacement

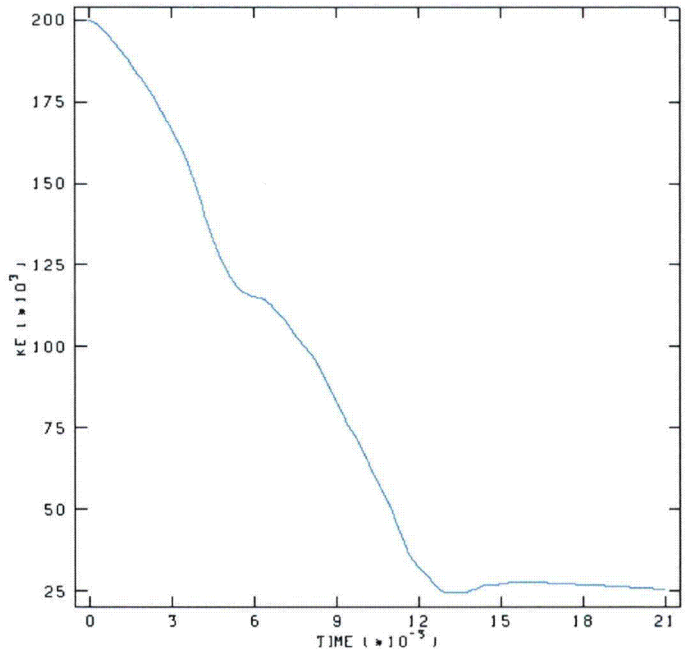

Figure 2-449. Kinetic Energy Time History for HAC Run 15, 831 g Angled Plutonium Metal Hollow Cylinder, CGOC Impact

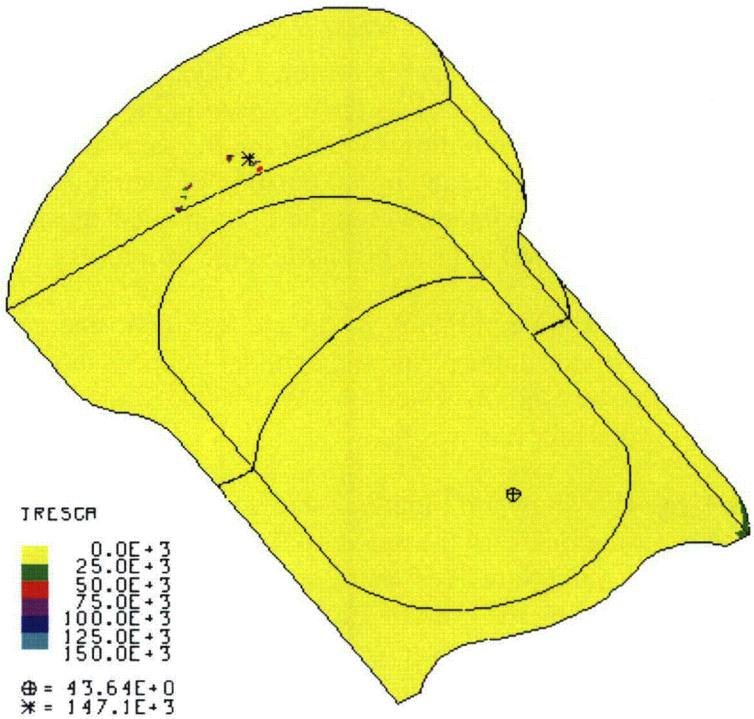

Figure 2-450. Plot of Tresca Stress in the TB-1 for HAC Run 15, 831 g Angled Plutonium Metal Hollow Cylinder, CGOC Impact

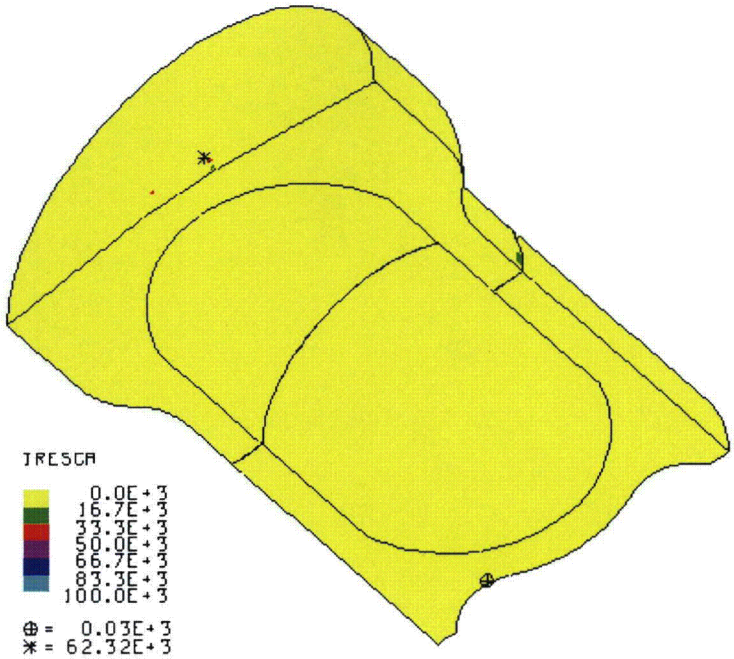

Figure 2-451. Plot of Tresca Stress in the TB-1 for HAC Run 15, 831 g Angled Plutonium Metal Hollow Cylinder, CGOC Impact when Plate Velocity Reaches Zero

2.12.5.6.16 HAC- Run 16, 731 g Plutonium Metal Hollow Cylinder, End Impact

The dynamic crush end impact HAC analysis run for the 731 g angled plutonium metal hollow cylinder uses the same model for the overpack as the one used in the previous 15 runs. The TB-1, T-Ampoule, and plutonium metal hollow cylinder are the same model as that used in the aircraft analysis. The finite element mesh and initial position of the model are shown in Figure 2-452. The plutonium metal hollow cylinder within the T-Ampoule is positioned at the bottom of the model because it was considered to be at rest at the time of impact.

The post-impact deformation is shown in Figure 2-453 and its kinetic energy history in Figure 2-454. The flanges on the overpack deform, and the cylinder bounces due to the impact of the plate. Zero elements extended beyond the tested Bao-Wierzbicki strain locus. The maximum Tearing Parameter value for this analysis was 0.

Peak EQPS in the TB-1 vessel is shown in Figures 2-455 and 2-456 to be 2.237e-3, and is localized in the outer contact regions with the redwood overpack. Figure 2-457 plots the Tresca stresses within the TB-1. The maximum Tresca stress in the TB-1 is 157.2 ksi, but there are no through thickness stresses exceeding the limit of 106.6 ksi, which can be seen clearly in the figure. Figure 2-458 is a plot of the Tresca stresses at the time when all of the kinetic energy of the plate has been transferred to the package, just as the plate begins to rebound. The maximum through thickness stress at this time is below 25.0 ksi, below the allowable through thickness stress of 106.6 ksi, as seen in the figure.

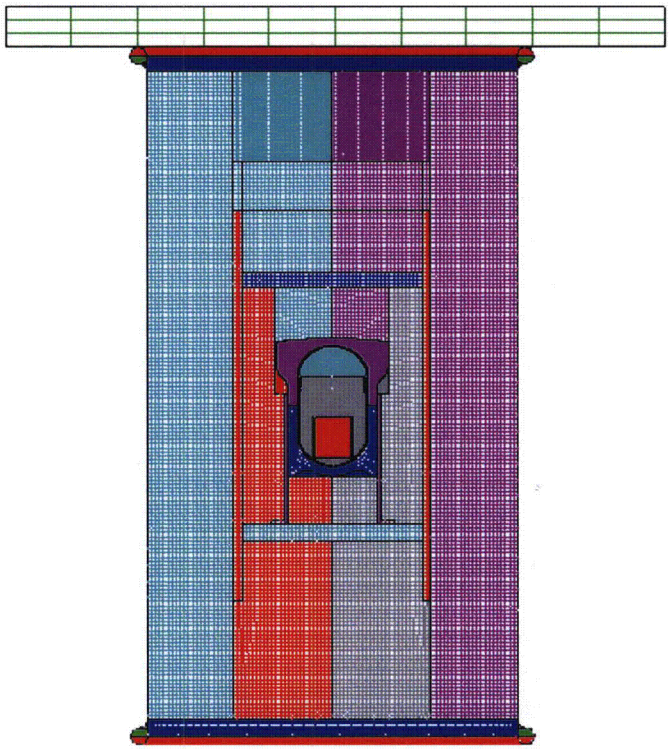

Figure 2-452. Finite Element Mesh for HAC Run 16, 731 g Plutonium Metal Hollow Cylinder, End Impact

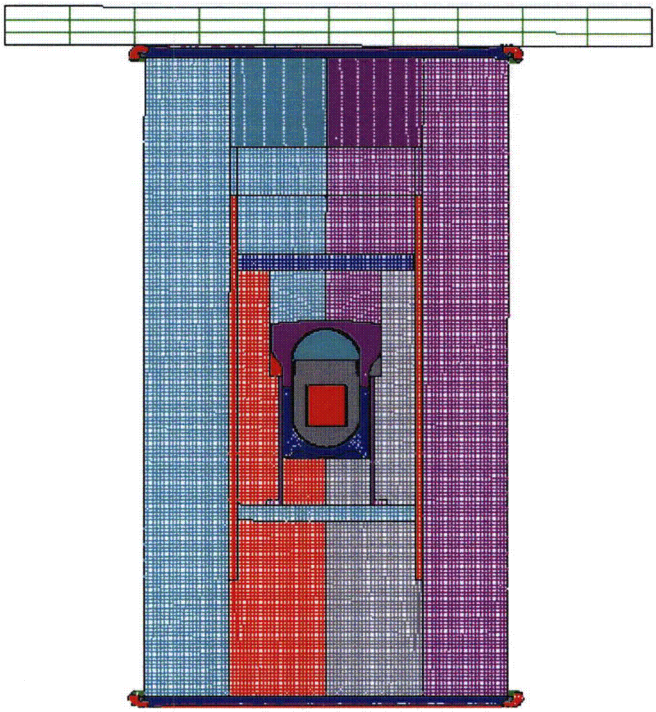

Figure 2-453. Finite Element Mesh for HAC Run 16, 731 g Plutonium Metal Hollow Cylinder, End Impact – Final Displacement

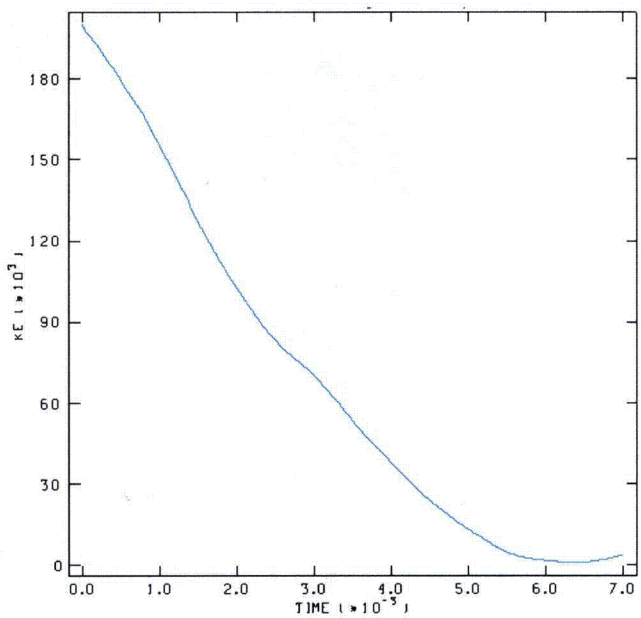

Figure 2-454. Kinetic Energy Time History for HAC Run 16, 731 g Plutonium Metal Hollow Cylinder, End Impact

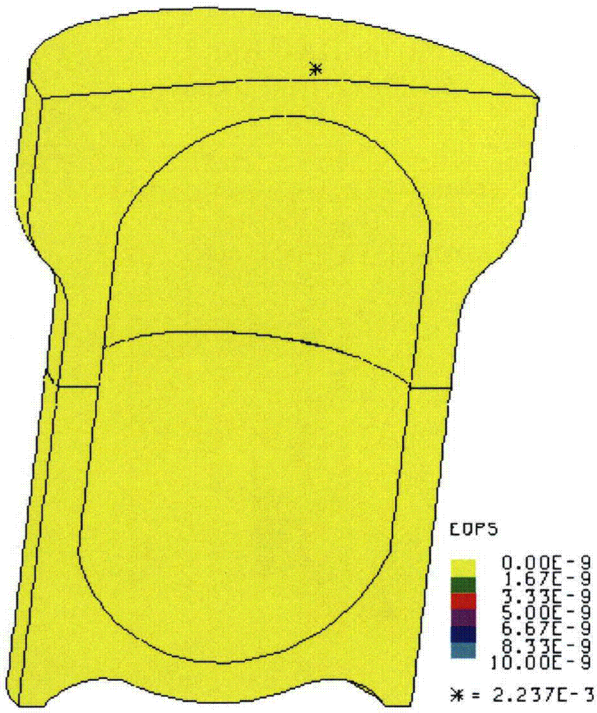

Figure 2-455. Plot of EQPS in the TB-1 for HAC Run 16, 731 g Plutonium Metal Hollow Cylinder, End Impact

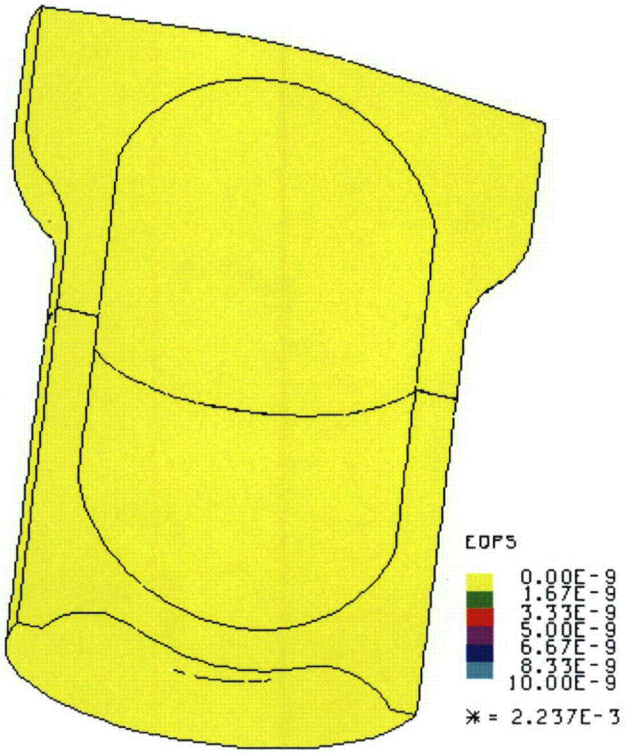

Figure 2-456. Plot of EQPS in the TB-1 for HAC Run 16, 731 g Plutonium Metal Hollow Cylinder, End Impact

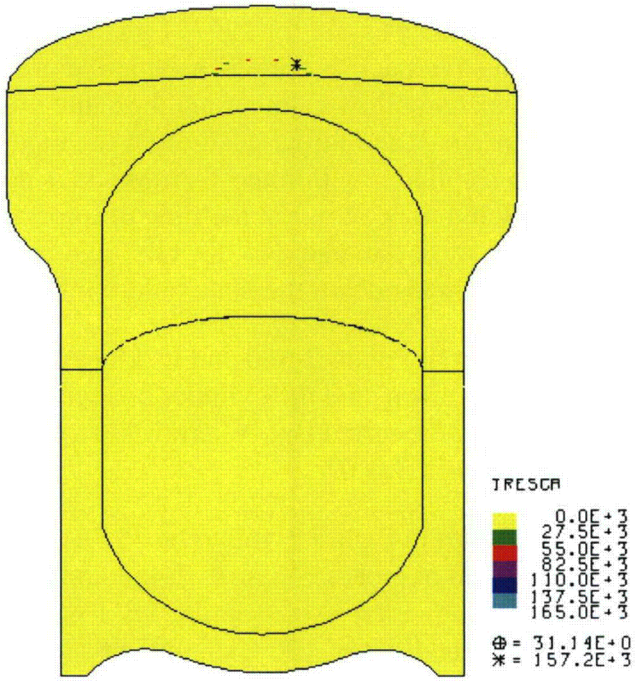

Figure 2-457. Plot of Tresca Stress in the TB-1 for HAC Run 16, 731 g Plutonium Metal Hollow Cylinder, End Impact

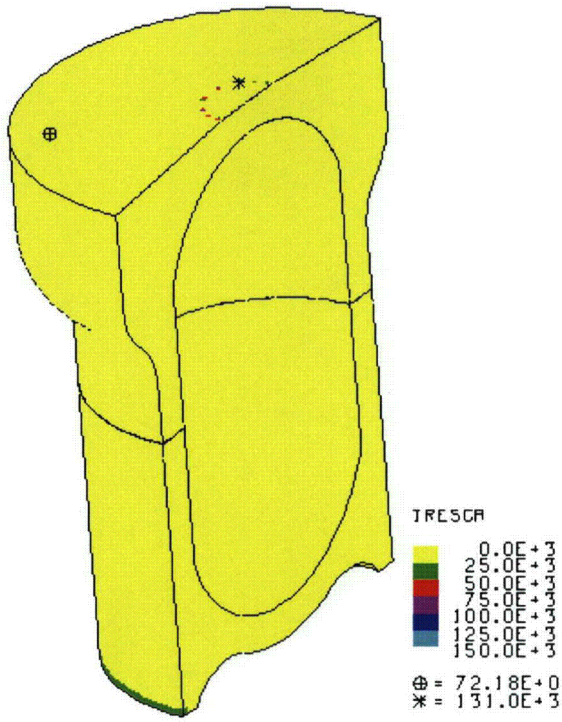

Figure 2-458. Plot of Tresca Stress in the TB-1 for HAC Run 16, 731 g Plutonium Metal Hollow Cylinder, End Impact when Plate Velocity Reaches Zero

2.12.5.6.17 HAC- Run 17, 731 g Plutonium Metal Hollow Cylinder, Side Impact

The dynamic crush side impact HAC analysis run for the 731 g angled plutonium metal hollow cylinder uses the same model for the overpack as the one used in the previous 16 runs. The TB-1, T-Ampoule, and plutonium metal hollow cylinder are the same model as that used in the aircraft analysis. The finite element mesh and initial position of the model are shown in Figure 2-459. The plutonium metal hollow cylinder within the T-Ampoule is positioned at the bottom of the model because it was considered to be at rest at the time of impact. The plate was positioned between the flanges to be most damaging to the TB-1 and contents by preventing the flanges from absorbing energy and slowing down the plate before it hits the overpack.

The post-impact deformation is shown in Figure 2-460 and its kinetic energy history in Figure 2-461. The flanges on the overpack deform, and the cylinder bounces due to the impact of the plate. Zero elements extended beyond the tested Bao-Wierzbicki strain locus. The maximum Tearing Parameter value for this analysis was 0.

Peak EQPS in the TB-1 vessel is shown in Figure 2-462 to be 45.76-3, and is localized in the outer contact regions with the redwood overpack. Figures 2-463 and 2-464 plot the Tresca stresses within the TB-1. The maximum Tresca stress in the TB-1 is 177.9 ksi, but there are no through thickness stresses exceeding the limit of 106.6 ksi, which can be seen clearly in the figure. Figure 2-465 is a plot of the Tresca stresses at the time when all of the kinetic energy of the plate has been transferred to the package, just as the plate begins to rebound. The maximum through thickness stress at this time is below 20.8 ksi, below the allowable through thickness stress of 106.6 ksi, as seen in the figure.

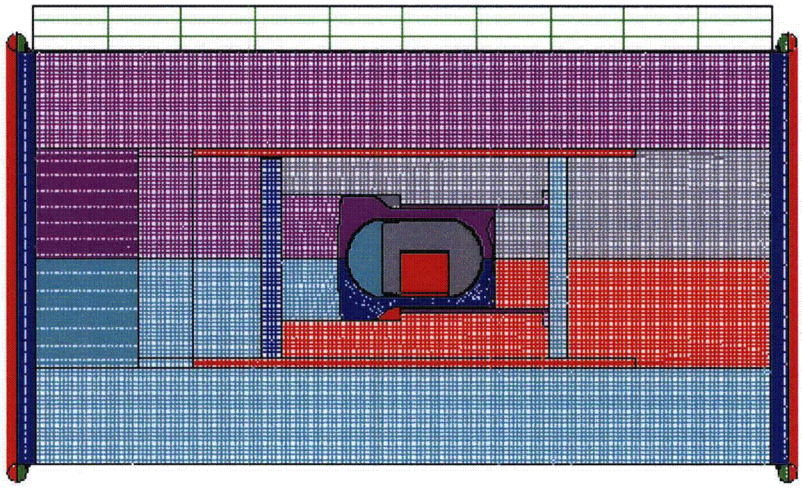

Figure 2-459. Finite Element Mesh for HAC Run 17, 731 g Plutonium Metal Hollow Cylinder, Side Impact

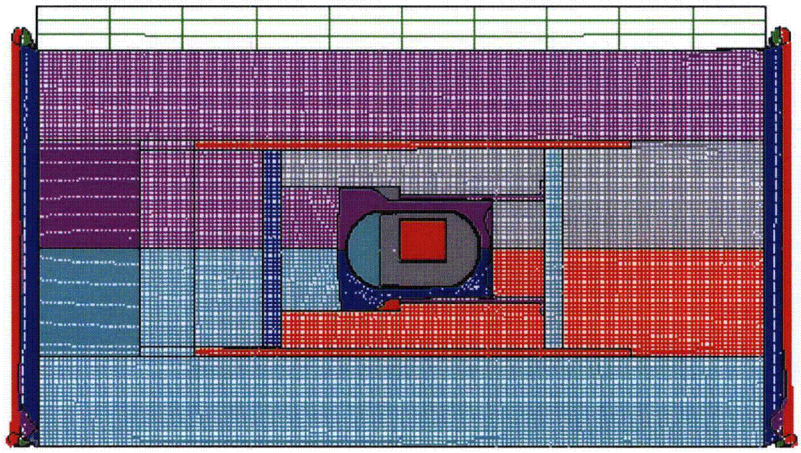

Figure 2-460. Finite Element Mesh for HAC Run 17, 731 g Plutonium Metal Hollow Cylinder, Side Impact – Final Displacement

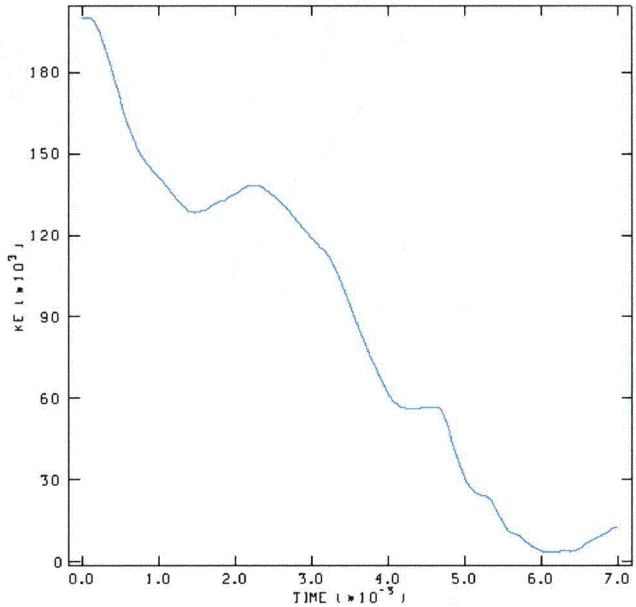

Figure 2-461. Kinetic Energy Time History for HAC Run 17, 731 g Plutonium Metal Hollow Cylinder, Side Impact

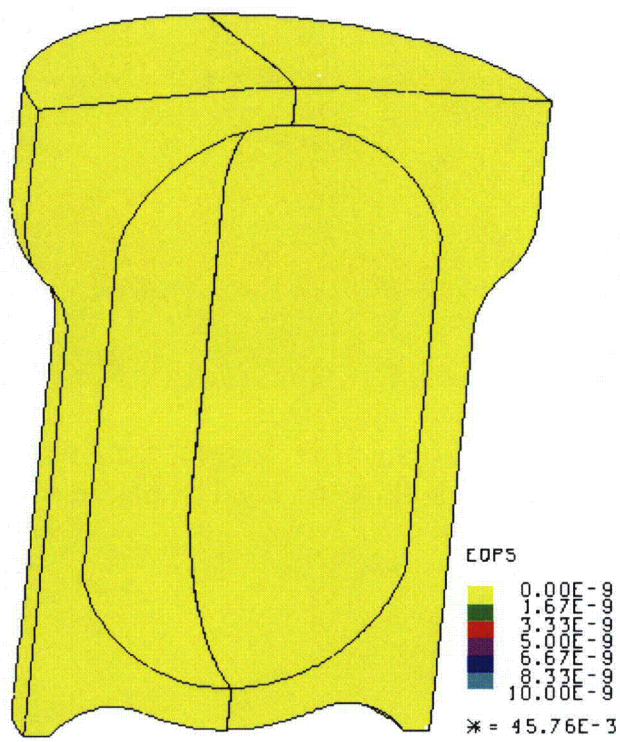

Figure 2-462. Plot of EQPS in the TB-1 for HAC Run 17, 731 g Plutonium Metal Hollow Cylinder, Side Impact

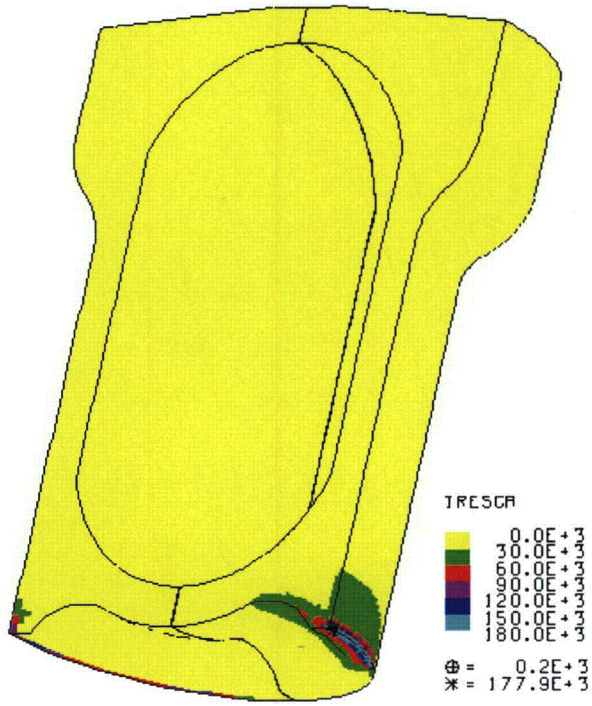

Figure 2-463. Plot of Tresca Stress in the TB-1 for HAC Run 17, 731 g Plutonium Metal Hollow Cylinder, Side Impact

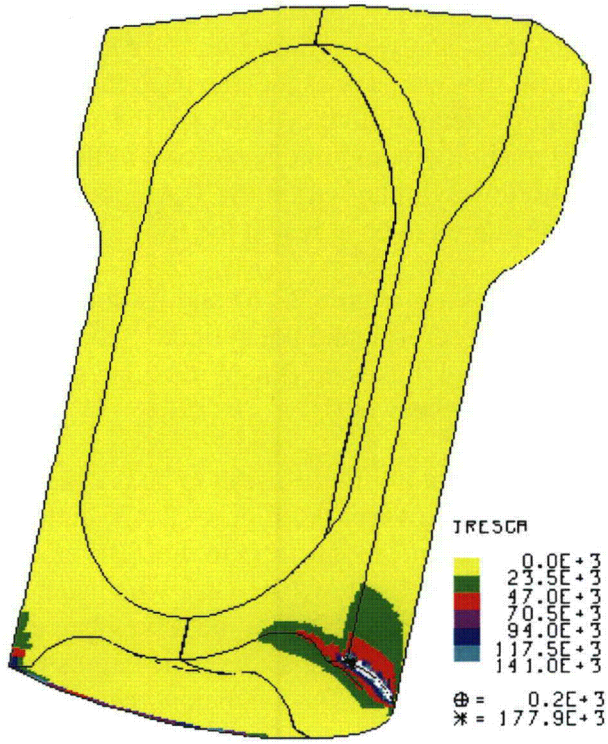

Figure 2-464. Plot of Tresca Stress in the TB-1 for HAC Run 17, 731 g Plutonium Metal Hollow Cylinder, Side Impact

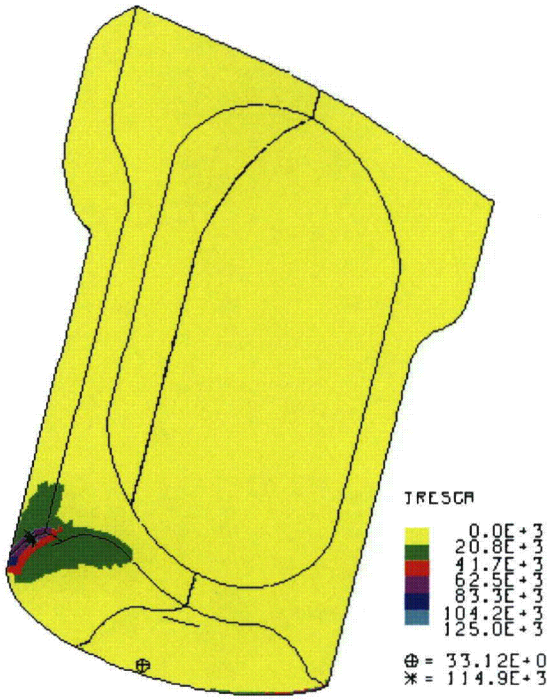

Figure 2-465. Plot of Tresca Stress in the TB-1 for HAC Run 17, 731 g Plutonium Metal Hollow Cylinder, Side Impact when Plate Velocity Reaches Zero

2.12.5.6.18 HAC- Run 18, 731 g Angled Plutonium Metal Hollow Cylinder, End Impact

The dynamic crush end impact HAC analysis run for the 731 g angled plutonium metal hollow cylinder uses the same model for the overpack as the one used in the previous 17 runs. The TB-1, T-Ampoule, and plutonium metal hollow cylinder are the same model as that used in the aircraft analysis. The finite element mesh and initial position of the model are shown in Figure 2-466. The plutonium metal hollow cylinder within the T-Ampoule is positioned at the bottom of the model because it was considered to be at rest at the time of impact.

The post-impact deformation is shown in Figure 2-467 and its kinetic energy history in Figure 2-468. The flanges on the overpack deform, and the cylinder bounces due to the impact of the plate. Zero elements extended beyond the tested Bao-Wierzbicki strain locus. The maximum Tearing Parameter value for this analysis was 0.

Peak EQPS in the TB-1 vessel is shown in Figure 2-469 to be 0.2813e-3, and is localized in the outer contact regions with the redwood overpack. Figures 2-470 and 2-471 plot the Tresca stresses within the TB-1. The maximum Tresca stress in the TB-1 is 157.3 ksi, but there are no through thickness stresses exceeding the limit of 106.6 ksi, which can be seen clearly in the figure. Figure 2-472 is a plot of the Tresca stresses at the time when all of the kinetic energy of the plate has been transferred to the package, just as the plate begins to rebound. The maximum through thickness stress at this time is below 20.8 ksi, below the allowable through thickness stress of 106.6 ksi, as seen in the figure.

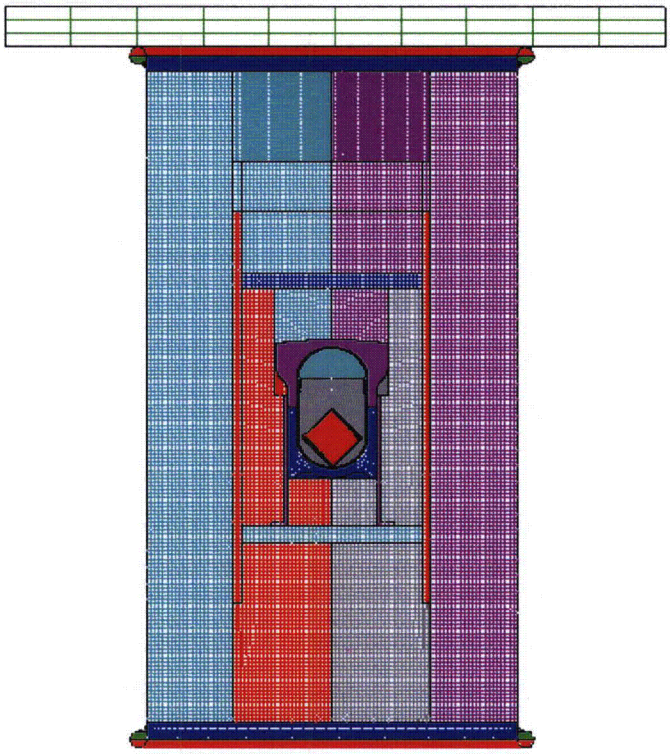

Figure 2-466. Finite Element Mesh for HAC Run 18, 731 g Angled Plutonium Metal Hollow Cylinder, End Impact

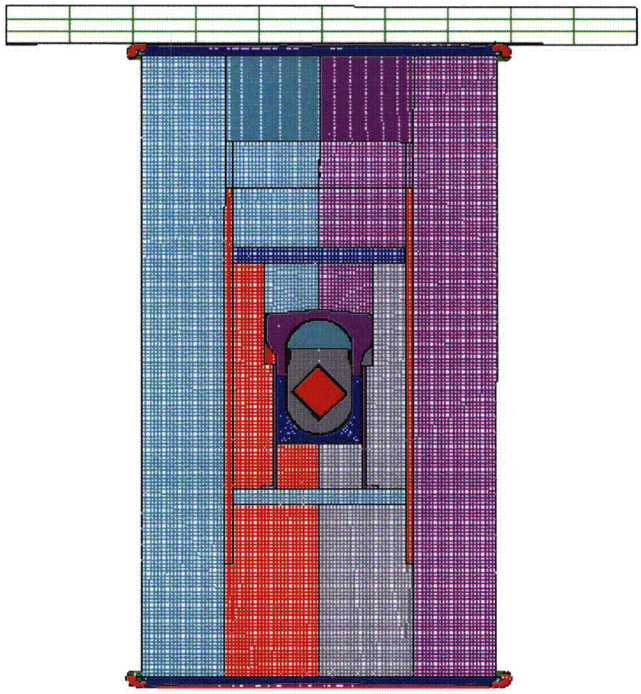

Figure 2-467. Finite Element Mesh for HAC Run 18, 731 g Angled Plutonium Metal Hollow Cylinder, End Impact – Final Displacement

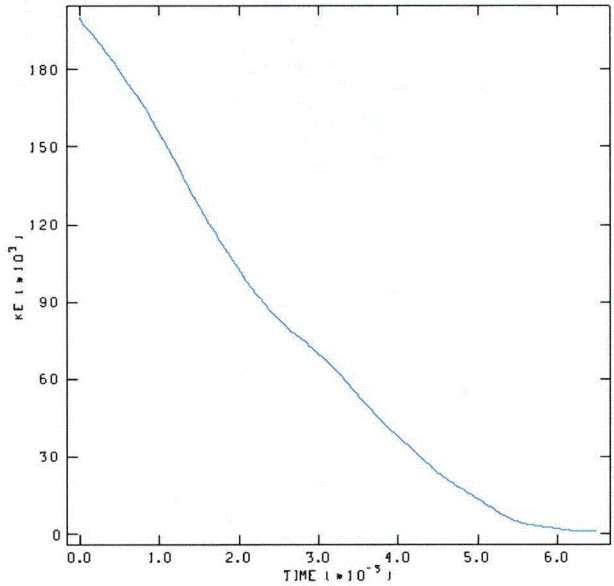

Figure 2-468. Kinetic Energy Time History for HAC Run 18, 731 g Angled Plutonium Metal Hollow Cylinder, End Impact

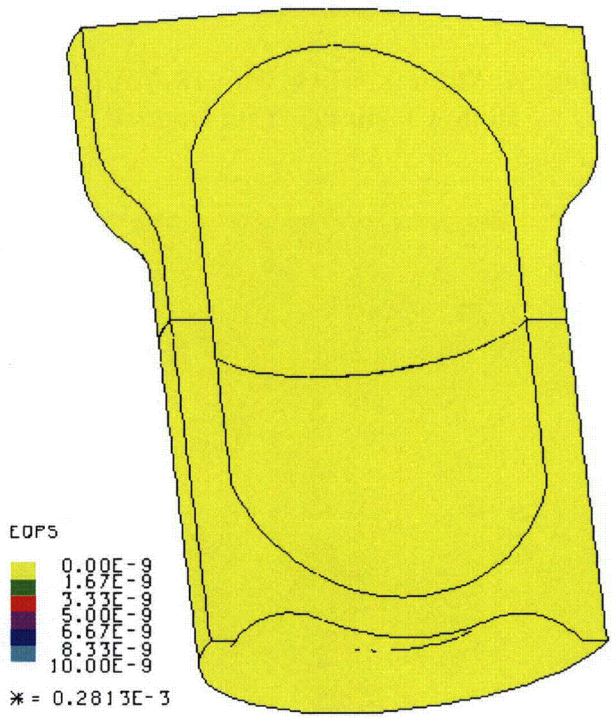

Figure 2-469. Plot of EQPS in the TB-1 for HAC Run 18, 731 g Angled Plutonium Metal Hollow Cylinder, End Impact

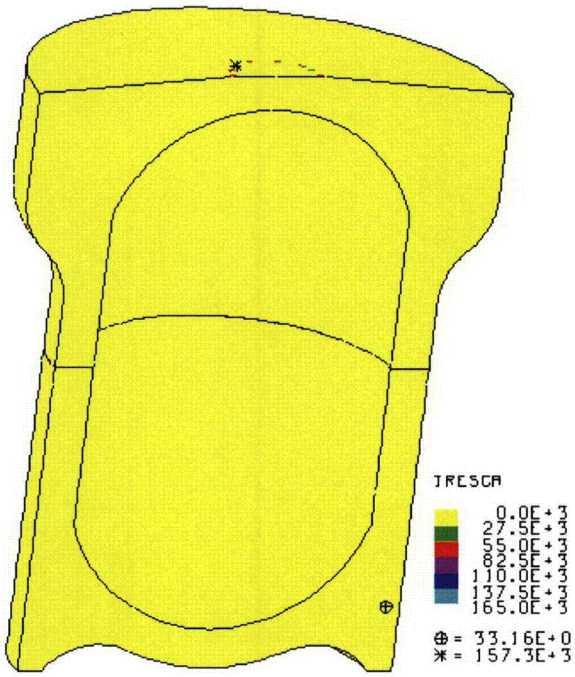

Figure 2-470. Plot of Tresca Stress in the TB-1 for HAC Run 18, 731 g Angled Plutonium Metal Hollow Cylinder, End Impact

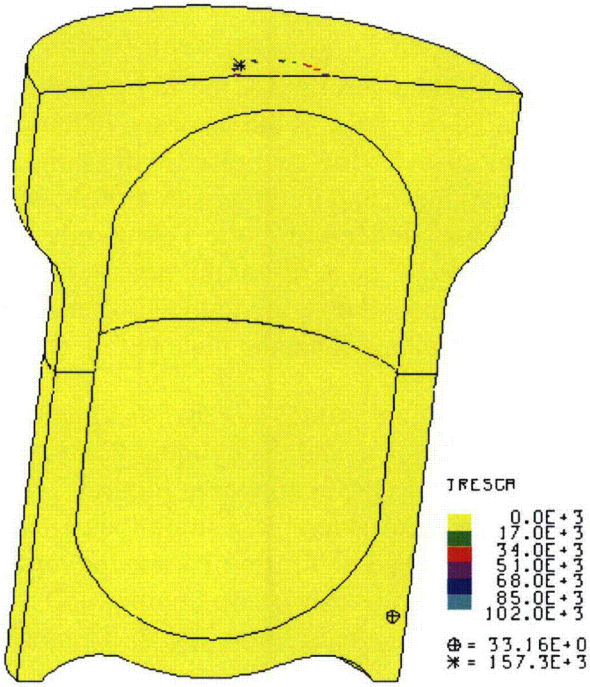

Figure 2-471. Plot of Tresca Stress in the TB-1 for HAC Run 18, 731 g Angled Plutonium Metal Hollow Cylinder, End Impact

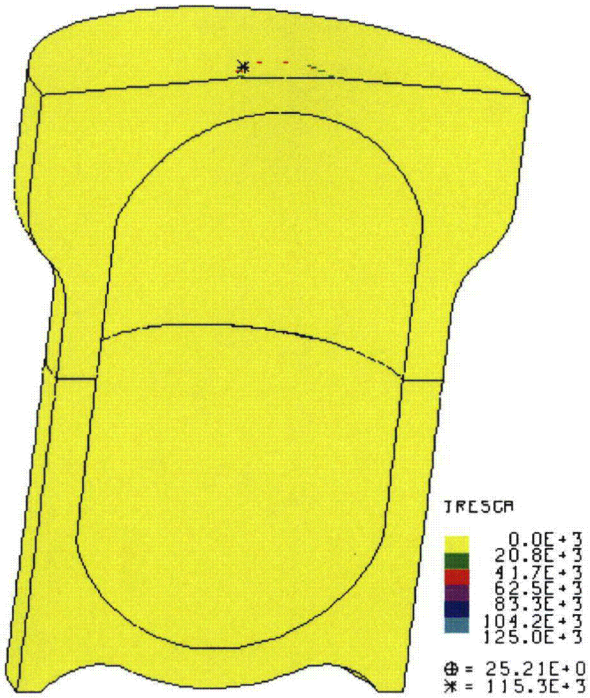

Figure 2-472. Plot of Tresca Stress in the TB-1 for HAC Run 18, 731 g Angled Plutonium Metal Hollow Cylinder, End Impact when Plate Velocity Reaches Zero

2.12.5.6.19 HAC- Run 19, 731 g Angled Plutonium Metal Hollow Cylinder, Side Impact

The dynamic crush side impact HAC analysis run for the 731 g angled plutonium metal hollow cylinder uses the same model for the overpack as the one used in the previous 18 runs. The TB-1, T-Ampoule, and plutonium metal hollow cylinder are the same model as that used in the aircraft analysis. The finite element mesh and initial position of the model are shown in Figure 2-473. The plutonium metal hollow cylinder within the T-Ampoule is positioned at the bottom of the model because it was considered to be at rest at the time of impact. The plate was positioned between the flanges to be most damaging to the TB-1 and contents by preventing the flanges from absorbing energy and slowing down the plate before it hits the overpack.

The post-impact deformation is shown in Figure 2-474 and its kinetic energy history in Figure 2-475. The flanges on the overpack deform, and the cylinder bounces due to the impact of the plate. Average stress-triaxiality versus EQPS is shown in Figures 2-476 and 2-477 for the elements extending beyond the tested Bao-Wierzbicki strain locus. These elements are at high stress triaxiality and low EQPS. The graph of Tearing Parameter versus EQPS for those elements extending beyond the strain locus is shown in Figure 2-478. The elements that exceeded the strain locus are highlighted in red Figure 2-479. The maximum Tearing Parameter value for this analysis was 5.092e-2, and is below the critical Tearing Parameter value of 1.012 for Ti-6Al-4V, thus T-Ampoule integrity is maintained.

Peak EQPS in the TB-1 vessel is shown in Figure 2-480 to be 0.1124, and is localized in the outer contact regions with the redwood overpack. Figures 2-481 and 2-482 plot the Tresca stresses within the TB-1. The maximum Tresca stress in the TB-1 is 201.7 ksi, but there are no through thickness stresses exceeding the limit of 106.6 ksi, which can be seen clearly in the

figures. Figure 2-483 is a plot of the Tresca stresses at the time when all of the kinetic energy of the plate has been transferred to the package, just as the plate begins to rebound. The maximum through thickness stress at this time is below 33.3 ksi, below the allowable through thickness stress of 106.6 ksi, as seen in the figure.

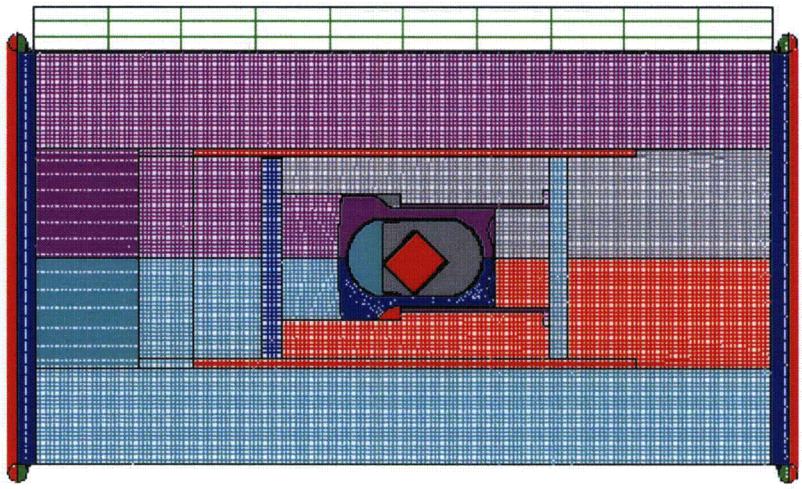

Figure 2-473. Finite Element Mesh for HAC Run 19, 731 g Angled Plutonium Metal Hollow Cylinder, Side Impact

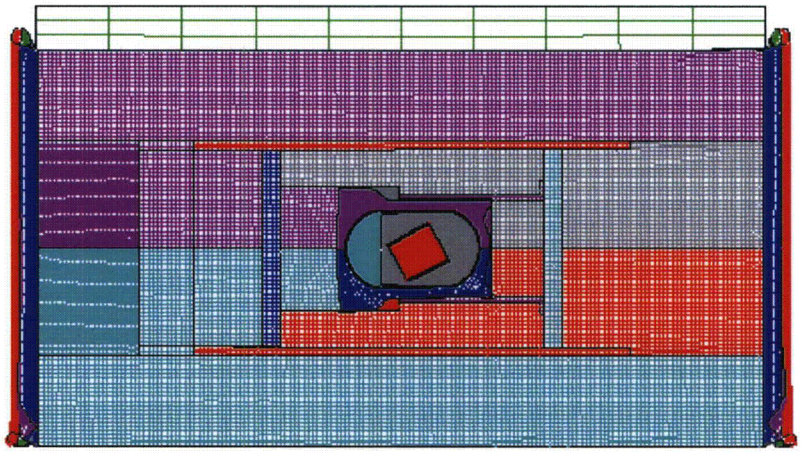

Figure 2-474. Finite Element Mesh for HAC Run 19, 731 g Angled Plutonium Metal Hollow Cylinder, Side Impact – Final Displacement

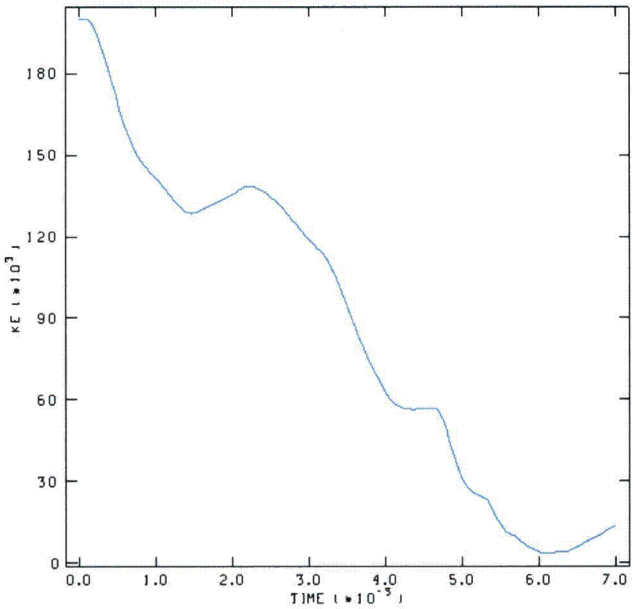

Figure 2-475. Kinetic Energy Time History for HAC Run 19, 731 g Angled Plutonium Metal Hollow Cylinder, Side Impact

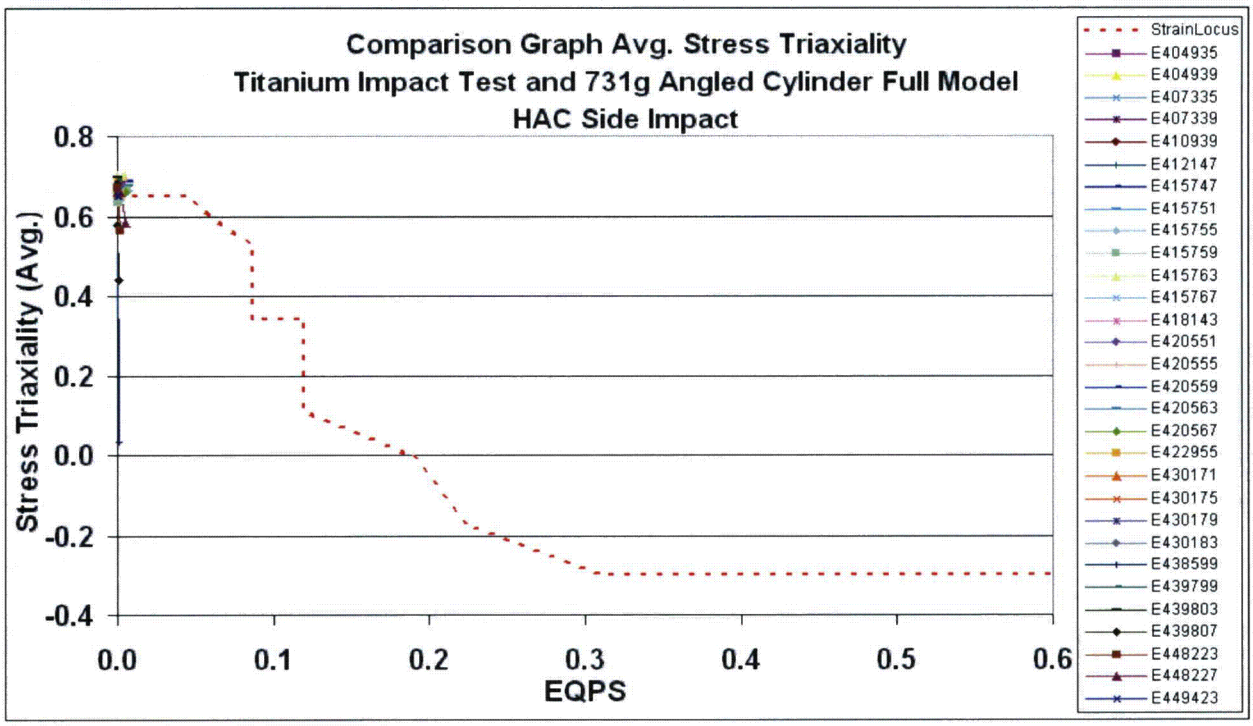

Figure 2-476. Graph of Average Stress Triaxiality versus EQPS for Elements Exceeding the Experimental Strain Locus for HAC Run 19, 731 g Angled Plutonium Metal Hollow Cylinder, Side Impact

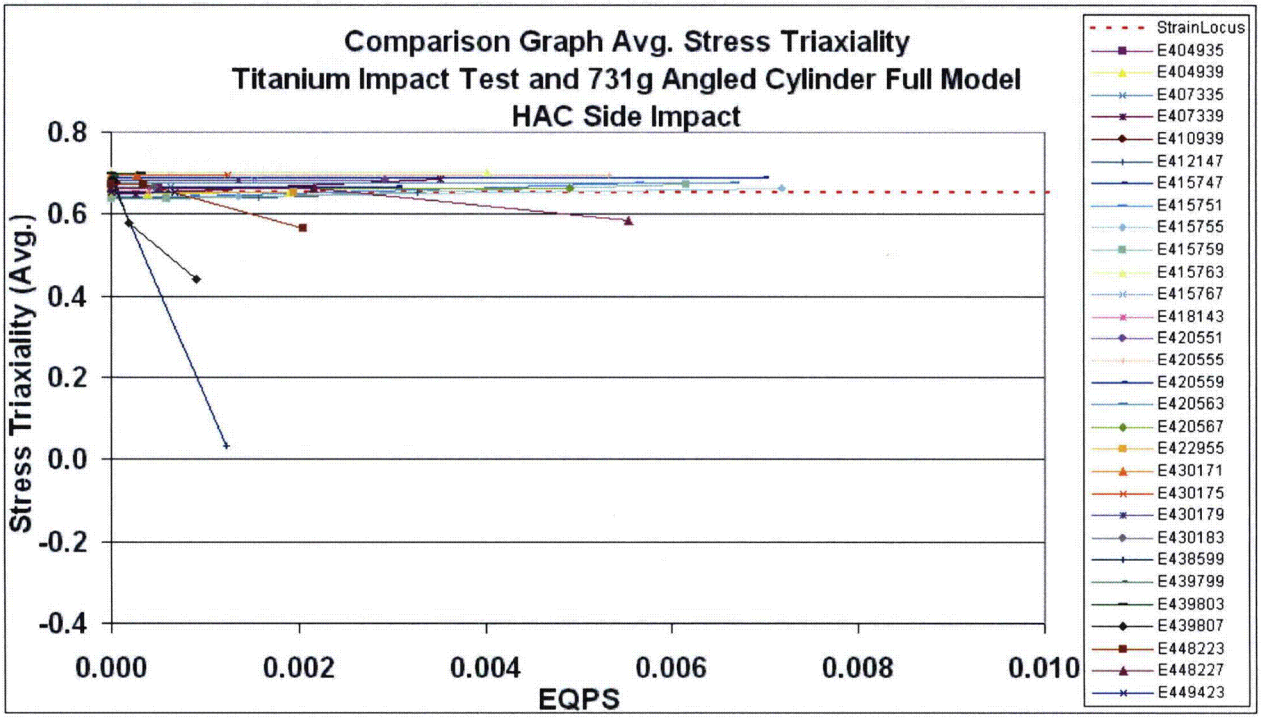

Figure 2-477. Graph of Average Stress Triaxiality versus EQPS for Elements Exceeding the Experimental Strain Locus (Zoomed In) for HAC Run 19, 731 g Angled Plutonium Metal Hollow Cylinder, Side Impact

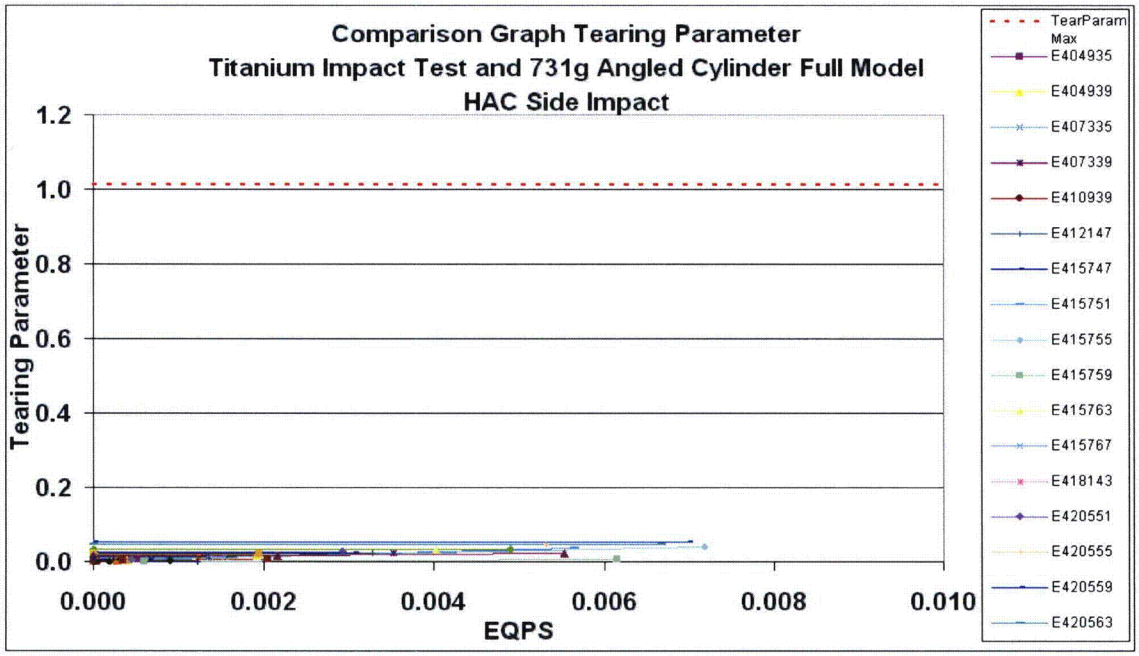

Figure 2-478. Graph of Tearing Parameter versus EQPS for Elements Exceeding the Experimental Strain Locus for HAC Run 19, 731 g Angled Plutonium Metal Hollow Cylinder, Side Impact

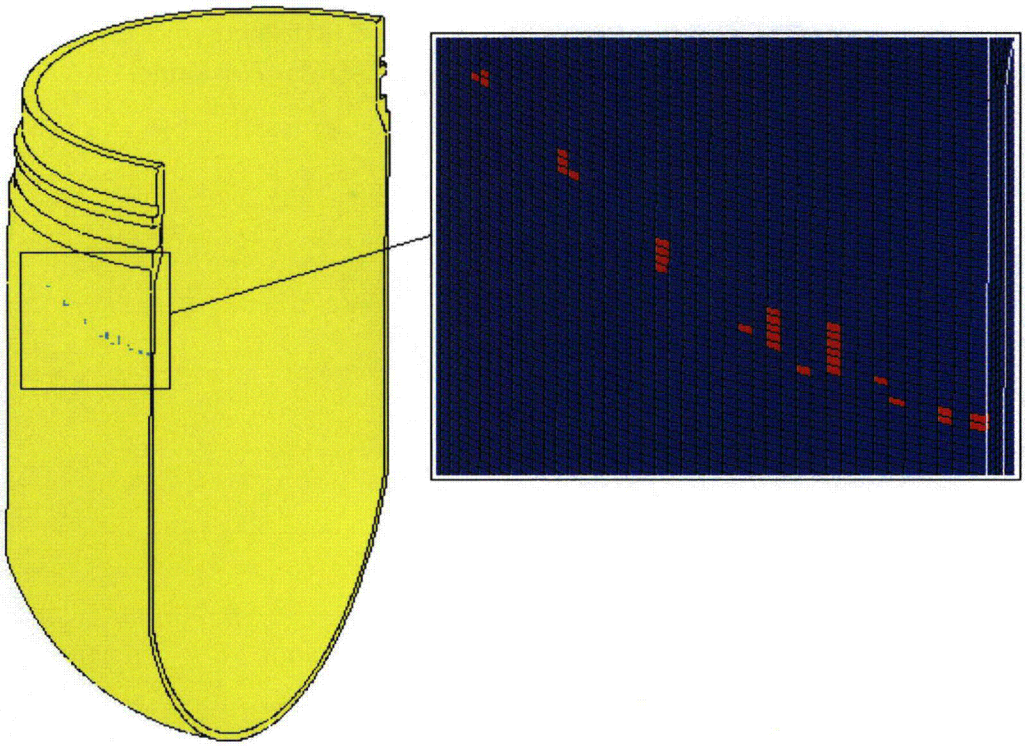

Figure 2-479. Plot of Elements Exceeding the Experimental Strain Locus for HAC Run 19, 731 g Angled Plutonium Metal Hollow Cylinder, Side Impact

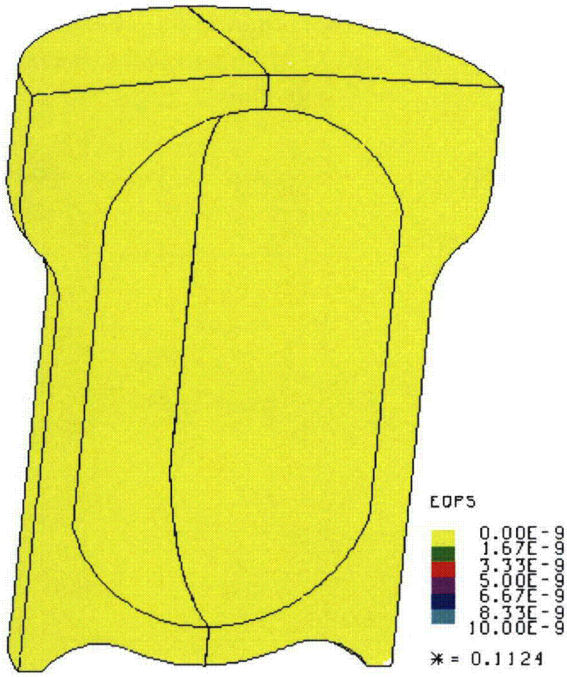

Figure 2-480. Plot of EQPS in the TB-1 for HAC Run 19, 731 g Angled Plutonium Metal Hollow Cylinder, Side Impact

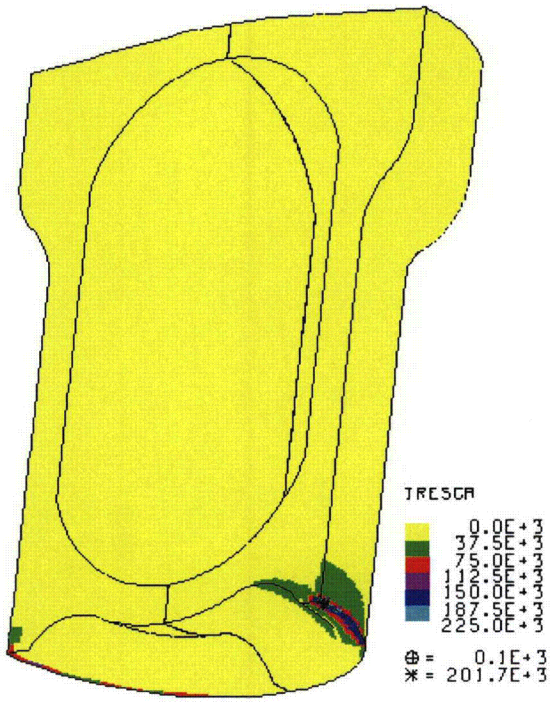

Figure 2-481. Plot of Tresca Stress in the TB-1 for HAC Run 19, 731 g Angled Plutonium Metal Hollow Cylinder, Side Impact

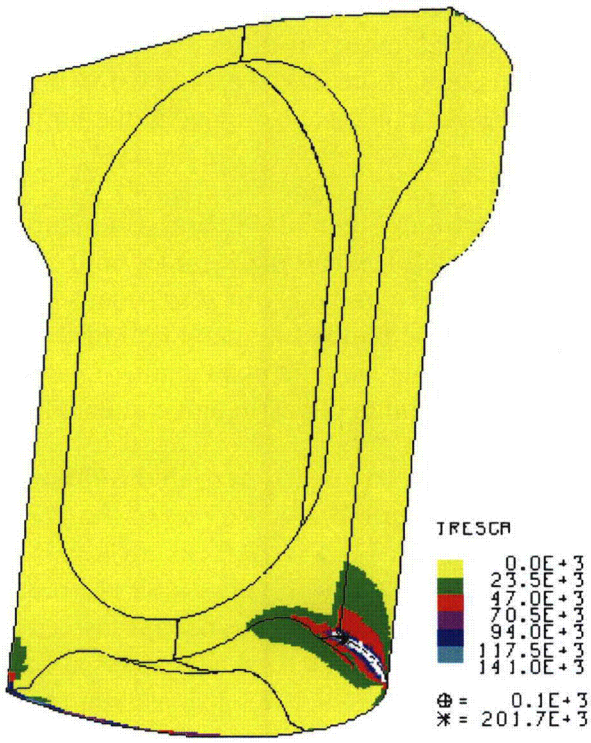

Figure 2-482. Plot of Tresca Stress in the TB-1 for HAC Run 19, 731 g Angled Plutonium Metal Hollow Cylinder, Side Impact

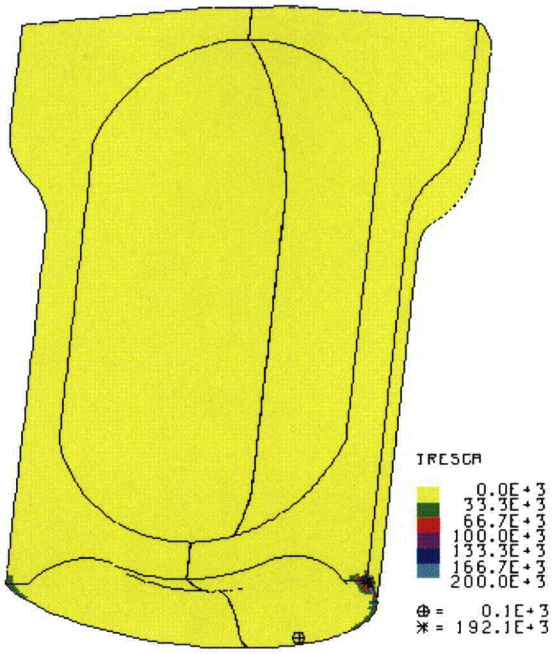

Figure 2-483. Plot of Tresca Stress in the TB-1 for HAC Run 19, 731 g Angled Plutonium Metal Hollow Cylinder, Side Impact when Plate Velocity Reaches Zero

2.12.5.6.20 HAC- Run 20, 731 g Angled Plutonium Metal Hollow Cylinder, CGOC Impact

The dynamic crush CGOC impact HAC analysis run for the 731 g angled plutonium metal hollow cylinder uses the same overpack model as those used in HAC runs 1 through 19. The finite element mesh and initial position of the model are shown in Figure 2-484. The plutonium metal hollow cylinder within the T-Ampoule is positioned at the bottom of the model because it was considered to be at rest.

The post-impact deformation is shown in Figure 2-485 and its kinetic energy history in Figure 2-486. The flanges on the overpack deform, and the cylinder bounces due to the impact of the plate. The kinetic energy does not drop completely to zero because the plate is still vibrating and internal contents are still in motion. The plutonium metal hollow cylinder has bounced off of the top and bottom surface of the T-Ampoule, and the plate is now rebounding slowly with the package, ensuring that the highest containment vessel and contents loadings have occurred.

There was zero EQPS in the T-Ampoule and nearly zero in the TB-1 (see Figure 2-487), and the maximum Tearing Parameter was 0. Figure 2-488 is a plot of the Tresca stresses within the TB-1. The maximum Tresca stress in the TB-1 is 70.57 ksi, which is below the maximum through thickness allowable stress of 106.6 ksi. Figure 2-489 is a plot of the Tresca stresses at the time when all of the kinetic energy of the plate has been transferred to the package, just as the plate begins to rebound. The maximum through thickness stress at this time is below 16.7 ksi, below the allowable through thickness stress of 106.6 ksi, as seen in the figure.

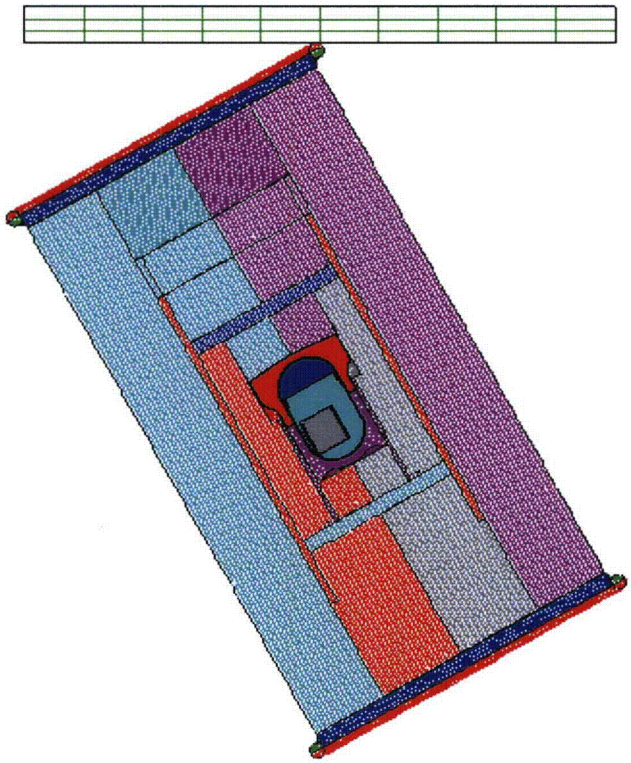

Figure 2-484. Finite Element Mesh for HAC Run 20, 731 g Angled Plutonium Metal Hollow Cylinder, CGOC Impact

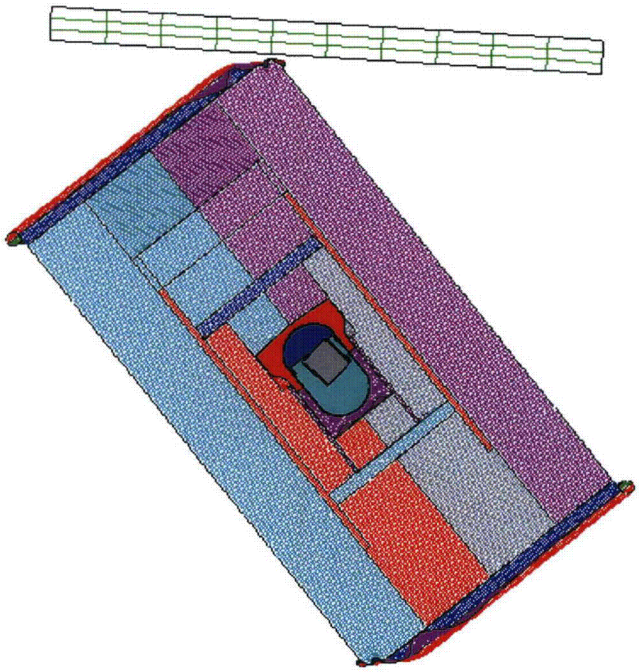

Figure 2-485. Finite Element Mesh for HAC Run 20, 731 g Angled Plutonium Metal Hollow Cylinder, CGOC Impact – Final Displacement

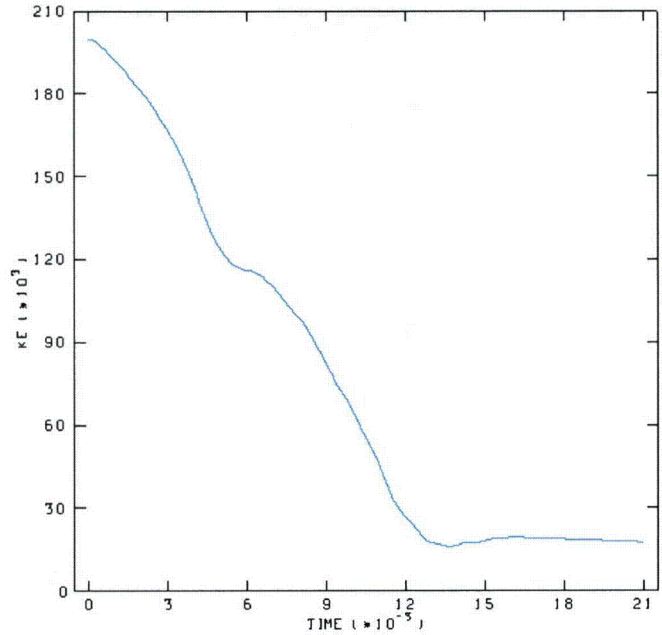

Figure 2-486. Kinetic Energy Time History for HAC Run 20, 731 g Angled Plutonium Metal Hollow Cylinder, CGOC Impact

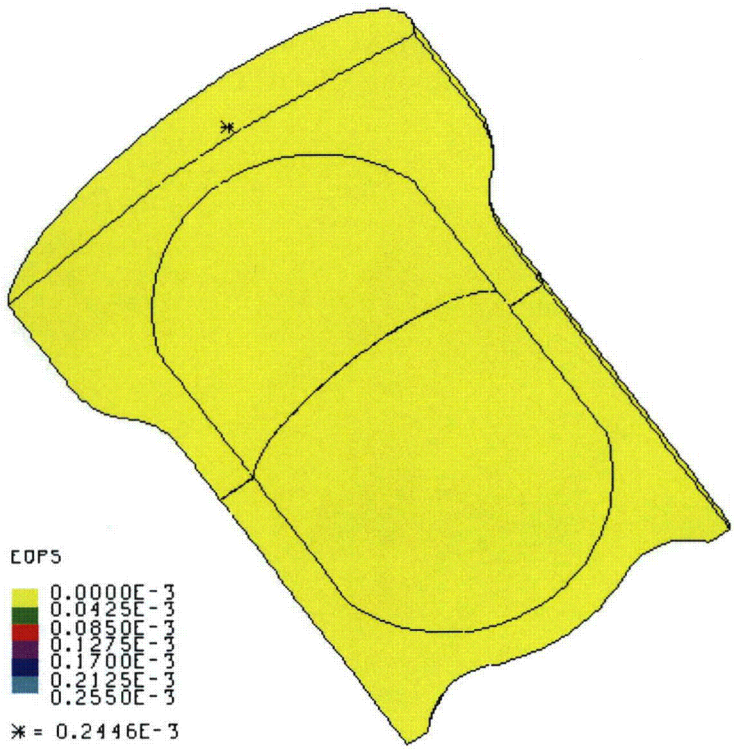

Figure 2-487. Plot of EQPS in the TB-1 for HAC Run 20, 731 g Angled Plutonium Metal Hollow Cylinder, CGOC Impact

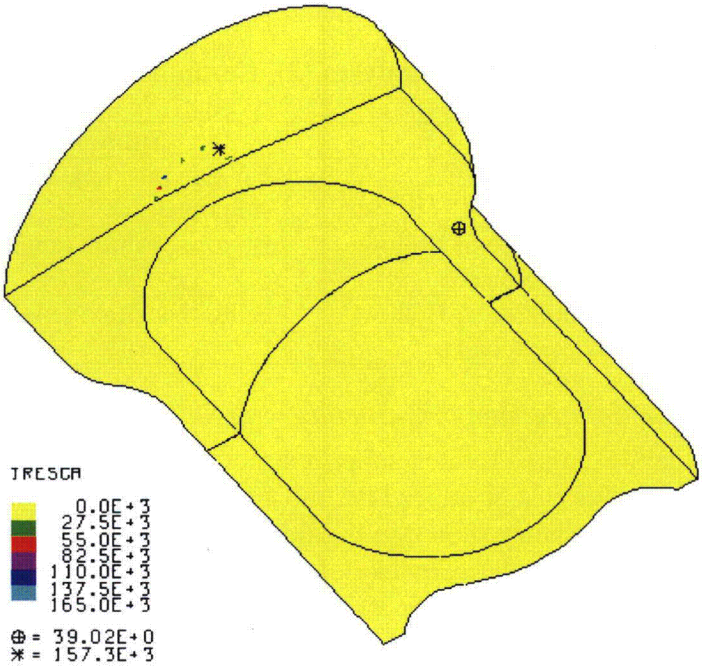

Figure 2-488. Plot of Tresca Stress in the TB-1 for HAC Run 20, 731 g Angled Plutonium Metal Hollow Cylinder, CGOC Impact

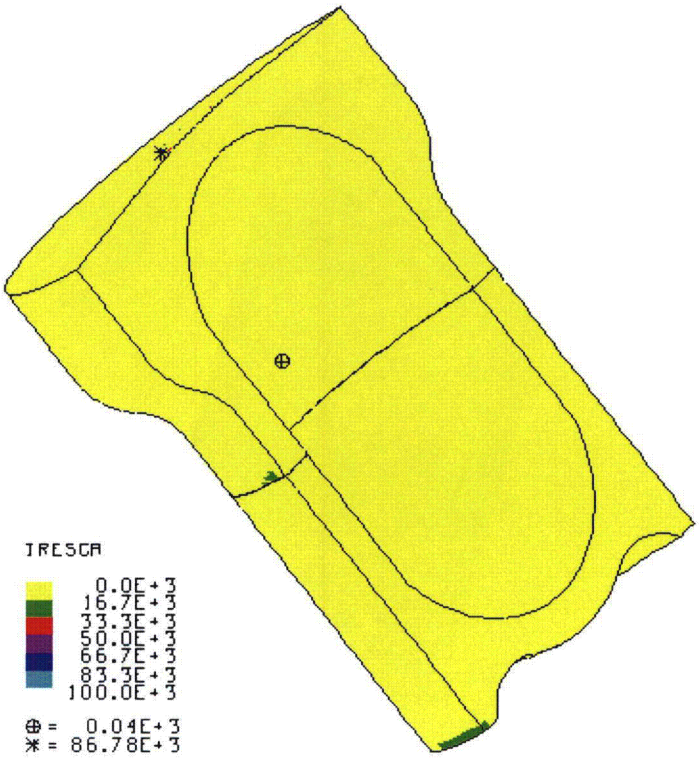

Figure 2-489. Plot of Tresca Stress in the TB-1 for HAC Run 20, 731 g Angled Plutonium Metal Hollow Cylinder, CGOC Impact when Plate Velocity Reaches Zero

2.12.5.7 30-foot Drop Analyses

Table 2-21. 30-ft Drop Impact Analyses (3), Components, and Orientations

Run No.	Component	Submodel Orientation
1	SC-2 - Pu	Far side position, support structure 45°, side impact
2	831 g Plutonium Metal Hollow Cylinder, alpha Pu	Bottom position (angled), top impact
3	831 g Plutonium Metal Hollow Cylinder, alpha Pu	Bottom position (angled), CGOC impact

2.12.5.7.1 SC-2 45 Degree Rotated Support Structure with Side Impact

The two-sample-container 45-degree rotated support structure contents was used for the 30-ft drop with side impact since this case produced the most severe loading of the aircraft side impacts. Pre-impact model geometry shown in Figure 2-490, and the final displacement shown in Figure 2-491. Note that the overall overpack deformation (rolled outer skin end closures, and slight denting of redwood) resulting from the 30-ft side impact analysis (half-symmetric model) compares well with the test result documented in the SAR,[1] shown in Figure 2-492. The kinetic energy history is shown in Figure 2-493 to verify that the analysis ran through the time of rebound. The negligible 0.26% equivalent plastic strain in the T-Ampoule eutectic boundary is shown in Figure 2-494. There were no T-Ampoule elements exceeding the experimental strain locus. Tresca stress in the TB-1 is shown in Figure 2-495, with through-thickness values below even the NCT allowables from Table 2-4.

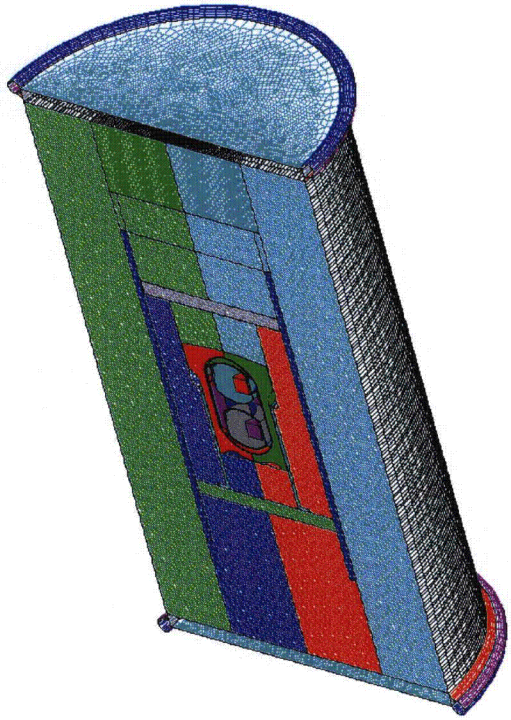

Figure 2-490. Finite Element Mesh for 30-ft Drop Run 1 – SC-2 with Support Structure Rotated 45 Degrees and Side Impact

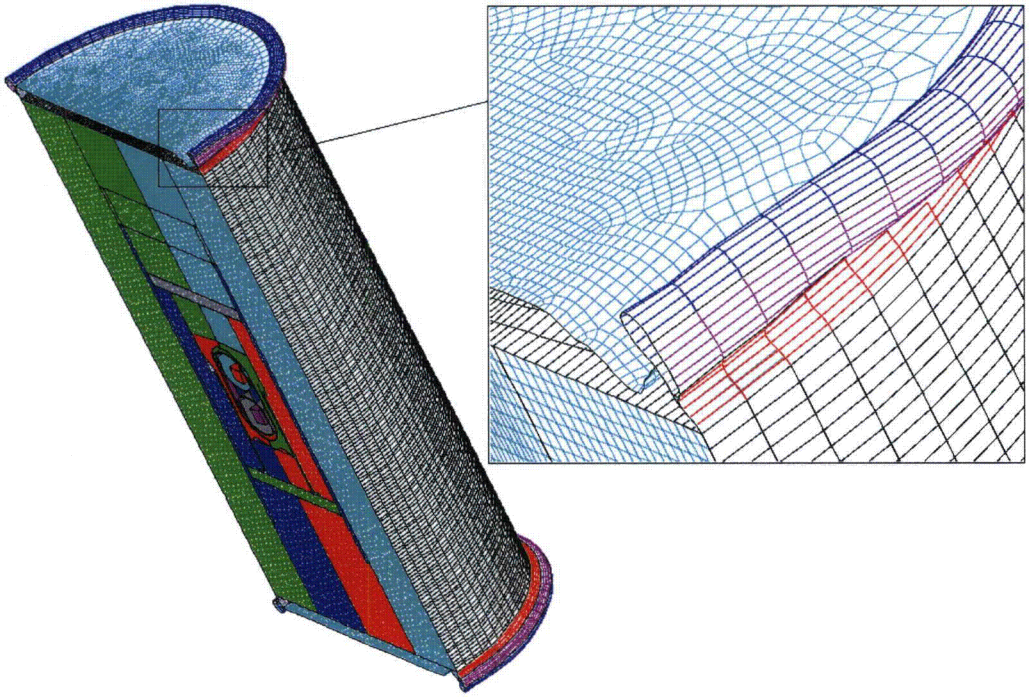

Figure 2-491. Final Displacement in Finite Element Mesh for 30-ft Drop Run 1 – SC-2 with Support Structure Rotated 45 Degrees and Side Impact

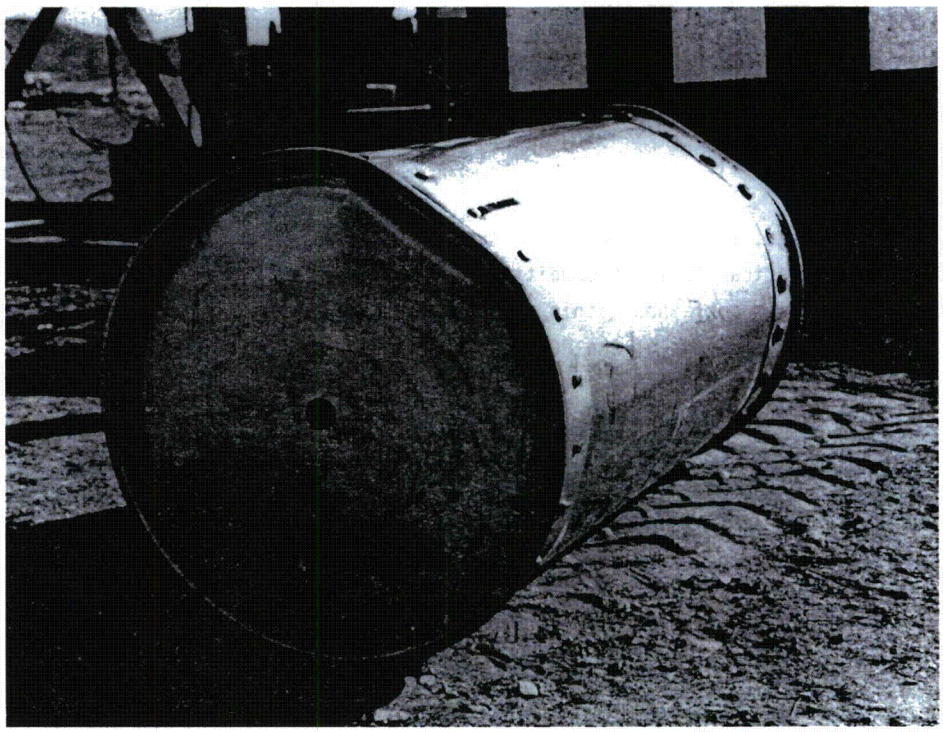

Figure 2-492. Final Displacement in SAR[1] Test for 30-ft Drop

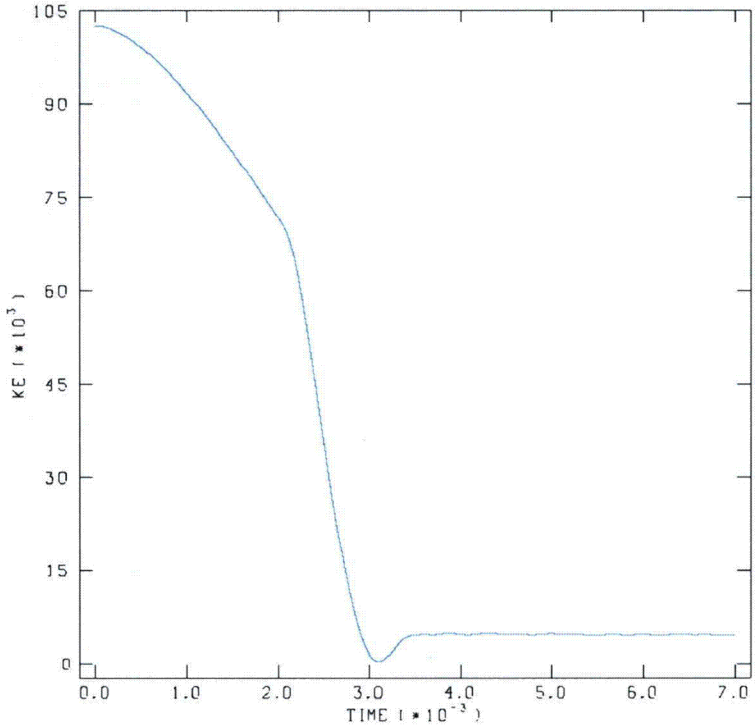

Figure 2-493. Kinetic Energy for 30-ft Drop Run 1 – SC-2 with Support Structure Rotated 45 Degrees and Side Impact

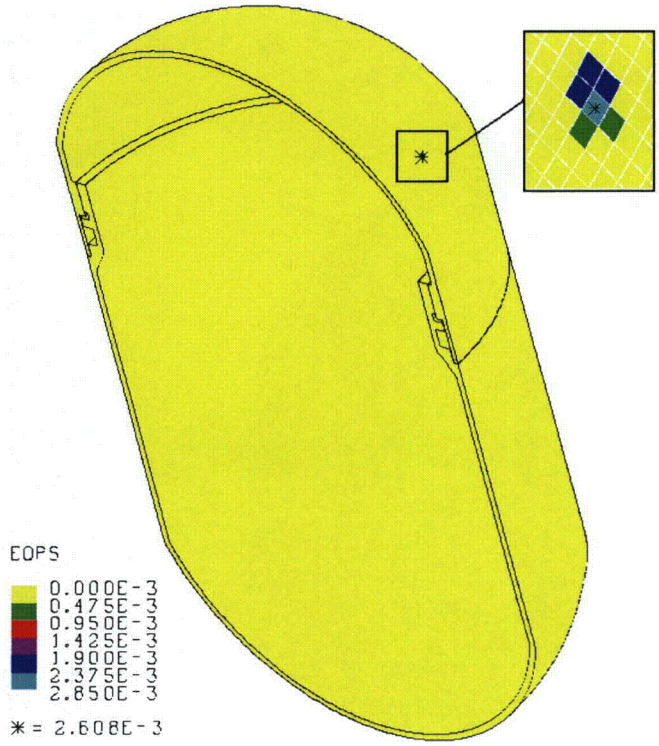

Figure 2-494. EQPS in the T-Amp for 30-ft Drop Run 1 – SC-2 with Support Structure Rotated 45 Degrees and Side Impact

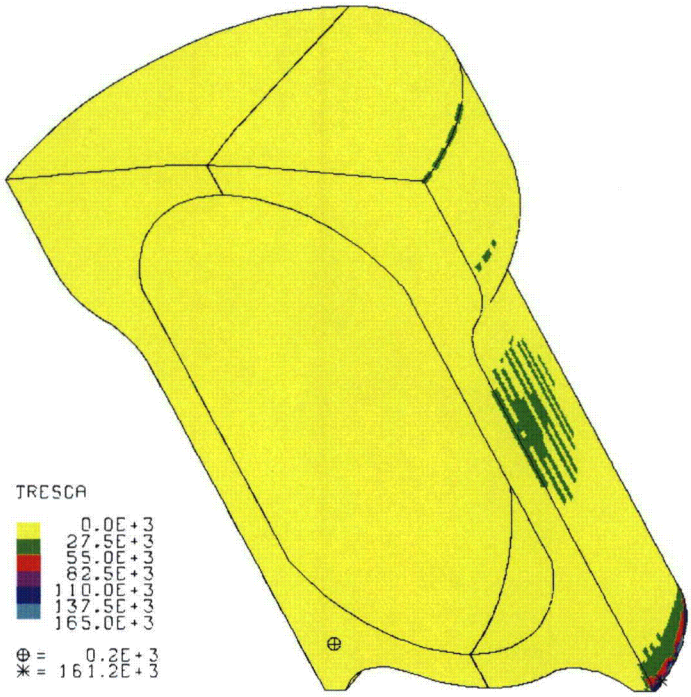

Figure 2-495. Tresca Stress in the TB-1 for 30-ft Drop Run 1 – SC-2 with Support Structure Rotated 45 Degrees and Side Impact

2.12.5.7.2 831g Plutonium Metal Hollow Cylinder Angled with End Impact

The 831g plutonium metal hollow cylinder contents was used for the 30-ft drop with end impact since this case produced one of the most severe loadings of the aircraft end impacts. Pre-impact model geometry shown in Figure 2-496, and the final displacement shown in Figure 2-497. The kinetic energy history is shown in Figure 2-498 to verify that the analysis ran through the time of rebound. The T-Ampoule equivalent plastic strain was zero, and there were no T-Ampoule elements exceeding the experimental strain locus. The negligible 0.255% equivalent plastic strain in the localized outer surface of the TB-1 (due to a minor contact modeling artifact) is shown in Figure 2-499. Tresca stress in the TB-1 is shown in Figure 2-500, with through-thickness values below even the NCT allowables from Table 2-4.

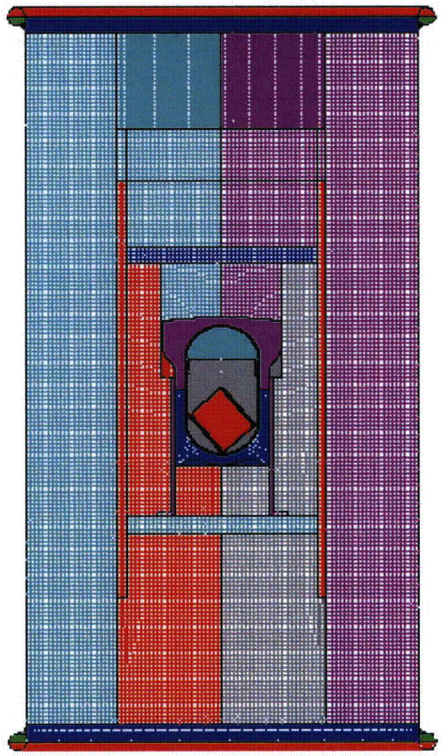

Figure 2-496. Finite Element Mesh for 30-ft Drop Run 2 – Angled 831 g Plutonium Metal Hollow Cylinder with End Impact

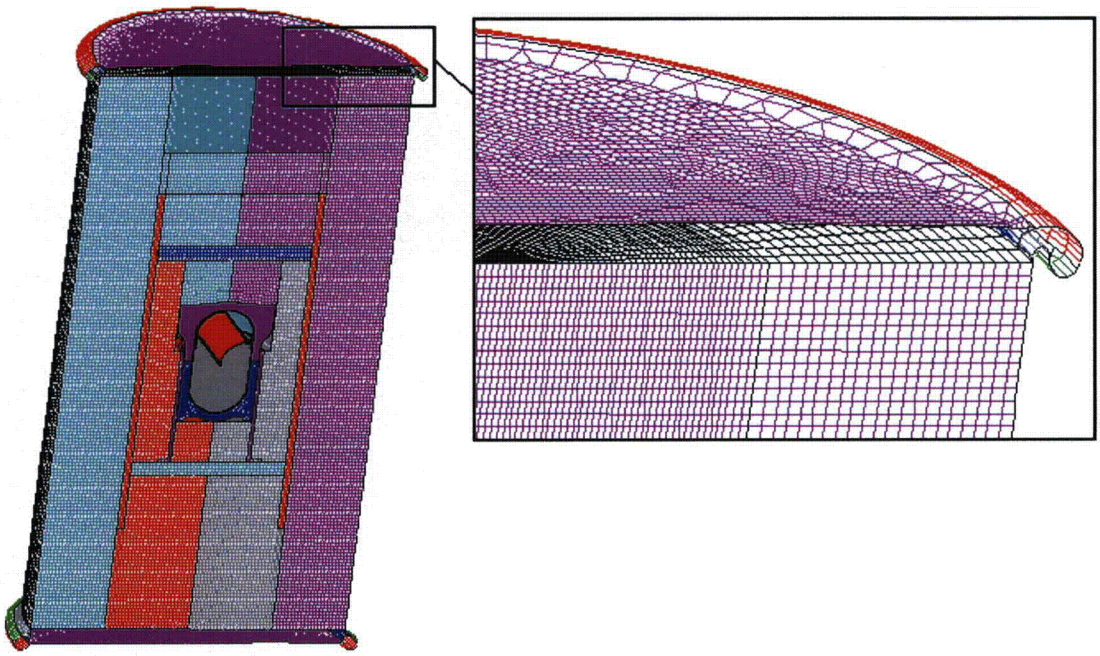

Figure 2-497. Final Displacement for 30-ft Drop Run 2 – Angled 831 g Plutonium Metal Hollow Cylinder with End Impact

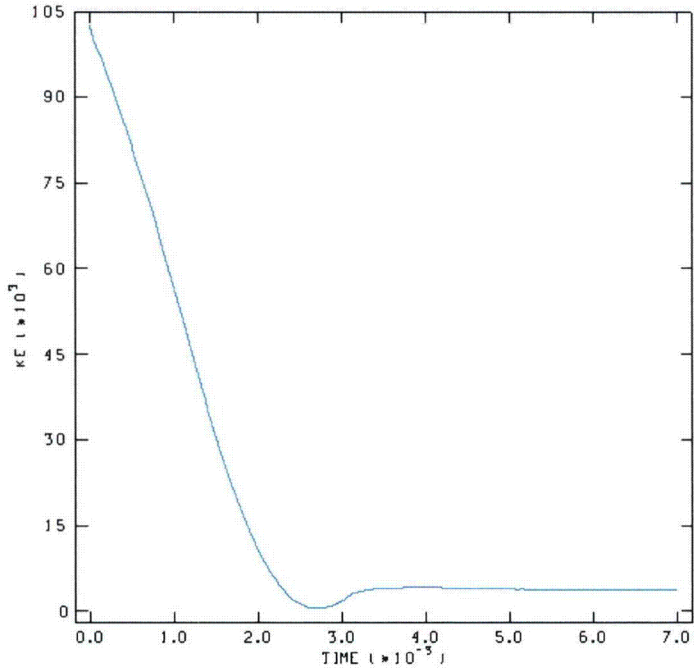

Figure 2-498. Kinetic Energy for 30-ft Drop Run 2 – Angled 831 g Plutonium Metal Hollow Cylinder with End Impact

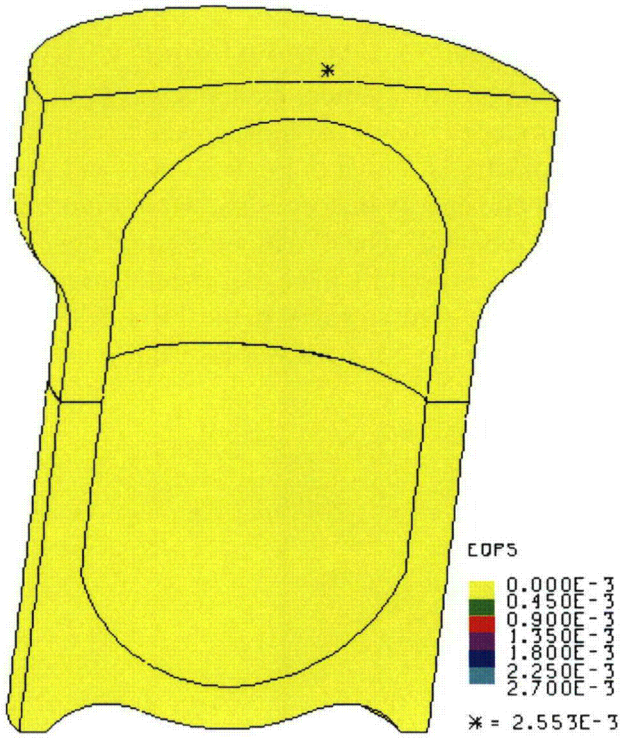

Figure 2-499. EQPS in TB-1 for 30-ft Drop Run 2 – Angled 831 g Plutonium Metal Hollow Cylinder with End Impact

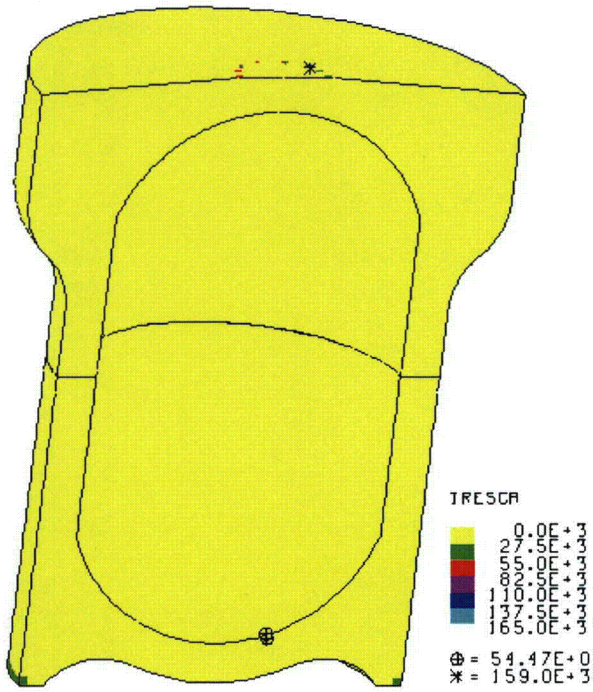

Figure 2-500. Tresca Stress in the TB-1 for 30-ft Drop Run 2 – Angled 831 g Plutonium Metal Hollow Cylinder with End Impact

2.12.5.7.3 831g Plutonium Metal Hollow Cylinder Angled with CGOC Impact

The angled 831g plutonium metal hollow cylinder contents was used for the 30-ft drop with corner impact since this case produced one of the most severe loadings of the aircraft CGOC impacts. Pre-impact model geometry is shown in Figure 2-501, and the final displacement shown in Figure 2-502. The kinetic energy history is shown in Figure 2-503 to verify that the analysis ran through the time of rebound. The T-Ampoule equivalent plastic strain was zero, and there were no T-Ampoule elements exceeding the experimental strain locus. There was zero equivalent plastic strain in the TB-1. Tresca stress in the TB-1 is shown in Figure 2-504, with through-thickness values below even the NCT allowables from Table 2-4.

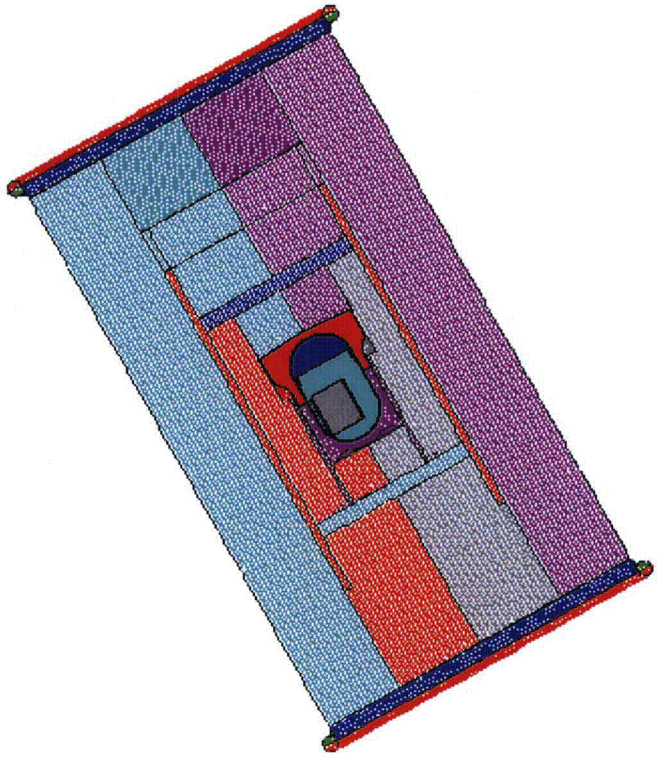

Figure 2-501. Finite Element Mesh for 30-ft Drop Run 3 – Angled 831 g Plutonium Metal Hollow Cylinder with CGOC Impact

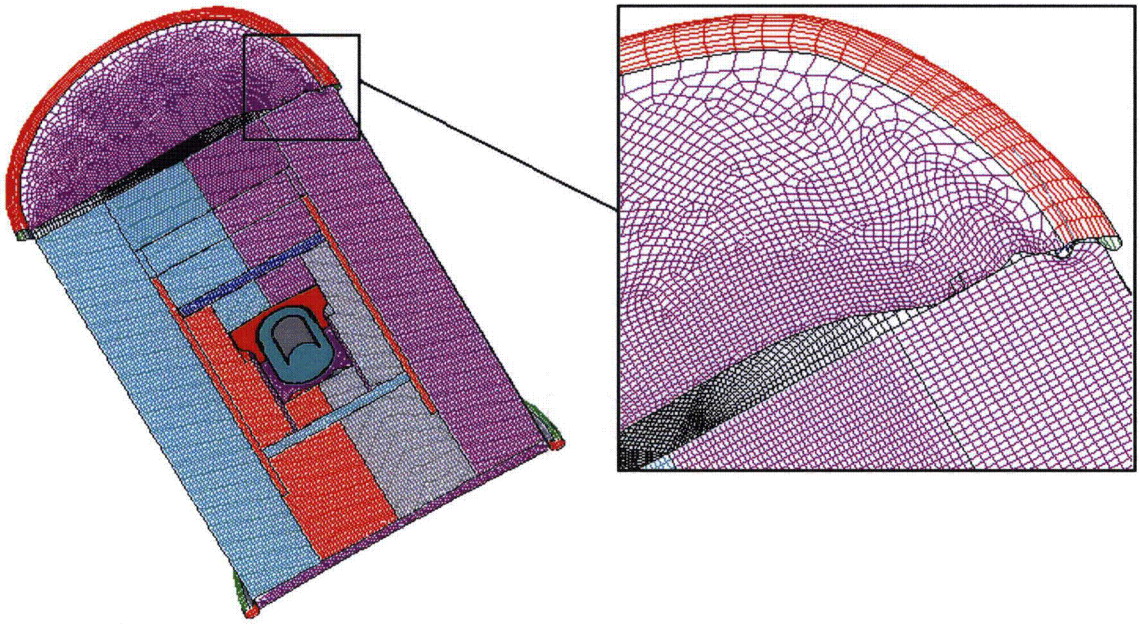

Figure 2-502. Final Displacement for 30-ft Drop Run 3 – Angled 831 g Plutonium Metal Hollow Cylinder with CGOC Impact

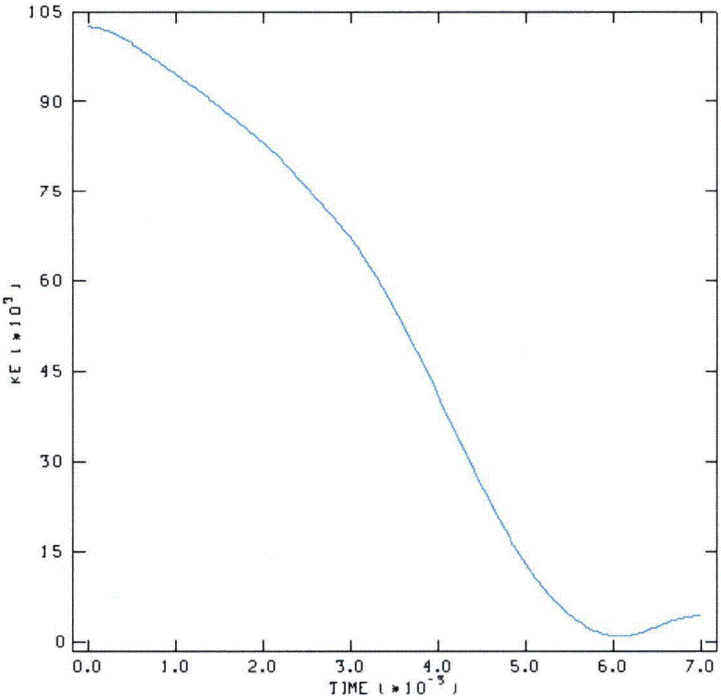

Figure 2-503. Kinetic Energy for 30-ft Drop Run 3 – Angled 831 g Plutonium Metal Hollow Cylinder with CGOC Impact

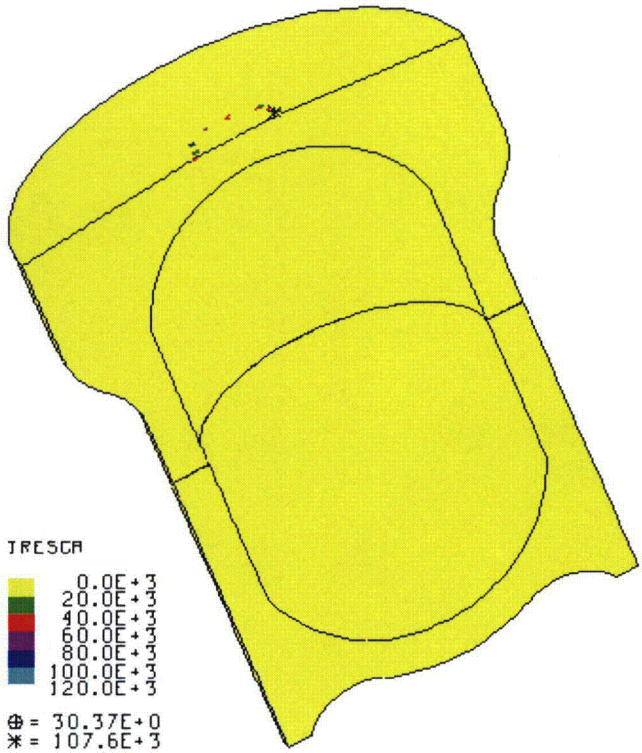

Figure 2-504. Tresca Stress in the TB-1 for 30-ft Drop Run 3 – Angled 831 g Plutonium Metal Hollow Cylinder with CGOC Impact

2.12.5.8 References

1. USNRC, NUREG-0361. Safety Analysis Report for the Plutonium Air Transportable Package, Model PAT-1. Washington, D.C. 1978.

2. EGR-Materials and Aerospace Corporation. "Compression Testing of DUOCEL C10100 Copper Alloy Foam." Report 11565. Oakland, CA. 2007.

3. Hecker, Siegfried S. and Michael F. Stevens. "Mechanical Behavior of Plutonium and Its Alloys." *Los Alamos Science* Number 26 (2000).

4. Wellman, G.W., Diegert, K.V., and Saizbrenner, R. "Two-Dimensional Quasistatic Modeling of Exclusion Region Barriers in Support of Design Guide Development." SAND93-0905. Sandia National Laboratories. Albuquerque, NM. 1993.

5. Bao, Y., and T. Wierzbicki. "On the Cut-Off Value of Negative Triaxiality for Fracture." Engineering Fracture Mechanics, 72, pp. 1049-1069, 2005..

6. Johnson, G.R., and Cook, W.H., "Fracture Characteristics of Three Metals Subjected to Various Strains, Strain Rates, Temperature and Pressures." *Engineering Fracture Mechanics* **21** (1985):31-48.

7. Bao, Y. "Prediction of Ductile Crack Formation in Uncracked Bodies," Report 100. Impact & Crash Worthiness Laboratory, Massachusetts Institute of Technology. Cambridge, MA. 2003.

8. Ame*rican Society of Mechanical Eng*ineers (ASME). "Boiler and Pressure Vessel Code," 2008a, Section II, Part D, Table 2A: Design Stress Intensity Values S_m for Ferrous Materials. pp. 298. 2008.

9. American Society of Mechanical Engineers (ASME). "Boiler and Pressure Vessel Code," Section III, Division 1--Appendices, Nonmandatory Appendix F: Article F-1000, Rules for Evaluation of Service Loadings with Level D Service Limits. pp. 232. 2007.

2.12.6 Bolt Analysis

The following section is an analysis of the bolts that secure the TB-1 lid when subjected to the loads applied during the high-speed aircraft accident test condition (10 CFR 71.74). The impulse loads are obtained from the component analyses (see Section 2.12.5).

The TB-1 lid is secured by (12) ½ -20 UNJF-3A bolts. The following calculation shows that the total bolt preload is approximately 108,000 lbs.

$$\text{Bolt torque}: T = 75 \text{ ft - lbs}$$

$$\text{Nominal bolt diameter } d = 0.5 \text{ in}$$

$$\text{Friction coefficient}: K = 0.2$$

$$\text{Shigley}^{1}\text{Boltforce}: F_i = \frac{T}{Kd}$$

$$Fi = \frac{900}{(0.2)(0.5)} = 9000 \text{ lbf}$$

$$(12 \text{ bolts}) \times 9000 = 108{,}000 \text{ lbf}$$

The contact force of the redwood pushing on the top of the TB-1 to decelerate it is shown as the dashed curve in Figure 2-505. The bolt preload is also shown along with the sum of the contact force and the total bolt preload. These are the forces holding the lid in place during the end impact event.

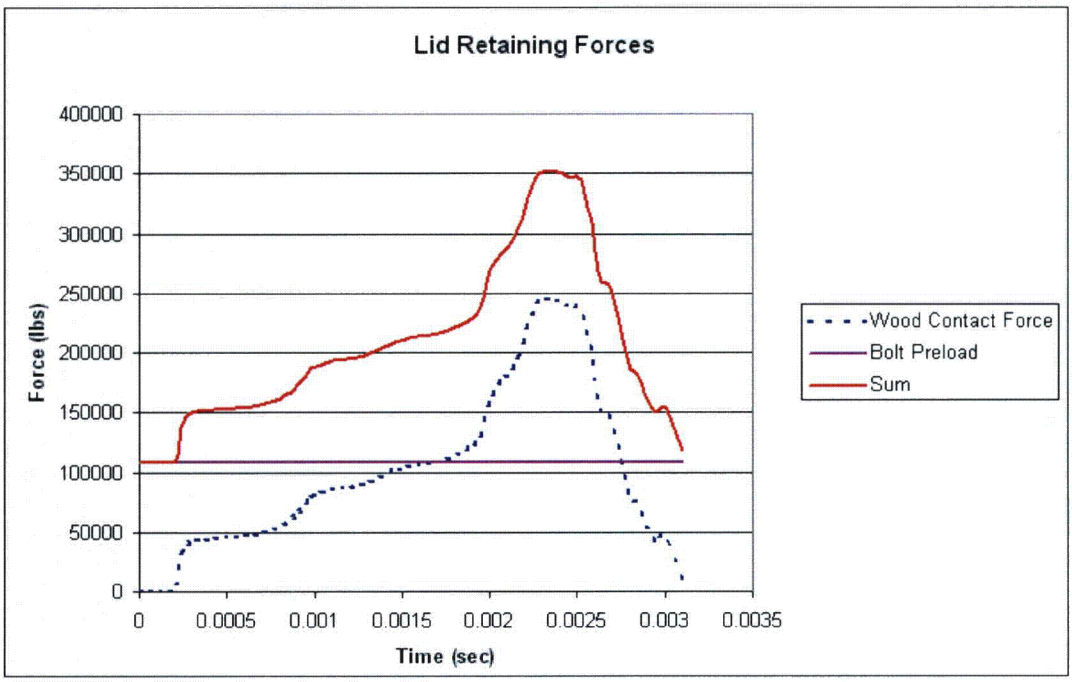

Figure 2-505. Contact Forces on the Top Surface of the TB-1 Lid

The force generated by the impacting components calculated in Section 2.12.5 along with the redwood contact force and bolt preload are shown in Figure 2-506. As shown in the figure, the forces from the components are only a fraction of the bolt preload. The peak impulse load is a factor of 2.1 less than the bolt preload and a factor of 6 less than the total of the sum of the wood retaining force and the bolt preload. Therefore, the lid of the TB-1 will remain tight and torqued during the aircraft impact accident.

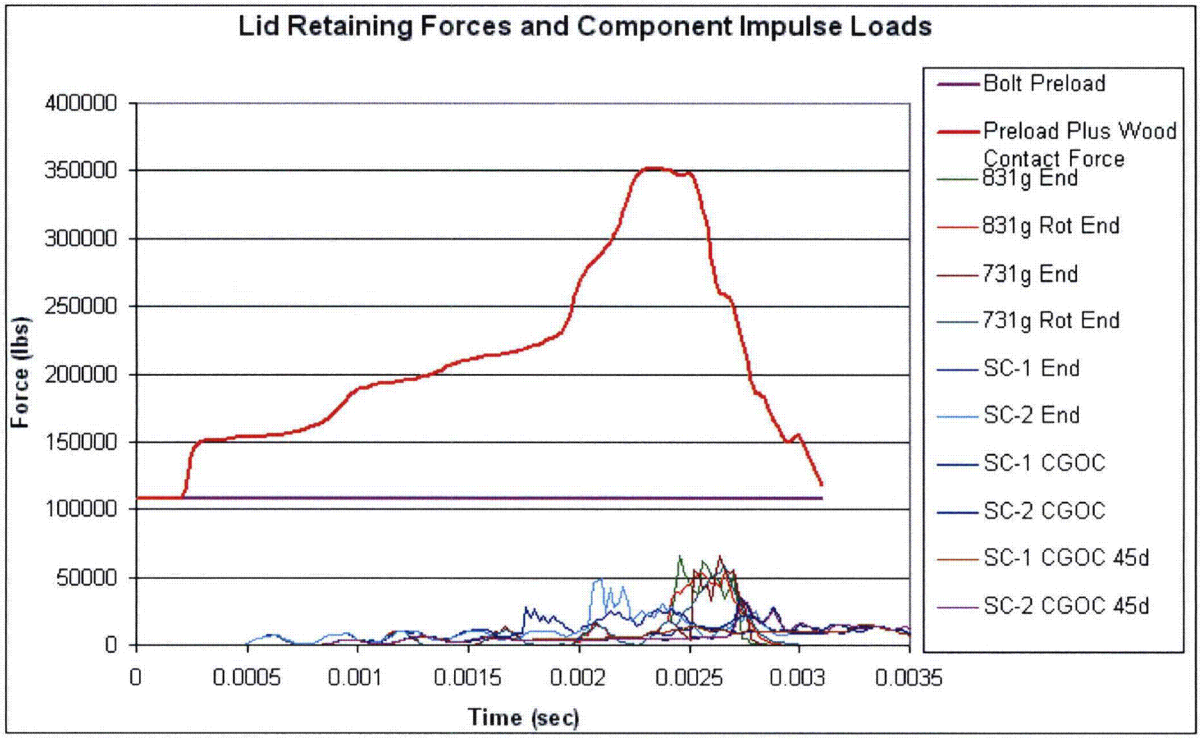

Figure 2-506. Contact Forces on the Top Surface of the TB-1 Lid Along with Impulse Loads from Various Contents

2.12.6.1 References

1. Shigley, J. E. *Mechanical Engineering Design*. McGraw-Hill, 1977.

2.12.7 Sample Input

The PRONTO3D input file for Run 3 of the high speed aircraft impact analysis (831 gram angled cylinder with CGOC impact) which resulted in the highest tearing parameter in the T-Ampoule is included below. Dollar signs designate comment lines.

```
TITLE
Full Overpack with TB1 with 831g cylinder top rot CGOC impact
$
TERM TIME,0.006
PLOT TIME,0.00003
PLOT NODAL,DISPLACEMENT, VELOCITY, ACCELERATION,reactions,force
PLOT ELEMENT, STRESS, VONMISES,DOPT, EPS
PLOT STATE, EQPS
SUM NODAL_MOMENTUMY MATERIAL 5
```

```
SUM CONTACT_FORCEY NODESET 500
SUM CONTACT_FORCEX NODESET 500
SUM CONTACT_FORCEZ NODESET 500
write restart .0005
$
$ symmetry boundary condition
$
$  no displ, y, 100
$  no displ, x, 100
  no displ, z, 100
  no displ, z, 101
$
$ hourglass control
$
$   assumed strain hourglass
    hourglass stiffening .08 .09
$
$ set up initial velocity
$
  initial velocity material 1   0.0  5064.0  0.0    $ cantop
  initial velocity material 2   0.0  5064.0  0.0    $ canbot
  initial velocity material 4   0.0  5064.0  0.0    $ TB-1 top
  initial velocity material 5   0.0  5064.0  0.0    $ PU cylinder (1)
  initial velocity material 6   0.0  5064.0  0.0    $ TB-1 bot
  initial velocity material 20  0.0  5064.0  0.0    $ spreader
  initial velocity material 21  0.0  5064.0  0.0    $ copper
  initial velocity material 22  0.0  5064.0  0.0    $ top plate 7075
  initial velocity material 23  0.0  5064.0  0.0    $ lower plate 7075
  initial velocity material 10  0.0  5064.0  0.0    $ shell
  initial velocity material 24  0.0  5064.0  0.0    $ wood 1 X
  initial velocity material 25  0.0  5064.0  0.0    $ wood 1 Z
  initial velocity material 26  0.0  5064.0  0.0    $ wood 1 X
  initial velocity material 27  0.0  5064.0  0.0    $ wood 2 X
  initial velocity material 28  0.0  5064.0  0.0    $ wood 2 Z
  initial velocity material 29  0.0  5064.0  0.0    $ wood 2 X
  initial velocity material 30  0.0  5064.0  0.0    $ wood 3 X
  initial velocity material 31  0.0  5064.0  0.0    $ wood 3 Z
  initial velocity material 32  0.0  5064.0  0.0    $ wood 3 X
  initial velocity material 33  0.0  5064.0  0.0    $ wood 4 X
  initial velocity material 34  0.0  5064.0  0.0    $ wood 4 Z
  initial velocity material 35  0.0  5064.0  0.0    $ wood 4 X
  initial velocity material 36  0.0  5064.0  0.0    $ wood 5 X
  initial velocity material 37  0.0  5064.0  0.0    $ wood 5 Z
  initial velocity material 38  0.0  5064.0  0.0    $ wood 5 X
  initial velocity material 39  0.0  5064.0  0.0    $ wood 6 X
  initial velocity material 40  0.0  5064.0  0.0    $ wood 6 Z
  initial velocity material 41  0.0  5064.0  0.0    $ wood 6 X
$
$ Death
$
$
$ set up contact by region for  model
$
  contact material 1
  contact material 2
  contact material 4
  contact material 5
```

```
  contact material 6
  contact material 20
  contact material 21
  contact material 22
  contact material 23
  contact material 24
  contact material 25
  contact material 26
  contact material 27
  contact material 28
  contact material 29
  contact material 30
  contact material 31
  contact material 32
  contact material 33
  contact material 34
  contact material 35
  contact material 36
  contact material 37
  contact material 38
  contact material 39
  contact material 40
  contact material 41
$ contact surfaces
  contact surface 30  $ mid tb1
  contact surface 31  $ mid tb1
  contact surface 800  $ top wood by pipe
  contact surface 801  $ top of pipe
$
$ define surface pairs
$
  contact data surface 800 surface 801 $
  kinematic partition 1.0
  friction static -1.0
  capture tolerance 0.005
  end
  contact data surface 30 surface 31 $
  kinematic partition 0.5
  friction static -1.0
  capture tolerance 0.005
  end
$
$ define friction
$
$ Top of Tamp and Cylinder
  contact data material 1 material 5
   kinematic partition 0.1
   friction static 0.36
   friction dynamic 0.3
  end
$ Bottom of Tamp and Cylinder
  contact data material 2 material 5
   kinematic partition 0.1
   friction static 0.36
   friction dynamic 0.3
  end
$
```

```
$ Rigid surface
$
 rigid surface 700 0.0 23.45 0.0 0.0 -1.0 0.0  $ top impact
$
$ define the shell thickness
$
  scale shell thickness 10 0.0625  $ can shell
$
$
$
$ define material properties
$
$
 MATERIAL, 1, ep power hardening, 0.000414, $  titanium
   YOUNGS MODULUS,       15.5E06
   POISSONS RATIO,        0.3
   YIELD STRESS,         141.7E03
   HARDENING constant,    12.6E04
   hardening exponent    0.6554
   luders strain         0.0
  END
 MATERIAL, 2, ep power hardening, 0.000414, $  titanium
   YOUNGS MODULUS,       15.5E06
   POISSONS RATIO,        0.3
   YIELD STRESS,         141.7E03
   HARDENING constant,    12.6E04
   hardening exponent    0.6554
   luders strain         0.0
  END
 Material, 4, ep power hardening, 0.00074, $  TB1 Top
   YOUNGS MODULUS,       30.E06
   POISSONS RATIO,        0.30
   YIELD STRESS,         141E03
   HARDENING constant,    30e4
   hardening exponent    1
   luders strain         0.0
  END
 MATERIAL, 5, ep power hardening, 0.001853, $  PU alpha phase 1
   YOUNGS MODULUS,       14.1E06
   POISSONS RATIO,        0.3
   YIELD STRESS,         36.0E03
   HARDENING constant,    85000
   hardening exponent    0.4
   luders strain         0.0
  END
 Material, 6, ep power hardening, 0.00074, $  TB1 Left
   YOUNGS MODULUS,       30.E06
   POISSONS RATIO,        0.30
   YIELD STRESS,         141E03
   HARDENING constant,    30e4
   hardening exponent    1
   luders strain         0.0
  END
 MATERIAL, 10, ep power hardening, 0.00074, $  304 stainless shell
   YOUNGS MODULUS,       28.E6
   POISSONS RATIO,        0.27
   YIELD STRESS,         40.E3
```

```
   HARDENING constant,    192746.
   hardening exponent    0.748190
   luders strain         0.0
  END
 MATERIAL, 20, ep power hardening, 0.0002536, $  6061
   YOUNGS MODULUS,       9.9E06
   POISSONS RATIO,        0.3
   YIELD STRESS,         45.0E03
   HARDENING constant,    37852
   hardening exponent    0.55
   luders strain         0.0
  END
 MATERIAL, 21, ep power hardening, 0.000414, $  copper
   YOUNGS MODULUS,       17.2E06
   POISSONS RATIO,        0.33
   YIELD STRESS,         45.0E03
   HARDENING constant,    38000
   hardening exponent    0.55
   luders strain         0.0
  END
 MATERIAL, 22, ep power hardening, 0.000264, $  7075
   YOUNGS MODULUS,       10.4E06
   POISSONS RATIO,        0.33
   YIELD STRESS,         73.0E03
   HARDENING constant,    37852
   hardening exponent    0.55
   luders strain         0.0
  END
 MATERIAL, 23, ep power hardening, 0.000264, $  7075
   YOUNGS MODULUS,       10.4E06
   POISSONS RATIO,        0.33
   YIELD STRESS,         73.0E03
   HARDENING constant,    37852
   hardening exponent    0.55
   luders strain         0.0
  END
MATERIAL 24 = ORTHOTROPIC CRUSH, 5.682e-5
        Compacted YOUNGS MODULUS = 1.5e6
        Compacted POISSONS RATIO = 0.3
        Compacted YIELD STRESS  = 20000.
        X ID = 1   Y ID = 1
        Z ID = 2   XY ID = 4
        YZ ID = 5   ZX ID = 4
        Full Compaction = 0.9 $ 0 = no compaction, 1 = very flat
        Modulus x = 1.5e6
        Modulus y = 0.3e6
        Modulus z = 0.3e6
        Modulus xy = 0.2e6
        Modulus yz = 0.25e6
        Modulus zx = 0.2e6
End
Function 1  $ x-direction ( T-Direction)
        0.       2000.
        0.14     4200.
        0.28     5100.
        0.42     5430.
        0.57     6100.
```

```
        0.71     10100.
        0.80     15000.
        0.90     20000.
End
Function 2    $  y-direction (L-Direction) z-direction approx the same
        0.       400.
        0.14     986.
        0.28     1200.
        0.42     1275.
        0.57     1432.
        0.71     2371.
        0.80     3521.
        0.90     4690.
End
Function 4   $ sigxy or sigxz vs volume
        0.0     1000.
        0.60    1000.
        0.70    10000.
        0.90    10000.
End
Function 5   $ sigyz vs volume
        0.0     1000.
        0.60    1000.
        0.70    10000.
        0.90    10000.
End
MATERIAL 25 = ORTHOTROPIC CRUSH, 5.682e-5
        Compacted YOUNGS MODULUS = 1.5e6
        Compacted POISSONS RATIO = 0.3
        Compacted YIELD STRESS  = 20000.
        X ID = 2   Y ID = 1
        Z ID = 1   XY ID = 4
        YZ ID = 5   ZX ID = 4
        Full Compaction = 0.9 $ 0 = no compaction, 1 = very flat
        Modulus x = 1.5e6
        Modulus y = 0.3e6
        Modulus z = 0.3e6
        Modulus xy = 0.2e6
        Modulus yz = 0.25e6
        Modulus zx = 0.2e6
End
Function 1  $ x-direction ( T-Direction)
        0.       2000.
        0.14     4200.
        0.28     5100.
        0.42     5430.
        0.57     6100.
        0.71     10100.
        0.80     15000.
        0.90     20000.
End
Function 2    $  y-direction (L-Direction) z-direction approx the same
        0.       400.
        0.14     986.
        0.28     1200.
        0.42     1275.
        0.57     1432.
```

```
        0.71     2371.
        0.80     3521.
        0.90     4690.
End
Function 4   $ sigxy or sigxz vs volume
        0.0     1000.
        0.60    1000.
        0.70    10000.
        0.90    10000.
End
Function 5   $ sigyz vs volume
        0.0     1000.
        0.60    1000.
        0.70    10000.
        0.90    10000.
End
MATERIAL 26 = ORTHOTROPIC CRUSH, 5.682e-5
        Compacted YOUNGS MODULUS = 1.5e6
        Compacted POISSONS RATIO = 0.3
        Compacted YIELD STRESS  = 20000.
        X ID = 1   Y ID = 1
        Z ID = 2   XY ID = 4
        YZ ID = 5   ZX ID = 4
        Full Compaction = 0.9 $ 0 = no compaction, 1 = very flat
        Modulus x = 1.5e6
        Modulus y = 0.3e6
        Modulus z = 0.3e6
        Modulus xy = 0.2e6
        Modulus yz = 0.25e6
        Modulus zx = 0.2e6
End
Function 1  $ x-direction ( T-Direction)
        0.       2000.
        0.14     4200.
        0.28     5100.
        0.42     5430.
        0.57     6100.
        0.71     10100.
        0.80     15000.
        0.90     20000.
End
Function 2    $  y-direction (L-Direction) z-direction approx the same
        0.       400.
        0.14     986.
        0.28     1200.
        0.42     1275.
        0.57     1432.
        0.71     2371.
        0.80     3521.
        0.90     4690.
End
Function 4   $ sigxy or sigxz vs volume
        0.0     1000.
        0.60    1000.
        0.70    10000.
        0.90    10000.
End
```

```
Function 5   $ sigyz vs volume
        0.0     1000.
        0.60    1000.
        0.70    10000.
        0.90    10000.
End
MATERIAL 27 = ORTHOTROPIC CRUSH, 5.682e-5
        Compacted YOUNGS MODULUS = 1.5e6
        Compacted POISSONS RATIO = 0.3
        Compacted YIELD STRESS  = 20000.
        X ID = 1   Y ID = 1
        Z ID = 2   XY ID = 4
        YZ ID = 5   ZX ID = 4
        Full Compaction = 0.9 $ 0 = no compaction, 1 = very flat
        Modulus x = 1.5e6
        Modulus y = 0.3e6
        Modulus z = 0.3e6
        Modulus xy = 0.2e6
        Modulus yz = 0.25e6
        Modulus zx = 0.2e6
End
Function 1  $ x-direction ( T-Direction)
        0.       2000.
        0.14     4200.
        0.28     5100.
        0.42     5430.
        0.57     6100.
        0.71     10100.
        0.80     15000.
        0.90     20000.
End
Function 2    $  y-direction (L-Direction) z-direction approx the same
        0.       400.
        0.14     986.
        0.28     1200.
        0.42     1275.
        0.57     1432.
        0.71     2371.
        0.80     3521.
        0.90     4690.
End
Function 4   $ sigxy or sigxz vs volume
        0.0     1000.
        0.60    1000.
        0.70    10000.
        0.90    10000.
End
Function 5   $ sigyz vs volume
        0.0     1000.
        0.60    1000.
        0.70    10000.
        0.90    10000.
End
MATERIAL 28 = ORTHOTROPIC CRUSH, 5.682e-5
        Compacted YOUNGS MODULUS = 1.5e6
        Compacted POISSONS RATIO = 0.3
        Compacted YIELD STRESS  = 20000.
```

```
        X ID = 2   Y ID = 1
        Z ID = 1   XY ID = 4
        YZ ID = 5   ZX ID = 4
        Full Compaction = 0.9 $ 0 = no compaction, 1 = very flat
        Modulus x = 1.5e6
        Modulus y = 0.3e6
        Modulus z = 0.3e6
        Modulus xy = 0.2e6
        Modulus yz = 0.25e6
        Modulus zx = 0.2e6
End
Function 1  $ x-direction ( T-Direction)
        0.       2000.
        0.14     4200.
        0.28     5100.
        0.42     5430.
        0.57     6100.
        0.71     10100.
        0.80     15000.
        0.90     20000.
End
Function 2    $  y-direction (L-Direction) z-direction approx the same
        0.       400.
        0.14     986.
        0.28     1200.
        0.42     1275.
        0.57     1432.
        0.71     2371.
        0.80     3521.
        0.90     4690.
End
Function 4   $ sigxy or sigxz vs volume
        0.0     1000.
        0.60    1000.
        0.70    10000.
        0.90    10000.
End
Function 5   $ sigyz vs volume
        0.0     1000.
        0.60    1000.
        0.70    10000.
        0.90    10000.
End
MATERIAL 29 = ORTHOTROPIC CRUSH, 5.682e-5
        Compacted YOUNGS MODULUS = 1.5e6
        Compacted POISSONS RATIO = 0.3
        Compacted YIELD STRESS  = 20000.
        X ID = 1   Y ID = 1
        Z ID = 2   XY ID = 4
        YZ ID = 5   ZX ID = 4
        Full Compaction = 0.9 $ 0 = no compaction, 1 = very flat
        Modulus x = 1.5e6
        Modulus y = 0.3e6
        Modulus z = 0.3e6
        Modulus xy = 0.2e6
        Modulus yz = 0.25e6
        Modulus zx = 0.2e6
```

```
End
Function 1  $ x-direction ( T-Direction)
        0.       2000.
        0.14     4200.
        0.28     5100.
        0.42     5430.
        0.57     6100.
        0.71     10100.
        0.80     15000.
        0.90     20000.
End
Function 2    $  y-direction (L-Direction) z-direction approx the same
        0.       400.
        0.14     986.
        0.28     1200.
        0.42     1275.
        0.57     1432.
        0.71     2371.
        0.80     3521.
        0.90     4690.
End
Function 4   $ sigxy or sigxz vs volume
        0.0     1000.
        0.60    1000.
        0.70    10000.
        0.90    10000.
End
Function 5   $ sigyz vs volume
        0.0     1000.
        0.60    1000.
        0.70    10000.
        0.90    10000.
End
MATERIAL 30 = ORTHOTROPIC CRUSH, 5.682e-5
        Compacted YOUNGS MODULUS = 1.5e6
        Compacted POISSONS RATIO = 0.3
        Compacted YIELD STRESS  = 20000.
        X ID = 1   Y ID = 1
        Z ID = 2   XY ID = 4
        YZ ID = 5   ZX ID = 4
        Full Compaction = 0.9 $ 0 = no compaction, 1 = very flat
        Modulus x = 1.5e6
        Modulus y = 0.3e6
        Modulus z = 0.3e6
        Modulus xy = 0.2e6
        Modulus yz = 0.25e6
        Modulus zx = 0.2e6
End
Function 1  $ x-direction ( T-Direction)
        0.       2000.
        0.14     4200.
        0.28     5100.
        0.42     5430.
        0.57     6100.
        0.71     10100.
        0.80     15000.
        0.90     20000.
```

```
End
Function 2     $  y-direction (L-Direction) z-direction approx the same
        0.       400.
        0.14     986.
        0.28     1200.
        0.42     1275.
        0.57     1432.
        0.71     2371.
        0.80     3521.
        0.90     4690.
End
Function 4   $ sigxy or sigxz vs volume
        0.0     1000.
        0.60    1000.
        0.70    10000.
        0.90    10000.
End
Function 5   $ sigyz vs volume
        0.0     1000.
        0.60    1000.
        0.70    10000.
        0.90    10000.
End
MATERIAL 31 = ORTHOTROPIC CRUSH, 5.682e-5
        Compacted YOUNGS MODULUS = 1.5e6
        Compacted POISSONS RATIO = 0.3
        Compacted YIELD STRESS  = 20000.
        X ID = 2   Y ID = 1
        Z ID = 1   XY ID = 4
        YZ ID = 5   ZX ID = 4
        Full Compaction = 0.9 $ 0 = no compaction, 1 = very flat
        Modulus x = 1.5e6
        Modulus y = 0.3e6
        Modulus z = 0.3e6
        Modulus xy = 0.2e6
        Modulus yz = 0.25e6
        Modulus zx = 0.2e6
End
Function 1  $ x-direction ( T-Direction)
        0.       2000.
        0.14     4200.
        0.28     5100.
        0.42     5430.
        0.57     6100.
        0.71     10100.
        0.80     15000.
        0.90     20000.
End
Function 2     $  y-direction (L-Direction) z-direction approx the same
        0.       400.
        0.14     986.
        0.28     1200.
        0.42     1275.
        0.57     1432.
        0.71     2371.
        0.80     3521.
        0.90     4690.
```

```
End
Function 4   $ sigxy or sigxz vs volume
        0.0     1000.
        0.60    1000.
        0.70    10000.
        0.90    10000.
End
Function 5   $ sigyz vs volume
        0.0     1000.
        0.60    1000.
        0.70    10000.
        0.90    10000.
End
MATERIAL 32 = ORTHOTROPIC CRUSH, 5.682e-5
        Compacted YOUNGS MODULUS = 1.5e6
        Compacted POISSONS RATIO = 0.3
        Compacted YIELD STRESS  = 20000.
        X ID = 1   Y ID = 1
        Z ID = 2   XY ID = 4
        YZ ID = 5   ZX ID = 4
        Full Compaction = 0.9 $ 0 = no compaction, 1 = very flat
        Modulus x = 1.5e6
        Modulus y = 0.3e6
        Modulus z = 0.3e6
        Modulus xy = 0.2e6
        Modulus yz = 0.25e6
        Modulus zx = 0.2e6
End
Function 1  $ x-direction ( T-Direction)
        0.       2000.
        0.14     4200.
        0.28     5100.
        0.42     5430.
        0.57     6100.
        0.71     10100.
        0.80     15000.
        0.90     20000.
End
Function 2    $  y-direction (L-Direction) z-direction approx the same
        0.       400.
        0.14     986.
        0.28     1200.
        0.42     1275.
        0.57     1432.
        0.71     2371.
        0.80     3521.
        0.90     4690.
End
Function 4   $ sigxy or sigxz vs volume
        0.0     1000.
        0.60    1000.
        0.70    10000.
        0.90    10000.
End
Function 5   $ sigyz vs volume
        0.0     1000.
        0.60    1000.
```

```
        0.70    10000.
        0.90    10000.
End
MATERIAL 33 = ORTHOTROPIC CRUSH, 5.682e-5
        Compacted YOUNGS MODULUS = 1.5e6
        Compacted POISSONS RATIO = 0.3
        Compacted YIELD STRESS  = 20000.
        X ID = 1   Y ID = 1
        Z ID = 2   XY ID = 4
        YZ ID = 5   ZX ID = 4
        Full Compaction = 0.9 $ 0 = no compaction, 1 = very flat
        Modulus x = 1.5e6
        Modulus y = 0.3e6
        Modulus z = 0.3e6
        Modulus xy = 0.2e6
        Modulus yz = 0.25e6
        Modulus zx = 0.2e6
End
Function 1  $ x-direction ( T-Direction)
        0.       2000.
        0.14     4200.
        0.28     5100.
        0.42     5430.
        0.57     6100.
        0.71     10100.
        0.80     15000.
        0.90     20000.
End
Function 2    $  y-direction (L-Direction) z-direction approx the same
        0.       400.
        0.14     986.
        0.28     1200.
        0.42     1275.
        0.57     1432.
        0.71     2371.
        0.80     3521.
        0.90     4690.
End
Function 4   $ sigxy or sigxz vs volume
        0.0     1000.
        0.60    1000.
        0.70    10000.
        0.90    10000.
End
Function 5   $ sigyz vs volume
        0.0     1000.
        0.60    1000.
        0.70    10000.
        0.90    10000.
End
MATERIAL 34 = ORTHOTROPIC CRUSH, 5.682e-5
        Compacted YOUNGS MODULUS = 1.5e6
        Compacted POISSONS RATIO = 0.3
        Compacted YIELD STRESS  = 20000.
        X ID = 2   Y ID = 1
        Z ID = 1   XY ID = 4
        YZ ID = 5   ZX ID = 4
```

```
        Full Compaction = 0.9 $ 0 = no compaction, 1 = very flat
        Modulus x = 1.5e6
        Modulus y = 0.3e6
        Modulus z = 0.3e6
        Modulus xy = 0.2e6
        Modulus yz = 0.25e6
        Modulus zx = 0.2e6
End
Function 1  $ x-direction ( T-Direction)
        0.       2000.
        0.14     4200.
        0.28     5100.
        0.42     5430.
        0.57     6100.
        0.71     10100.
        0.80     15000.
        0.90     20000.
End
Function 2    $  y-direction (L-Direction) z-direction approx the same
        0.       400.
        0.14     986.
        0.28     1200.
        0.42     1275.
        0.57     1432.
        0.71     2371.
        0.80     3521.
        0.90     4690.
End
Function 4   $ sigxy or sigxz vs volume
        0.0     1000.
        0.60    1000.
        0.70    10000.
        0.90    10000.
End
Function 5   $ sigyz vs volume
        0.0     1000.
        0.60    1000.
        0.70    10000.
        0.90    10000.
End
MATERIAL 35 = ORTHOTROPIC CRUSH, 5.682e-5
        Compacted YOUNGS MODULUS = 1.5e6
        Compacted POISSONS RATIO = 0.3
        Compacted YIELD STRESS  = 20000.
        X ID = 1   Y ID = 1
        Z ID = 2   XY ID = 4
        YZ ID = 5   ZX ID = 4
        Full Compaction = 0.9 $ 0 = no compaction, 1 = very flat
        Modulus x = 1.5e6
        Modulus y = 0.3e6
        Modulus z = 0.3e6
        Modulus xy = 0.2e6
        Modulus yz = 0.25e6
        Modulus zx = 0.2e6
End
Function 1  $ x-direction ( T-Direction)
        0.       2000.
```

```
        0.14     4200.
        0.28     5100.
        0.42     5430.
        0.57     6100.
        0.71     10100.
        0.80     15000.
        0.90     20000.
End
Function 2    $  y-direction (L-Direction) z-direction approx the same
        0.       400.
        0.14     986.
        0.28     1200.
        0.42     1275.
        0.57     1432.
        0.71     2371.
        0.80     3521.
        0.90     4690.
End
Function 4   $ sigxy or sigxz vs volume
        0.0     1000.
        0.60    1000.
        0.70    10000.
        0.90    10000.
End
Function 5   $ sigyz vs volume
        0.0     1000.
        0.60    1000.
        0.70    10000.
        0.90    10000.
End
MATERIAL 36 = ORTHOTROPIC CRUSH, 5.682e-5
        Compacted YOUNGS MODULUS = 1.5e6
        Compacted POISSONS RATIO = 0.3
        Compacted YIELD STRESS  = 20000.
        X ID = 1   Y ID = 1
        Z ID = 2   XY ID = 4
        YZ ID = 5   ZX ID = 4
        Full Compaction = 0.9 $ 0 = no compaction, 1 = very flat
        Modulus x = 1.5e6
        Modulus y = 0.3e6
        Modulus z = 0.3e6
        Modulus xy = 0.2e6
        Modulus yz = 0.25e6
        Modulus zx = 0.2e6
End
Function 1  $ x-direction ( T-Direction)
        0.       2000.
        0.14     4200.
        0.28     5100.
        0.42     5430.
        0.57     6100.
        0.71     10100.
        0.80     15000.
        0.90     20000.
End
Function 2    $  y-direction (L-Direction) z-direction approx the same
        0.       400.
```

```
        0.14      986.
        0.28      1200.
        0.42      1275.
        0.57      1432.
        0.71      2371.
        0.80      3521.
        0.90      4690.
End
Function 4   $ sigxy or sigxz vs volume
        0.0      1000.
        0.60     1000.
        0.70     10000.
        0.90     10000.
End
Function 5   $ sigyz vs volume
        0.0      1000.
        0.60     1000.
        0.70     10000.
        0.90     10000.
End
MATERIAL 37 = ORTHOTROPIC CRUSH, 5.682e-5
        Compacted YOUNGS MODULUS = 1.5e6
        Compacted POISSONS RATIO = 0.3
        Compacted YIELD STRESS  = 20000.
        X ID = 2   Y ID = 1
        Z ID = 1   XY ID = 4
        YZ ID = 5   ZX ID = 4
        Full Compaction = 0.9 $ 0 = no compaction, 1 = very flat
        Modulus x = 1.5e6
        Modulus y = 0.3e6
        Modulus z = 0.3e6
        Modulus xy = 0.2e6
        Modulus yz = 0.25e6
        Modulus zx = 0.2e6
End
Function 1  $ x-direction ( T-Direction)
        0.       2000.
        0.14     4200.
        0.28     5100.
        0.42     5430.
        0.57     6100.
        0.71     10100.
        0.80     15000.
        0.90     20000.
End
Function 2    $  y-direction (L-Direction) z-direction approx the same
        0.       400.
        0.14     986.
        0.28     1200.
        0.42     1275.
        0.57     1432.
        0.71     2371.
        0.80     3521.
        0.90     4690.
End
Function 4   $ sigxy or sigxz vs volume
        0.0      1000.
```

```
        0.60    1000.
        0.70    10000.
        0.90    10000.
End
Function 5   $ sigyz vs volume
        0.0     1000.
        0.60    1000.
        0.70    10000.
        0.90    10000.
End
MATERIAL 38 = ORTHOTROPIC CRUSH, 5.682e-5
        Compacted YOUNGS MODULUS = 1.5e6
        Compacted POISSONS RATIO = 0.3
        Compacted YIELD STRESS  = 20000.
        X ID = 1   Y ID = 1
        Z ID = 2   XY ID = 4
        YZ ID = 5   ZX ID = 4
        Full Compaction = 0.9 $ 0 = no compaction, 1 = very flat
        Modulus x = 1.5e6
        Modulus y = 0.3e6
        Modulus z = 0.3e6
        Modulus xy = 0.2e6
        Modulus yz = 0.25e6
        Modulus zx = 0.2e6
End
Function 1  $ x-direction ( T-Direction)
        0.       2000.
        0.14     4200.
        0.28     5100.
        0.42     5430.
        0.57     6100.
        0.71     10100.
        0.80     15000.
        0.90     20000.
End
Function 2    $  y-direction (L-Direction) z-direction approx the same
        0.       400.
        0.14     986.
        0.28     1200.
        0.42     1275.
        0.57     1432.
        0.71     2371.
        0.80     3521.
        0.90     4690.
End
Function 4   $ sigxy or sigxz vs volume
        0.0     1000.
        0.60    1000.
        0.70    10000.
        0.90    10000.
End
Function 5   $ sigyz vs volume
        0.0     1000.
        0.60    1000.
        0.70    10000.
        0.90    10000.
End
```

```
MATERIAL 39 = ORTHOTROPIC CRUSH, 5.682e-5
        Compacted YOUNGS MODULUS = 1.5e6
        Compacted POISSONS RATIO = 0.3
        Compacted YIELD STRESS  = 20000.
        X ID = 1   Y ID = 1
        Z ID = 2   XY ID = 4
        YZ ID = 5   ZX ID = 4
        Full Compaction = 0.9 $ 0 = no compaction, 1 = very flat
        Modulus x = 1.5e6
        Modulus y = 0.3e6
        Modulus z = 0.3e6
        Modulus xy = 0.2e6
        Modulus yz = 0.25e6
        Modulus zx = 0.2e6
End
Function 1  $ x-direction ( T-Direction)
        0.       2000.
        0.14     4200.
        0.28     5100.
        0.42     5430.
        0.57     6100.
        0.71     10100.
        0.80     15000.
        0.90     20000.
End
Function 2    $  y-direction (L-Direction) z-direction approx the same
        0.       400.
        0.14     986.
        0.28     1200.
        0.42     1275.
        0.57     1432.
        0.71     2371.
        0.80     3521.
        0.90     4690.
End
Function 4   $ sigxy or sigxz vs volume
        0.0     1000.
        0.60    1000.
        0.70    10000.
        0.90    10000.
End
Function 5   $ sigyz vs volume
        0.0     1000.
        0.60    1000.
        0.70    10000.
        0.90    10000.
End
MATERIAL 40 = ORTHOTROPIC CRUSH, 5.682e-5
        Compacted YOUNGS MODULUS = 1.5e6
        Compacted POISSONS RATIO = 0.3
        Compacted YIELD STRESS  = 20000.
        X ID = 2   Y ID = 1
        Z ID = 1   XY ID = 4
        YZ ID = 5   ZX ID = 4
        Full Compaction = 0.9 $ 0 = no compaction, 1 = very flat
        Modulus x = 1.5e6
        Modulus y = 0.3e6
```

```
        Modulus z = 0.3e6
        Modulus xy = 0.2e6
        Modulus yz = 0.25e6
        Modulus zx = 0.2e6
End
Function 1  $ x-direction ( T-Direction)
        0.       2000.
        0.14     4200.
        0.28     5100.
        0.42     5430.
        0.57     6100.
        0.71     10100.
        0.80     15000.
        0.90     20000.
End
Function 2    $  y-direction (L-Direction) z-direction approx the same
        0.       400.
        0.14     986.
        0.28     1200.
        0.42     1275.
        0.57     1432.
        0.71     2371.
        0.80     3521.
        0.90     4690.
End
Function 4   $ sigxy or sigxz vs volume
        0.0     1000.
        0.60    1000.
        0.70    10000.
        0.90    10000.
End
Function 5   $ sigyz vs volume
        0.0     1000.
        0.60    1000.
        0.70    10000.
        0.90    10000.
End
MATERIAL 41 = ORTHOTROPIC CRUSH, 5.682e-5
        Compacted YOUNGS MODULUS = 1.5e6
        Compacted POISSONS RATIO = 0.3
        Compacted YIELD STRESS  = 20000.
        X ID = 1   Y ID = 1
        Z ID = 2   XY ID = 4
        YZ ID = 5   ZX ID = 4
        Full Compaction = 0.9 $ 0 = no compaction, 1 = very flat
        Modulus x = 1.5e6
        Modulus y = 0.3e6
        Modulus z = 0.3e6
        Modulus xy = 0.2e6
        Modulus yz = 0.25e6
        Modulus zx = 0.2e6
End
Function 1  $ x-direction ( T-Direction)
        0.       2000.
        0.14     4200.
        0.28     5100.
        0.42     5430.
```

```
        0.57     6100.
        0.71     10100.
        0.80     15000.
        0.90     20000.
End
Function 2    $  y-direction (L-Direction) z-direction approx the same
        0.       400.
        0.14     986.
        0.28     1200.
        0.42     1275.
        0.57     1432.
        0.71     2371.
        0.80     3521.
        0.90     4690.
End
Function 4   $ sigxy or sigxz vs volume
        0.0     1000.
        0.60    1000.
        0.70    10000.
        0.90    10000.
End
Function 5   $ sigyz vs volume
        0.0     1000.
        0.60    1000.
        0.70    10000.
        0.90    10000.
End
 exit
```

2.12.8 Design Pressure Calculations for the T-Ampoule (in Accordance with Section VIII Division 1 of the ASME Boiler and Pressure Vessel Code

See stand-alone document below.

Design Pressure Calculations for the T-Ampoule in Accordance with Section VIII Division 1 of the ASME Boiler and Pressure Vessel Code

The objective of the T-Ampoule (Drawing 2A0261) is to provide a eutectic prevention barrier between the plutonium contents it contains and the PH13-8Mo shell of TB-1 containment vessel, TB-1, to minimize the formation of a Pu/Fe eutectic under an elevated temperature of 1080°F from a fire accident. The approach taken to ensure this separation was to design a pressure envelope that could maintain a glove box atmosphere during normal conditions of transport and hypothetical accident conditions and to provide the eutectic prevention barrier during the accident conditions for air transport of plutonium. The analyses contained in this report and in the addendum for plutonium metal demonstrate that the T-Ampoule will accomplish these goals.

The first aspect of pressure vessel design requires the preparation of a pressure-temperature map. of this paper fulfill this requirement. The second aspect is to use a set of design criteria by which to demonstrate integrity. The criteria selected for the T-Ampoule is the ASME Boiler and Pressure Vessel Code, Section VIII, Division 1 [1]. The T-Ampoule's unusual design has some aspects (i.e., its small size or the use of O-ring seals) that require exception to Section VIII. Section 2 of this document enumerates these exceptions. This section also identifies specific paragraphs of the code that apply to the T-Ampoule design. Section 3 describes the analyses performed in accordance with Section VII. Finally, Section 3.8 addresses the O-ring seal, a device not covered by Section VIII.

1 Pressure/Temperature Map

1.1 Summary

A previous analysis by Rubin [2] addresses increased pressure inside the TB-1 pressure vessel, in an aircraft accident scenario. Rubin treats the TB-1 interior as a single volume subjected to a uniform temperature of 1080°F and a uniform internal pressure was determined by analysis. However, the T-Ampoule is a pressure vessel itself, creating two zones within the TB-1 containment. The T-Ampoule forms the first zone. The second zone consists of the annulus between the T-Ampoule and the TB-1 wall. Once the O-rings inside the vessels begin to decompose, these two zones will respond differently to temperature increase..

This analysis uses Rubin's conclusion that packing configuration #3 is the worst case.

Consider the assembly drawing contained in Figure 1. Three sample containers with plutonium reside within the T-Ampoule (see Figure 1). These three containers are designed to carry plutonium metal contents and are not pressure vessels. The T-Ampoule with the three containers fits snuggly within the TB-1 containment vessel leaving a small annulus volume between the TB-1 wall and the T-Ampoule. Both the T-Ampoule and the TB-1 vessel contain pressure. As assembly temperature increases, as a result of the fire accident condition, the O-rings will decompose, increasing the mass of vapor within each pressure vessel. The combination of increasing temperature and increasing molar mass within each pressure vessel combine to rapidly increase pressure inside each zone, as documented below. The additional mass is approximately the same however, the volumes of the two zones differ by orders of magnitude. These volume differences cause the pressure response to differ.

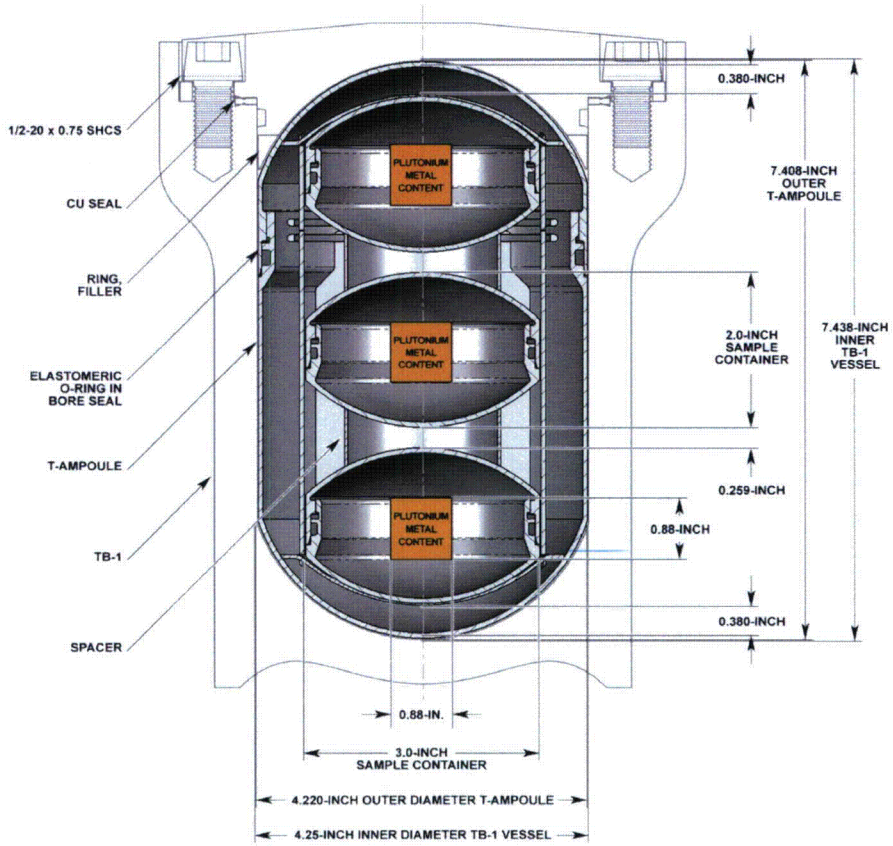

Figure 1: TB-1 Assembly for Packing Configuration #3

The following analysis tracks the response of three individual volumes. The first volume, is the annulus, which is the space between the TB-1 containment vessel and the T-Ampoule. The second volume, is the T-Ampoule, which consists of all volume and components within the T-Ampoule. The third volume, is the TB-1 which is the sum of the first two volumes. This third volume is meaningful only after the T-Ampoule's seal fails and the pressure equilibrates between the first two zones.

The volumes listed in Table 1 were taken from the Rubin paper. An exception to these volumes is the empty, internal T-Ampoule volume of 1280 cm^3, which was estimated specifically for this analysis. The vapor volume of the TB-1 container remains 1103 cm^3. The T-Ampoule, designed to nestle within the TB-1 container, is only slightly smaller with an internal volume of 1065 cm^3. The difference between these two volumes is the volume of the annulus at 37.7 cm^3.

Table 1: Summary of Component Volumes

Description	TB-1	T-Ampoule	Annulus	Units
Empty Volume	1460	1280		cm^3
Metal Volume		128		cm^3
Occupied Volume		1410		cm^3
Filler Ring	14.75			cm^3
T-Amp Contents Volume		214		cm^3
Vapor Volume	1103	1065	37.7	cm^3
	0.001103	0.001065	0.000377	m^3

Table 2 provides a summary of O-ring volumes and masses with the initial volumes extracted from Rubin's paper. The T-Ampoule contains three O-rings, one for each sample container seal. In addition, this analysis allocates one half of the O-ring volume used to seal the T-Ampoule to the T-Ampoule volume. The remaining one half of the T-Ampoule, O-ring seal is allocated to the annulus. Additionally, this small volume must also accommodate all of the TB-1 O-ring seal. The copper gasket, which seals the TB-1 containment vessel, ensures all of this O-ring's mass is trapped in the annulus. The TB-1 column contains the sum of the T-Ampoule and the annulus. The masses listed on the last line of Table 1 are based on an O-ring density of 1.8 g/cm^3.

Table 2: O-ring Volumes

	TB-1	T-Ampoule	Annulus	Units
T-Ampoule Seal	3.2209	1.6105	1.6105	cm^2
TB-1 Seal	3.1233	0	3.1233	cm^3
SC-1 Seals (3 times)	3.5748	3.5748	0	cm^3
Total Volume	9.9190	5.1853	4.7338	cm^3
Total O-ring mass	17.8542	9.3335	8.5208	g

According to Rubin, a fluoro-elastomeric O-ring decomposes per equation 1

$$0.217CF_2CH_2(s)+0.026C_3F_6(s)\rightarrow 0.473C(s)+0.434HF(g)+0.039CF_4(g) \qquad 1$$

Rubin asserts, based on references, that the O-ring initially contains 78% by mass CF_2HC_2 and 22% by mass C_3F_6. He also assumes complete O-ring decomposition at 1080 °F.

In fact fluorocarbon decomposition, or pyrolysis, is a function of temperature also shown in Figure 2 [Reference 3, p. 300]. The first steep loss of mass between 700 and 900°F marks the loss of hydrogen fluoride (HF). The remaining slow decline traces the conversion of the remaining material to CF_4. At 1080 °F, approximately 78% of the O-ring material has pyrolized.

Table 1: Summary of Component Volumes

Description	TB-1	T-Ampoule	Annulus	Units
Empty Volume	1460	1280		cm^3
Metal Volume		128		cm^3
Occupied Volume		1410		cm^3
Filler Ring	14.75			cm^3
T-Amp Contents Volume		214		cm^3
Vapor Volume	1103	1065	37.7	cm^3
	0.001103	0.001065	0.000377	m^3

Table 2 provides a summary of O-ring volumes and masses with the initial volumes extracted from Rubin's paper. The T-Ampoule contains three O-rings, one for each sample container seal. In addition, this analysis allocates one half of the O-ring volume used to seal the T-Ampoule to the T-Ampoule volume. The remaining one half of the T-Ampoule, O-ring seal is allocated to the annulus. Additionally, this small volume must also accommodate all of the TB-1 O-ring seal. The copper gasket, which seals the TB-1 containment vessel, ensures all of this O-ring's mass is trapped in the annulus. The TB-1 column contains the sum of the T-Ampoule and the annulus. The masses listed on the last line of Table 1 are based on an O-ring density of 1.8 g/cm^3.

Table 2: O-ring Volumes

	TB-1	T-Ampoule	Annulus	Units
T-Ampoule Seal	3.2209	1.6105	1.6105	cm^2
TB-1 Seal	3.1233	0	3.1233	cm^3
SC-1 Seals (3 times)	3.5748	3.5748	0	cm^3
Total Volume	9.9190	5.1853	4.7338	cm^3
Total O-ring mass	17.8542	9.3335	8.5208	g

According to Rubin, a fluoro-elastomeric O-ring decomposes per equation 1

$$0.217CF_2CH_2(s)+0.026C_3F_6(s)\rightarrow 0.473C(s)+0.434HF(g)+0.039CF_4(g) \qquad 1$$

Rubin asserts, based on references, that the O-ring initially contains 78% by mass CF_2HC_2 and 22% by mass C_3F_6. He also assumes complete O-ring decomposition at 1080 °F.

In fact fluorocarbon decomposition, or pyrolysis, is a function of temperature also shown in Figure 2 [Reference 3, p. 300]. The first steep loss of mass between 700 and 900°F marks the loss of hydrogen fluoride (HF). The remaining slow decline traces the conversion of the remaining material to CF_4. At 1080 °F, approximately 78% of the O-ring material has pyrolized.

Table 3: Weight Loss from O-rings at 1080°F

Reactant	TB-1	T-Ampoule	Annulus	Units
CF_2CH_2	10.7	5.57	5.09	g
C_3F_6	3.016	1.58	1.43	g
Total Decomposed O-ring Mass	13.7	7.15	6.52	g

Table 4 contains some useful statistics for the pyrolysis process, including molecular mass ratios for the reactants and products. The last column contains molar coefficients for products and reactants after the reactants have been normalized to 1 mol. This last column is units of mols per total mol of O-ring reactants.

Table 4: Viton Pyrolysis Statistics

Compound	mol fractions based on Equation 1	MW (g/mol)	molprod/-Total Reactant
CF_2CH_2	0.217	64.0341	0.8930
C_3F_6	0.026	150.0225	0.107
C	0.473	12.0107	1.947
HF	0.434	20.00634	1.786
CF_4	0.039	88.0043	0.160

In addition to the above, it is conservative to assume that both the TB-1 lid and body and the T-Ampoule lid and body were assembled in air. While user loading procedures could allow assembly of the T-Ampoule into TB-1 in air, they require assembly of the T-Ampoule in a glove box with an inert atmosphere. Assembly of the T-Ampoule with contents and packing in air is not permitted in the loading procedures. Nonetheless it is conceivable and, therefore, is considered here. With this assumption, some or all of the solid carbon, or graphite char identified in equation 1 will be oxidized to CO_2. With this assumption, some or all of the solid carbon, or graphite char identified in equation will be oxidized to CO_2. At temperatures less than 3000°F (1500 K) the carbon monoxide/carbon dioxide equilibrium favors carbon dioxide. This analysis assumes that all gas formed is in fact CO_2. Incorporating the above, equation 2 can be rewritten as:

$$
\begin{aligned}
0.21r_3O_2(g)+0.79r_3N_2(g)+r_1CF_2CH_2(s)+r_2C_3F_6(s) \rightarrow\ & p_1C(s) \\
& +p_2HF(g) \\
& +p_3CF_4(g) \\
& +p_4O_2(g) \\
& +p_5CO_2(g) \\
& +0.79r_3N_2(g)
\end{aligned}
\qquad 2
$$

At assembly pressure, p_o, and temperature, T_o, assumed to be 1 bar and 25 °C respectively, atmospheric gas behaves ideally. Hence, the reactant coefficient for initial atmosphere, r_2, in equation 2 can be estimated using the ideal gas laws:

$$
r_3 = \frac{VP_o}{R_u T_o} \qquad 3
$$

The volumes used for this calculation are listed in Table 1.

The reactant coefficients for the O-ring material can be estimated using the following relationships:

$$
r_1 = \frac{0.78 \cdot m_{O-ring} f_d}{M_{CF_2CH_2}},\ r_2 = \frac{0.22 \cdot m_{O-ring} f_d}{M_{C_3F_6}} \qquad 4
$$

Molecular mass ratios, $M_{CF_2CH_2}$ and $M_{C_3F_6}$, are available from Table 4. The O-ring masses are listed in Table 2. The fraction of O-ring decomposing, f_d, is plotted in Figure 2 as a function of temperature.

The product relationships are as follows:

$$
p_1 = \begin{cases} 1.947(r_1+r_2)-0.21r_3 & 0.21r_3 < 1.947(r_1+r_2) \\ 0 & 0.21r_3 \geq 1.947(r_1+r_2) \end{cases} \qquad 5
$$

$$
p_2 = 1.782(r_1+r_2) \qquad 6
$$

$$
p_3 = 0.160(r_1+r_2) \qquad 7
$$

$$
p_4 = \begin{cases} 0 & 0.21r_3 \leq 1.947(r_1+r_2) \\ 0.21r_3 - 1.947(r_1+r_2) & 0.21r_3 > 1.947(r_1+r_2) \end{cases} \qquad 8
$$

$$p_5 = \begin{cases} 0.21r_3 & 0.21r_3 \geq 1.947(r_1 + r_2) \\ 1.947(r_1 + r_2) & 0.21r_3 < 1.947(r_1 + r_2) \end{cases} \qquad 9$$

The quantity of O_2, C, and CO_2 is dependent on initial, relative quantities of reactants. If there is more carbon than O_2, then the reaction consumes all oxygen and leaves some carbon as char or graphite. The reverse is also true. The constants in these equations have units of mols per total mols or O-ring reactants and are listed in Table 4.

Table 5 contains a listing of coefficients for equation 2 for the case where temperature equals 1080°F. These values change with temperature because the degree of decomposition changes with temperature.

Table 5: Summary of Coefficients at 1080°F

Compound	Coefficient	TB-1	T-Ampoule	Annulus
Reactants				
CF_2CH_2	r_1	0.167	0.0871	0.0795
C_3F_6	r_2	0.020	0.0105	0.00957
Total mols O-ring reactants	r_1+r_2	0.187	0.0975	0.0890
O_2	$0.21r_3$	0.00929	0.00897	0.000317
N_2	$0.79r_3$	0.0349	0.0337	0.00119
Products				
Total C		0.363	0.190	0.173
C as Char	p_1	0.354	0.181	0.173
HF	p_2	0.333	0.174	0.159
CF_4	p_3	0.0299	0.0157	0.0142
O_2	p_4	0.000	0.000	0.000
CO_2	p_5	0.00929	0.00897	0.000317
N_2	$0.79r_3$	0.0349	0.00119	0.0337
Total mols of Vapor		0.407	0.200	0.207

At the high reaction temperatures and pressures relative to their critical values, the reactants behave as ideal gases. As a consequence the following is true:

$$P = \rho' R_u T = \left(\frac{n}{V}\right) R_u T \qquad 10$$

For this equation, the number of mols, n, is taken directly from the bottom line of Table 5. The volume, V, is taken from the bottom line of Table 1. The universal gas constant, R_u, equals 8.314 N·m/mol·K for all cases. Temperature T is the independent variable in the equation.

Table 6 provides a tabulation of results from the above equations for the maximum temperature, T = 1080°F = 855.4 K. Pressures in the table are presented using three different sets of units, N/m^2, bar, and psia.

It is important to recognize the impact of volume on the resultant pressure. From Table 5, the total number of mols of vapor is relatively the same for the T-Ampoule and the annulus. Even when they are added together to make the TB-1 column, the quantities are of the same order of magnitude. However, when reviewing Table 1 the volume of the annulus is very small compared to the T-Ampoule. As a consequence of this volume difference, pressure in the annulus is an order of magnitude higher than the pressure of the T-Ampoule.

Table 6: Tabulation of Equation 10 Results for T = 1080°F

Parameter	VB-1	T-Ampoule	Annulus	units
molar density,ρ'	369	188	5502	m^3/mol
Temperature T	855.4	855.4	855.4	K
Gas Constant R_u	8.314	8.314	8.314	Nm/mol.K
Pressure P	1,553,000	2,627,000	32,988,000	N/m^2
	15.53	26.27	329.88	bar
	225.19	380.92	4,783.26	psia

Figure 3 is a plot of pressure versus temperature for the three volumes under consideration in this analysis. The plots were developed using the tables and equations detailed above.

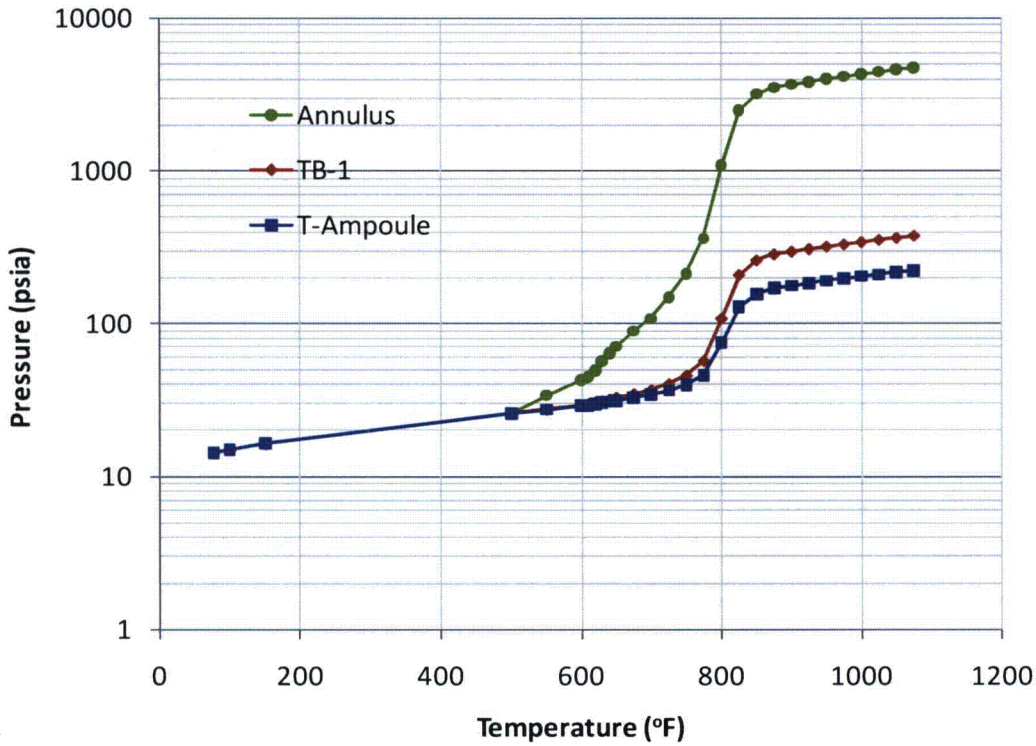

Figure 3: Pressure versus Temperature

Figure 3 shows that the annulus pressure gets large quickly, as is expected, given the relatively large quantity of vapors generated in such a confined space. The figure presents pressure in absolute terms. In fact stress analyses, including the Section VIII, use gauge pressure, or the difference between the pressures internal to a vessel and the pressure external to the same vessel. Figure 5 contains a plot of the pressure difference between the annulus and the T-Ampoule based on Figure 3.

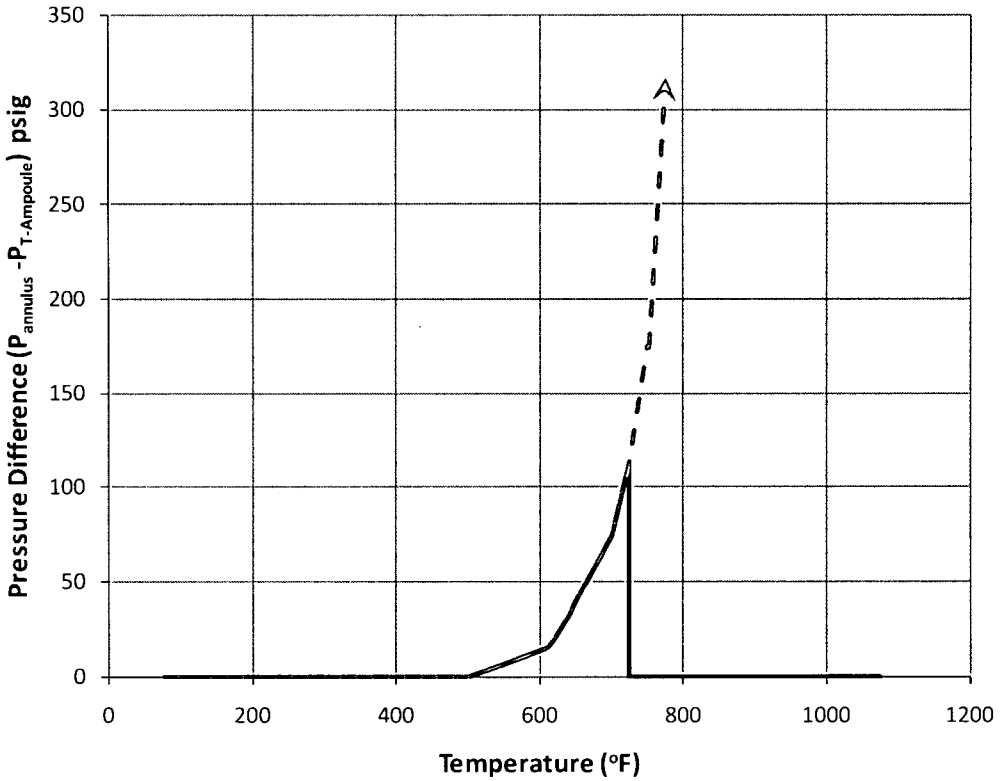

Figure 4: Pressure Difference Between Annulus and T-Ampoule

If the T-Ampoule and the annulus were to remain separated, the pressure difference would follow the trajectory of the dashed line, growing rapidly after approximately 700°F to extremely high pressures. However, the O-ring seal of the T-Ampoule has a gland designed to yield with back pressure at approximately 150 psig. When this occurs, the T-Ampoule and the annulus equilibrate and behave as initially predicted by Rubin. After the seal between the T-Ampoule and annulus opens, all volumes within the TB-1 experience the same pressure, or the difference is zero.

Figure 5 contains a plot of absolute pressure within the annulus. Prior to seal failure, pressure follows the dashed trajectory beginning to increase rapidly as the O-rings start to decompose. However, with seal failure at 150 psig, all volumes within TB-1 experience the same pressure and the vessel begins to act as Rubin initially predicted.

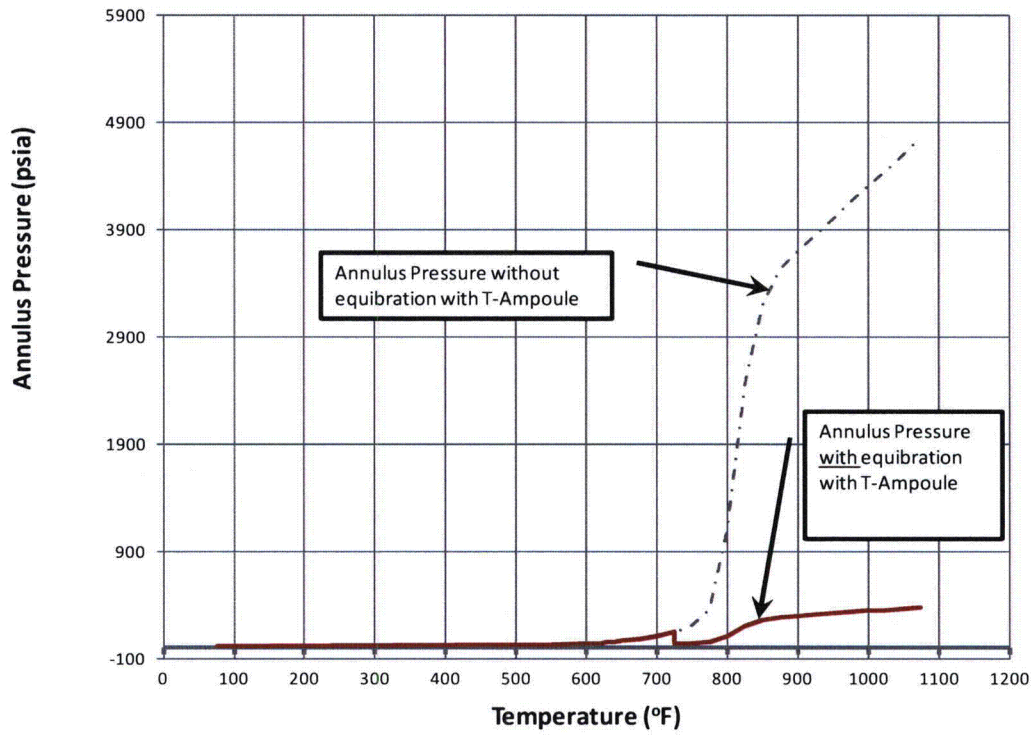

Figure 5: Pressure Trajectories for TB-1

2 *Adjustments to the ASME Boiler and Pressure Vessel Code*

With the exception of the elastomeric (O-ring) seal, the T-Ampoule (Drawing 2A0261) was designed, and will be fabricated and inspected to meet the requirements of the ASME Boiler and Pressure Vessel Code (Section VIII) [0]. However, the following exceptions or explanations apply:

1. The T-Ampoule was designed to Section VIII as modified by this document:

    a. The size requirements in section *U-1(c)(2)(i)* of Section VIII, do not apply.

    b. The marking requirements of parts UG 115-119 do not apply. T-Ampoules will be marked with part and serial numbers as specified in fabrication specification PAT-1040 [5] .

2. Given the dry inert gaseous initial atmosphere and the general non-reactivity of titanium with the vessel contents, the design requires a no corrosion allowance.

3. T-Ampoule MAWP will be established with calculations as set forth in this document. Allowable pressure calculations will be performed based on the following paragraphs of Section VIII:

   a. Torispherical Head allowable pressure was calculated based on the requirements of Section VIII's Mandatory Appendix 1, Supplementary Design Formulas, paragraph 1-4(d).

   b. Allowable pressure, based on membrane stress in the hemispherical head, was estimated based on the criteria set forth in paragraph UG-32.

   c. Allowable pressures in the both the longitudinal and circumferential direction of the shell and lid are estimated based on the criteria set forth in paragraph UG-27 of Section VIII.

   d. T-Ampoule is exempt from the requirements of paragraph UG-32, *Thickness of Shells and Tubes Under External Pressure.* As the T-Ampoule will be subject to impact loading and a separate impact analysis will be conducted as described in Chapter 2 of the PAT-1 Safety Analysis Report Addendum Docket No. 71-0361, Rev. 0, August 2009.

4. T-Ampoule design specifies no welded joints. Consequently joint efficiency, E, in all subsequent Section VIII equations will be applied as 1.0.

5. The requirements of paragraph UG-125 regarding pressure relief devices do not apply. Over pressure response will be discussed in detail in the body of this paper.

6. T-Ampoule will be fabricated from Ti-6Al-4V titanium alloy produced to material specification ASTM 348 except, as modified below:

   a. Titanium alloy will have procurement specified values of 150,000 psi ultimate strength and 140,000 psi yield strength, both at 77°F (room temperature).

   b. Temperature dependant allowable stress criteria will be determined using the procedures outlined in the ASME Boiler and Pressure Vessel Code, Section IID, *Mandatory Appendix 1 Basis for Establishing Stress Values in Tables 1A and 1B.*

   c. In either case, titanium maintains ductility at low temperatures and is therefore, exempt from the requirements of Sections UCS 66 through 68 pertaining to derating allowable stress for low temperature operation.

7. In the case of analysis of the torispherical heads, and in accordance with Section UG-32(e), allowable stress will be limited to 20,000 psi for temperatures below 77°F, and will be reduced proportional to the curves developed in 2.b above for temperatures above 77°F.

8. The T-Ampoule quality program will meet the requirements of Section VIII with the following exceptions:

    a. The standard hydrostatic test of paragraph UG-99 or the pneumatic test from paragraph UG-100, are not required.

    b. The requirements of paragraph UF-55 regarding ultrasonic examination do not apply. Inspection will consist of visual inspection and physical measurement of specified dimensions.

    c. As the T-Ampoule components are either formed or spun without welding, the requirements of part UW and part UB do not apply.

9. In lieu of the requirements of paragraph UG-91, the inspector will meet the requirements listed below:

    a. Inspector will demonstrate experience with spinning and fabrication processes, and

    b. Inspector will demonstrate experience with Section VIII.

The elastomeric (O-ring) seal and the associated threaded joint were analyzed using accepted engineering practices and manufacturers' recommendations.

3 Analysis

Within this section:

- Sections 3.1 and 3.2 summarize the results used for future analyses. Section 3.1 provides a summary of results for internal pressure while Section 3.2 does the same for external pressure calculations.

- Section 3.3 addresses calculations required to provide metal properties for subsequent calculations. The T-Ampoule will be built using an alloy of titanium not addressed, in detail within Section II.

Sections 3.5 through 3.8 summarize individual analyses.

Figure 6 contains a map of the T-Ampoule features that require analysis.

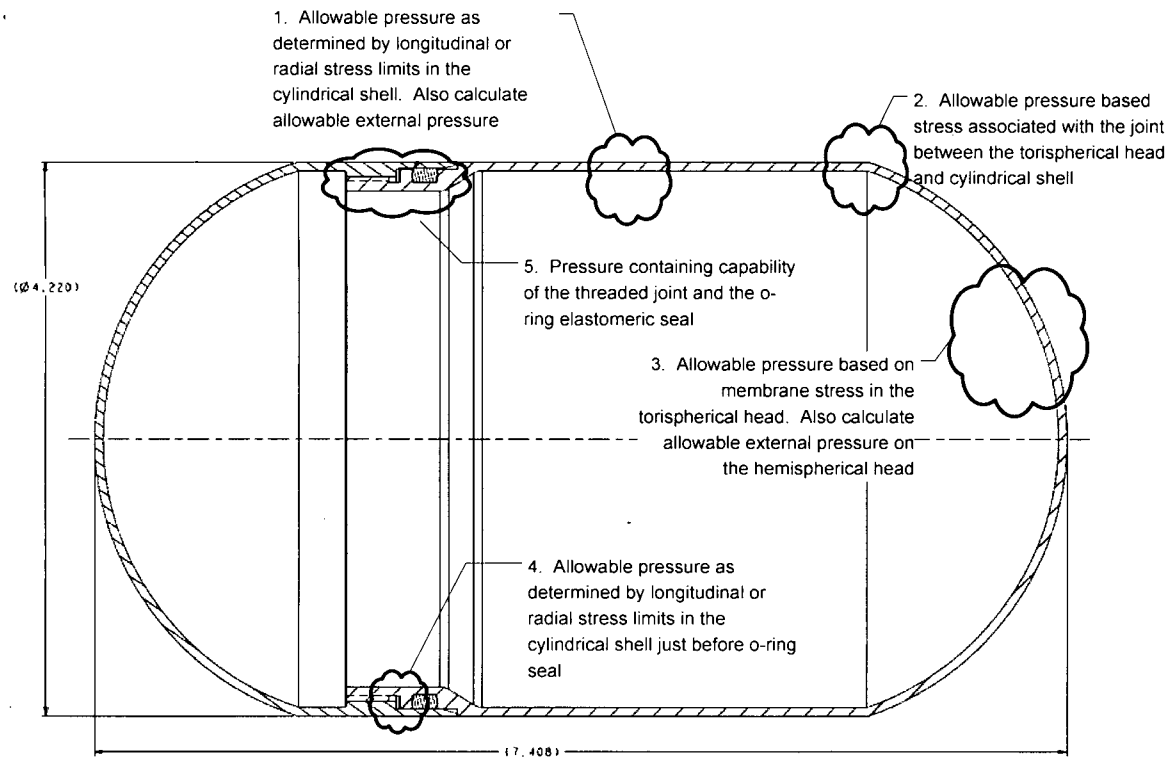

Figure 6: Five Analyses Performed for MAWP Determination

3.1 Maximum Allowable Working Pressure

Figure 7 contains a plot of maximum allowable working pressure (MAWP) as a function of temperature. The MAWP declines with temperature from 617 psig at room temperature (77°F) to 263 psig at 1080°F. At temperatures exceeding 1080°*F*, the T-Ampoule's O-ring seal has failed and pressure has equilibrated with the external environment resulting in zero pressure stress on the T-Ampoule.

It is important to later recall that MAWP is presented as gauge pressure, the difference between external and internal pressures.

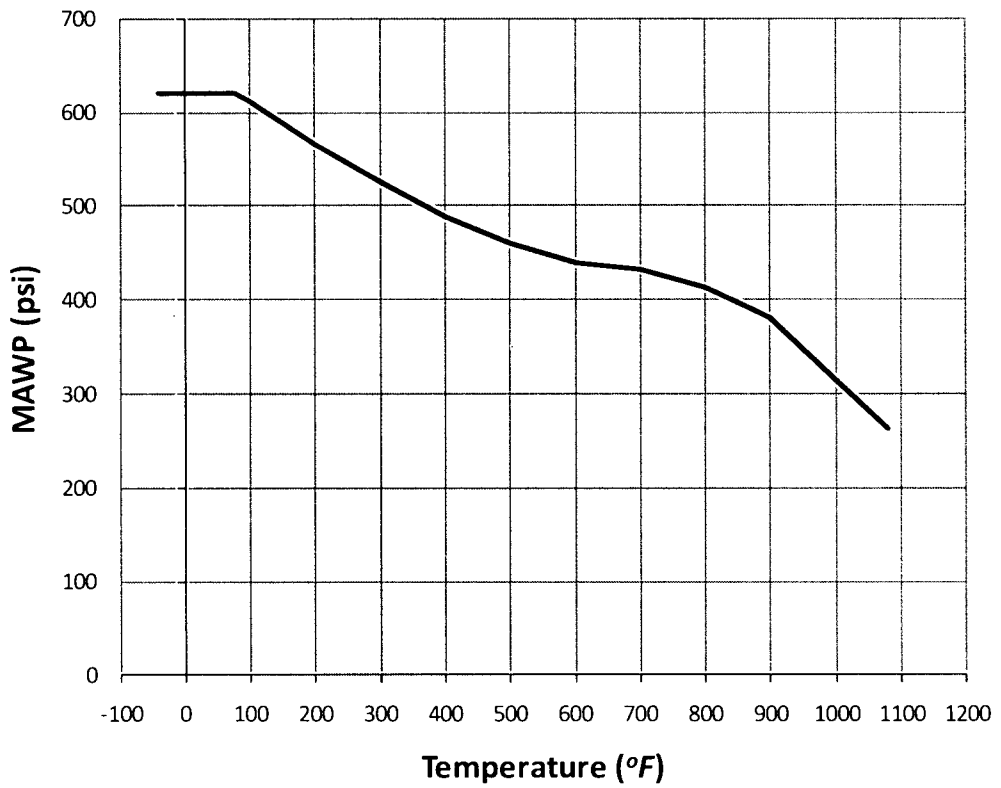

Figure 7: Maximum Allowable Working Pressure (MAWP) for T-Ampoule

Table 7 contains a summary of the results.

Table 7: Summary of Allowable Internal Pressure by Analysis Area

Analysis Area	Description	Allowable Pressure (psig) @ 77°F	Allowable Pressure (psig) @ 1080°F
1	Cylindrical Shell Longitudinal Stress	2790	1180
1	Cylindrical Shell Circumferential Stress	1360	576
2	**Joint, Torispherical Head to Shell**	**624**	**263**
3	Torispherical head, membrane stress	2600	1100
4	Seal Area Longitudinal Stress	1910	809
4	Seal Area Circumferential Stress	935	396
5	O-Ring Seal	900	n/a

The MAWP is set to the lowest allowable pressure for the analysis areas. For this design, the joint between the torispherical head and the cylindrical shell, determined MAWP. The five analyses are summarized below, preceded by a review of the methodology used to determine temperature dependant allowable stresses.

3.2 External Pressure Limits

Figure 7 contains a plot of maximum allowable, external pressure as a function of temperature for the cylindrical shell and the hemispherical head. Allowable pressure for the cylindrical head is the lower of the two and would provide the limiting criteria for the T-Ampoule as a pressure vessel. As is discussed in the applicable sections, this is a conservative calculation.

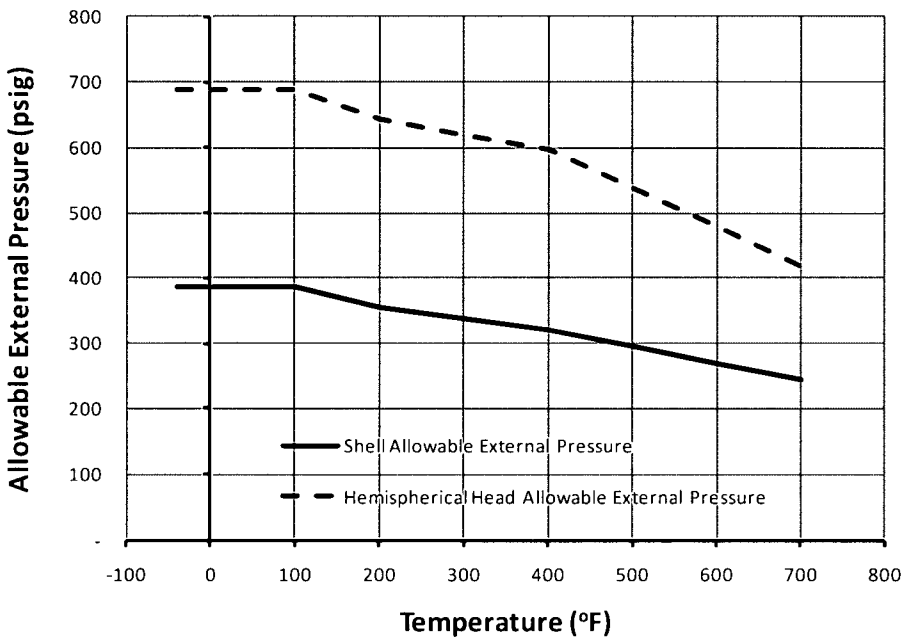

Figure 8: Allowable External Pressure

Table 8 contains a summary of allowable external pressures. This table lists values for room temperature (71°F) and for 700°F, the temperature at which the T-Ampoule's O-ring seal is expected to fail.

Table 8: Summary of Allowable External Pressure by Analysis Area

Analysis Area	Description	Allowable Pressure (psig) @ 71°F	Allowable Pressure (psig) @ 700°F
1	Cylindrical Shell	386	244
3	Torispherical head	687	478
5	O-Ring Seal	80	80

3.3 Titanium Properties

The document controlling design and fabrication of the T-Ampoule [Reference 4, paragraph 3.1.1] specifies that the titanium alloy Ti-6Al-4V will be procured with a minimum tensile (ultimate) strength, S_T, of 150,000 psi and minimum yield strength, S_Y, of 140,000 psi at room temperature (77°F). The analyses below require allowable stress, S_A, values at temperatures, both below and well above room temperature. Allowable stress values should be for a wrought non-ferrous metal.

Section VIII references Section II part D (Section II) for allowable stress values. However, Section II does not tabulate properties for this material. In the event allowable stresses are not published in Tables 1A or 1B of that document, Section II refers the user to an internal appendix, *Mandatory Appendix 1 Basis for Establishing Stress Values in Tables 1A and 1B*. The following criteria were extracted from TABLE 1-100 of that appendix:

$$S_A = \begin{cases} \dfrac{S_T}{3.5} & temperature \leq 77\,°F \\ \dfrac{1.1 S_T R_T}{3.5} & temperature > 77\,°F \end{cases} \qquad 11$$

The Parameter R_T is defined as the ratio of the average temperature dependent, trend curve value of tensile strength to the room temperature tensile strength, the value of which was extracted from the curve F_{tu} in Figure 9.

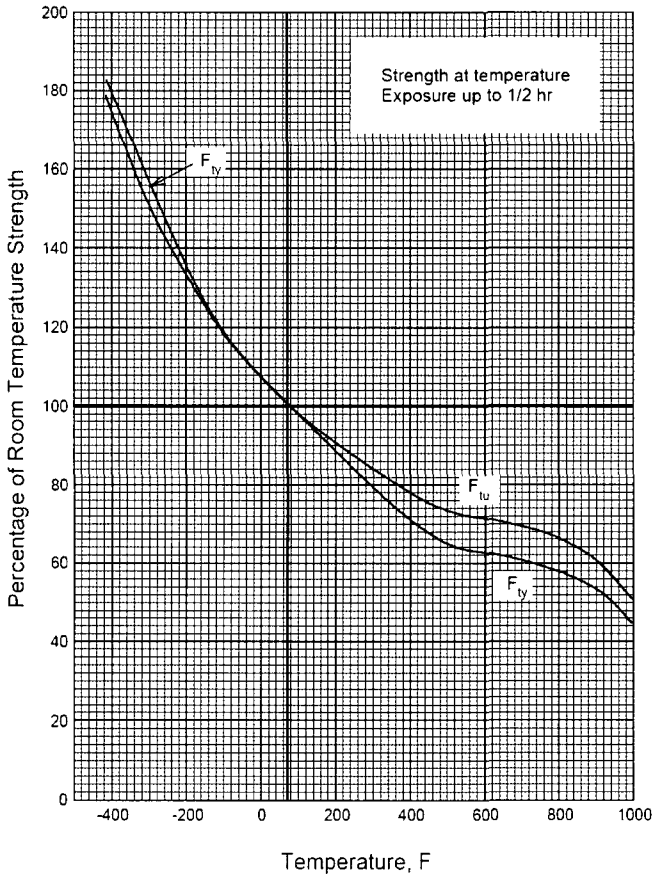

Figure 9: The Effect of Temperature on the Tensile Ultimate Strength of Annealed Ti-6Al-4V Alloy [Ref. 5, Figure 5.4.1.1.1]

For titanium, the useful temperature range is from -320 to 750°F [Reference 6, p 5-51]. Unlike ferritic steels, titanium maintains ductility throughout its operating range, as shown in Figure 10. For these reasons, allowable stresses for temperatures below room temperature were extended down to -40°F.

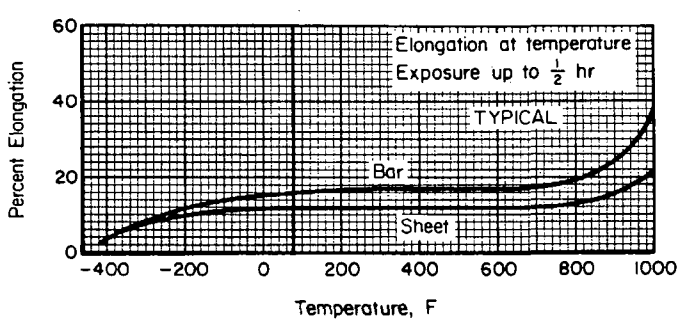

Figure 10: The Effect of Temperature on the Elongation of Annealed Ti-6Al-4V [Ref. 5, Figure Fig 5.4.1.1.5]

The temperature factor for this analysis was extrapolated to 1080°F, 80°F beyond the data presented in Figure 9 and Figure 10 in order to estimate the response of the T-Ampoule at the theoretical accident temperature (1080°F).

The torispherical head analysis, per Section VIII, paragraph UG-32(e), mandates lower allowable stresses. In this single case, the following applies:

Torispherical Head

$$S_A = \begin{cases} 20,000 & temperature \leq 77\,°F \\ 20,000 R_T & temperature > 77\,°F \end{cases} \qquad 12$$

Figure 11 contains plots of the allowable stress values that result from the above equations.

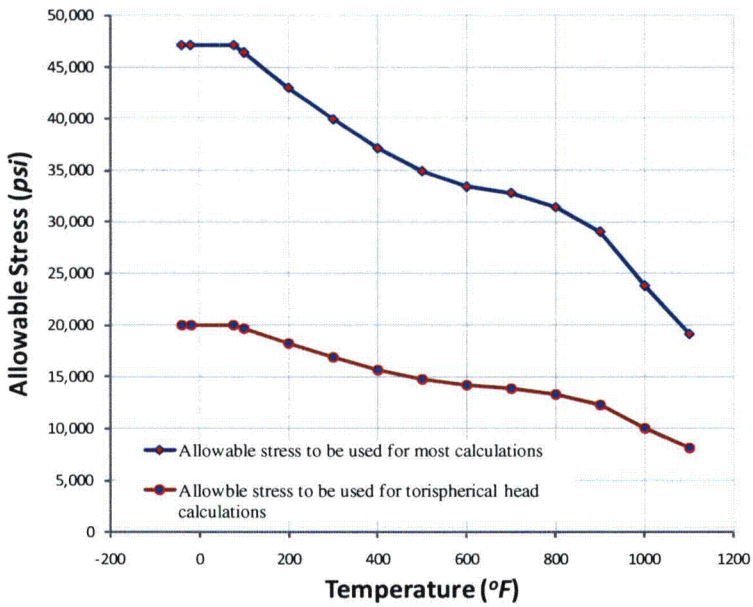

Figure 11: Allowable Stress Values for Ti-6Al-4V

Section VIII references Section II part D (Section II) for computation of yield stress values. In the event yield stresses are not published in Tables 1A or 1B of that document, Section II refers the user to an internal appendix, *Mandatory Appendix 1 Basis for Establishing Stress Values in Tables 1A and 1B*. The following criteria were extracted from TABLE 1-100 of that appendix:

$$Y = \begin{cases} \frac{2}{3} S_Y & temperature \leq 77\,°F \\ \frac{2}{3} S_Y R_Y & temperature > 77\,°F \end{cases} \qquad 13$$

The Parameter R_Y is defined as the ratio of the average temperature dependent value of yield strength to the room temperature yield strength, the value of which was extracted from the curve F_{ty} in Figure 9. The results of equation 13 are plotted in Figure 12.

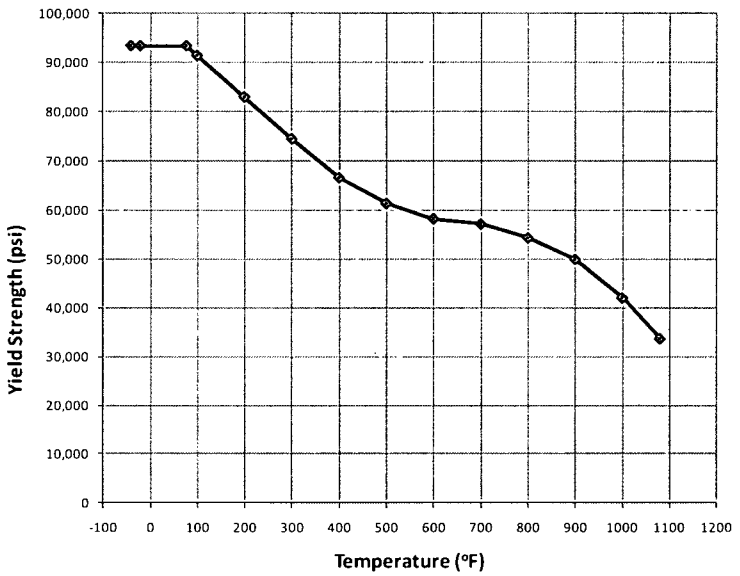

Figure 12: Yield Strength for Ti-6Al-4V

As with tensile strength, the curve is extended to -40°F based on low temperature ductility arguments.

External pressure calculations incorporate the modulus of elasticity at temperature. Figure 13 contains a plot for the T-Ampoule's material based data from a metals handbook published by the U.S. Department of Transportation [5].

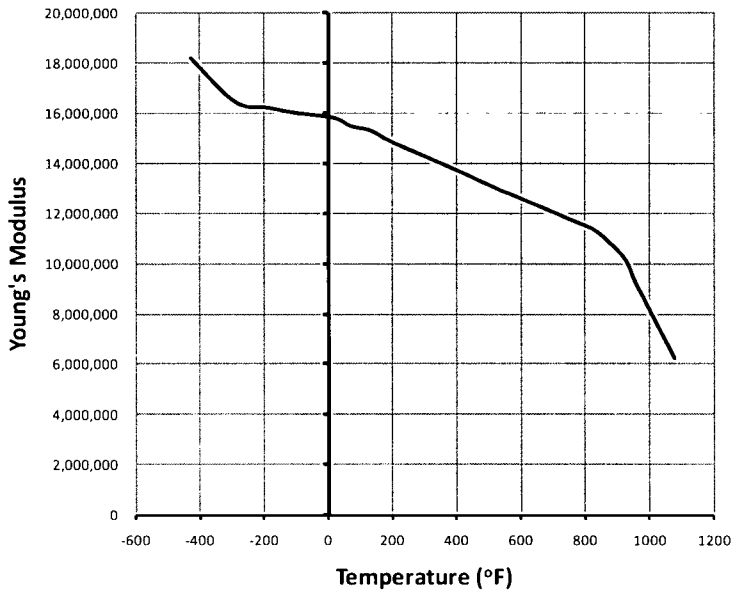

Figure 13: Effect of Temperature on the Young's Modulus of Annealed Ti-6Al-4V [Ref. 5, Figure 5.4.1.1.4]

Figure 14 contains the chart extracted from Section II, from which Factor B was extracted for external pressure calculations. This chart is in fact for an alloy of titanium with similar elastic moduli, but of yield strength half that of Ti-6Al-4V.

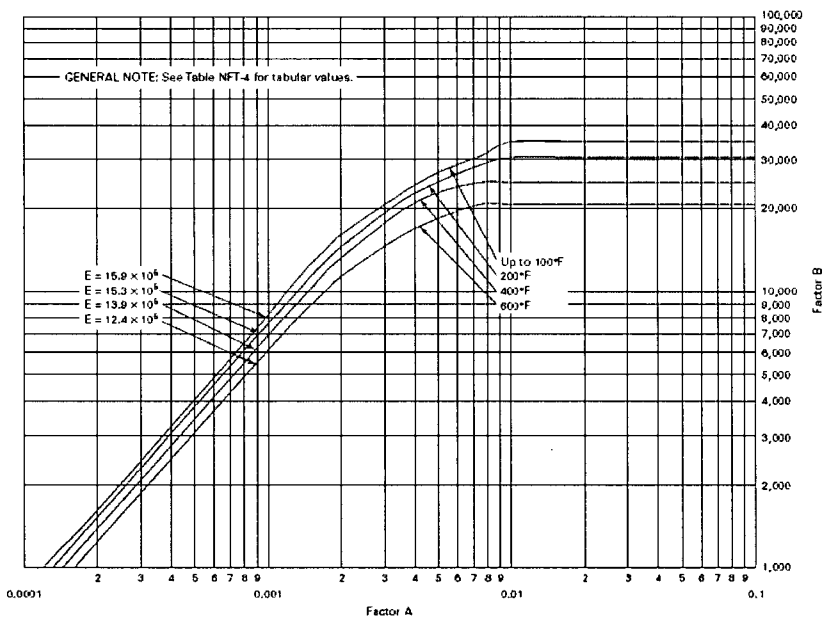

Figure 14: Fig. NFT-4 Chart for Determining Shell Thickness of Components Under External Pressure Developed For Titanium Grade 9 Alloy (Uns R56320) [1]

3.4 Analysis 1, Cylindrical Shell

3.4.1 Internal Pressure - This section summarizes the analysis performed on the cylindrical shell, the area designated as analysis area 1 in Figure 6. Allowable pressures in the both the longitudinal and circumferential direction of the shell are based on the criteria set forth in Section UG-27 of Section VIII.

Longitudinal Limit, shell

$$P_L = \frac{2S_A Et}{R_i - 0.4t} \qquad 14$$

Circumferential Limit, shell

$$P_\phi = \frac{S_A Et}{R_i + 0.6t} \qquad 15$$

The analyst should use data from the upper curve of Figure 11 for allowable stress, S_A. Since Because the device in question has a formed joint efficiency, E, of 1.0. The internal radius, R_i, is based on dimensions taken from Figure 15, and uses specified minimum/maximum values that result in the smallest radius value. Wall thickness, t, is derived from the same dimensions. It is based on the difference between outer and inner diameters using tolerances to obtain the largest value.

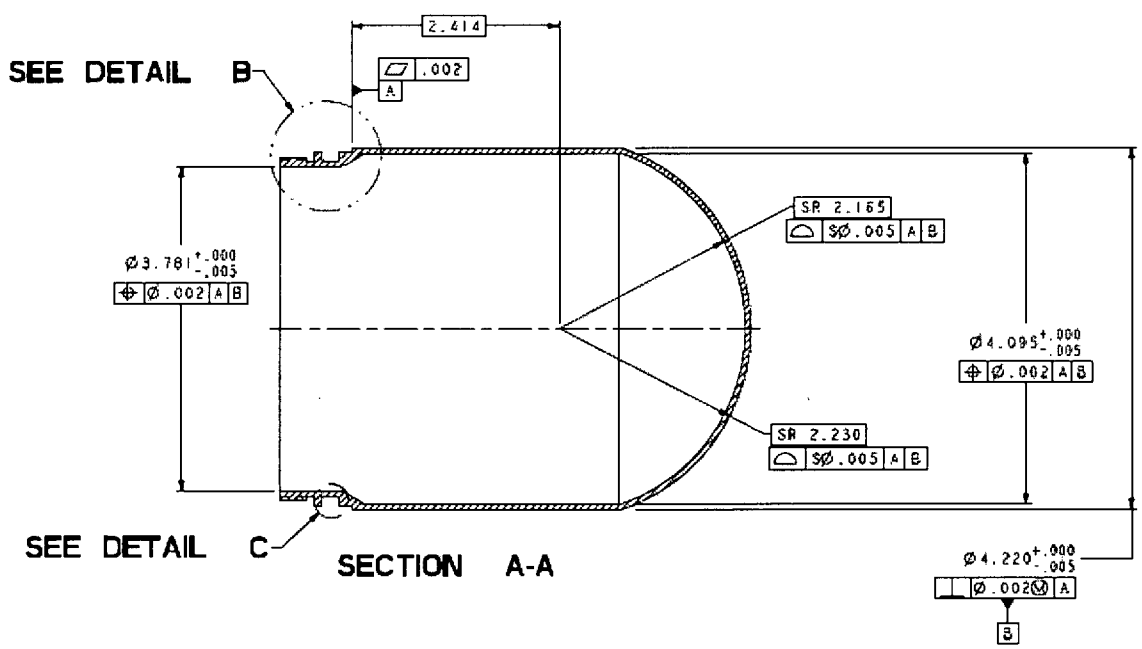

Figure 15: Dimensional Sketch of T-Ampoule Body

Table 9 contains both the input parameters to equations 14 and 15 as well as the final results. The allowable pressure for this analysis area is the pressure determined based on allowable circumferential stress with a value of 1356 psig at room temperature.

Table 9: Parameters and Calculated Values Analysis Area 1

Parameter	Value	Units
d_i	4.095	in
d_o	4.215	in
R_i	2.0475	in
R_o	2.1075	in
t	0.06	in
E	1	n/a
S_A	47100	psi
P_L	**2790**	**psi**
$P\phi$	**1360**	**psi**

Values for allowable stress and therefore, pressure are at room temperature.

3.4.2 External Pressure - This external pressure calculation is conservative. Given the snug fit between the T-Ampoule and the TB-1 containment vessel, it is unlikely that the T-Ampoule will be allowed to flex enough to buckle elastically. The Section VIII external pressure analysis ignores this type of external support and the analysis assumes no support exists. In addition, B factor charts for the Ti-6Al-4V material used for the T-Ampoule do not exist. The curve for a titanium alloy with UNS designation R56320 will be assumed instead. This substitute alloy has a room temperature yield strength of 70,000, a factor of 2 lower than the alloy actually in use. These two assumptions combine to under-predict allowable external pressure. Since the predicted pressures are still sufficiently high that failure is not predicted, no attempt was made to refine the analysis.

Rules for calculating allowable external pressure are presented in Section VIII, paragraph UG-33(d). The methodology is graphic oriented. The first important parameter, A, is obtained from the graph in Section II, Figure G, which correlates A to geometric parameters derived from external diameter, D_o, shell length, SL, and wall thickness, t. Using this value, one can determine the allowable stress, B, from Figure 14. This value of B for room temperature is 18,800 psi.

A B factor feeds into the following equation:

$$P_{ex} = \frac{4B}{3\left(\frac{L_o}{t}\right)} \qquad 16$$

Table 13 summarizes the results of the above calculations. Allowable external pressure is 481 psig. At 700°F when the T-Ampoule equilibrates with the annulus pressure, the allowable

external pressure difference will be 244 psig, providing a reasonable margin above the estimated equilibration threshold of 150 psig difference.

Table 10: Allowable External Pressure of Hemispherical Head

Parameter	Value	Units
D_o	4.22	In.
t	0.06	In.
SL	4.426	length
SL/D_o	2.098	
D_o/t	64.9	
A	0.00250	
B	18,800	psi
P_{ex}	386	psi

3.5 Analysis Area 2, Torispherical Head Joint

Criteria for analysis area 2 are based on paragraph UG-32 *Formed Heads, and Sections, Pressure on the Concave Side* of Section VIII. This paragraph refers in turn to Section VIII's Mandatory Appendix 1, Supplementary Design Formulas, paragraph 1-4(d) which applies the following criteria:

Torispherical Head Joint

$$P_T = \frac{2S_A E t_s}{LM + 0.2t_s} \qquad 17$$

Where

$$M = \frac{1}{4}\left(3 + \sqrt{\frac{L}{r}}\right) \qquad 18$$

In this case the analyst should employ the lower curve of Figure 11 for allowable stress. Dimensions were obtained from Figure 15. The crown radius, L, or the radius of the head, must be the minimum value possible when considering tolerances. The head wall thickness, t_s, should also be the minimum possible value. The parameter M is based on the ratio of crown radius, L, to knuckle radius, r. Knuckle radius is the radius of curvature of the titanium at the joint between the head and the cylindrical shell. This value is specified to be 0.125 inch. As above, the joint efficiency, E, is 1.0 since no joint exists.

In addition to the above, the following criteria apply:

$$\frac{t_s}{L} \geq 0.002, \qquad 19$$
$$L \leq d_o$$

Table 11 contains input parameters and results for the torispherical head joint. The value for t_s is based on the difference between outer and inner crown radii with tolerances chosen to minimize thickness. The allowable stress at room temperature is limited to a maximum of 20,000 psi at room temperature. The two criteria of equation 19 are met. The ratio of head thickness to crown radius is 0.0277, an order of magnitude above the criterion. The crown radius itself, at 2.225 inches is less than the outer diameter of the shell which equals 4.095 inches. All of this results in an allowable pressure of 624 psig. This is, in fact, the lowest allowable pressure of all calculated for the five analysis areas, and as such provides the criteria for MAWP.

Table 11: Parameters and Calculated Values Analysis Area 2

Parameter	Value	Units
d_i	4.095	in
d_o	4.215	in
R_i	2.0475	in
R_o	2.1075	in
L	2.225	in
t_s	0.06	in
E	1	n/a
t_s/L	**0.0277**	nd
S_A	**20,000**	psi
M	**1.790**	nd
P_T	**624**	psi

3.6 Analysis Area 3, Head Membrane

3.6.1 Internal Pressure - Stress in the hemispherical head away from the joint is uniform in all directions normal to the radius and is governed by the criteria of paragraph UG-32 of Section VIII, Formed Heads and Sections.

Hemispherical Head Membrane

$$P_H = \frac{2S_A E t_s}{L + 0.2t_s} \qquad 20$$

The following additional constraints apply:

$$\frac{t_s}{L} < 0.356$$
$$\frac{P_H}{SE} < 0.665 \qquad 21$$

Values and definitions are as defined in the previous section.

Table 12 contains input parameters and results for the hemispherical head membrane. The two supplemental criteria of equation 21 are satisfied. The calculated value for allowable pressure of 2600 psig is well above the previously calculated allowable pressure for the torispherical joint.

Table 12: Parameters and Calculated Values Analysis Area 3

Parameter	Value	Units
d_i	4.095	*in*
d_o	4.215	*in*
R_i	2.048	*in*
R_o	2.108	*in*
L	2.225	*in*
t_s	0.060	*in*
E	1	*n/a*
S_A	47100	*psi*
t_s/L	0.0277	*nd*
P_H/SE	0.0551	*nd*
P_H	2600	*psi*

3.6.2 External Pressure - This external pressure calculation is conservative. Given the snug fit between the T-Ampoule and the TB-1 containment vessel, it is unlikely that the T-Ampoule will be allowed to flex enough to buckle elastically. The Section VIII external pressure analysis ignores this type of external support and the analysis assumes no support exists. In addition, B factor charts for the Ti-6Al-4V material used for the T-Ampoule do not exist. The curve for a titanium alloy with UNS designation R56320 will be assumed instead. This substitute alloy has a room temperature yield strength of 70,000, a factor of 2 lower than the alloy actually in use. These two assumptions combine to under-predict allowable external pressure. Since the predicted pressures are still sufficiently high that failure is not predicted, no attempt was made to refine the analysis.

Rules for calculating allowable external pressure are presented in Section VIII, paragraph UG-33(e). Methods are graphic oriented. First important parameter, A, is calculated as:

$$A = 0.125\left(\frac{t}{L_o}\right) \qquad 22$$

Note: This equation uses the external crown radius, L_o. Using this value, allowable stress, B from Figure 14 can be determined. This value at room temperature is 23,400 psi. The B factor feeds into the following equation:

$$P_{ex} = \frac{B}{\left(\frac{L_o}{t}\right)} \qquad 23$$

Table 13 summarizes the results of the above calculations. Allowable external pressure is 687 psig. At 700°F when the T-Ampoule equilibrates with the annulus pressure, the allowable external pressure difference will be 419 psig, providing a reasonable margin above the estimated equilibration threshold of 150 psig, difference between the annulus and the T-Ampoule.

Table 13: Allowable External Pressure of Hemispherical Head

Parameter	Value	Units
L_o	2.22	In.
t	0.065	In.
L	4.43	
L_o/t	34.1	
A	0.00367	psi
B	23,400	psi
P_{ext}	687	

3.7 Analysis 4, Seal Area

This section summarizes the analysis performed on the cylindrical shell in the area designated as area 5. Figure 16 shows the area in extreme close-up. The thin cap section just after the threads, but before the O-ring is of concern. This section still experiences internal pressure and yet, is substantially thinner than the T-Ampoule body. This analysis ignores possible rib reinforcement from the threaded area.

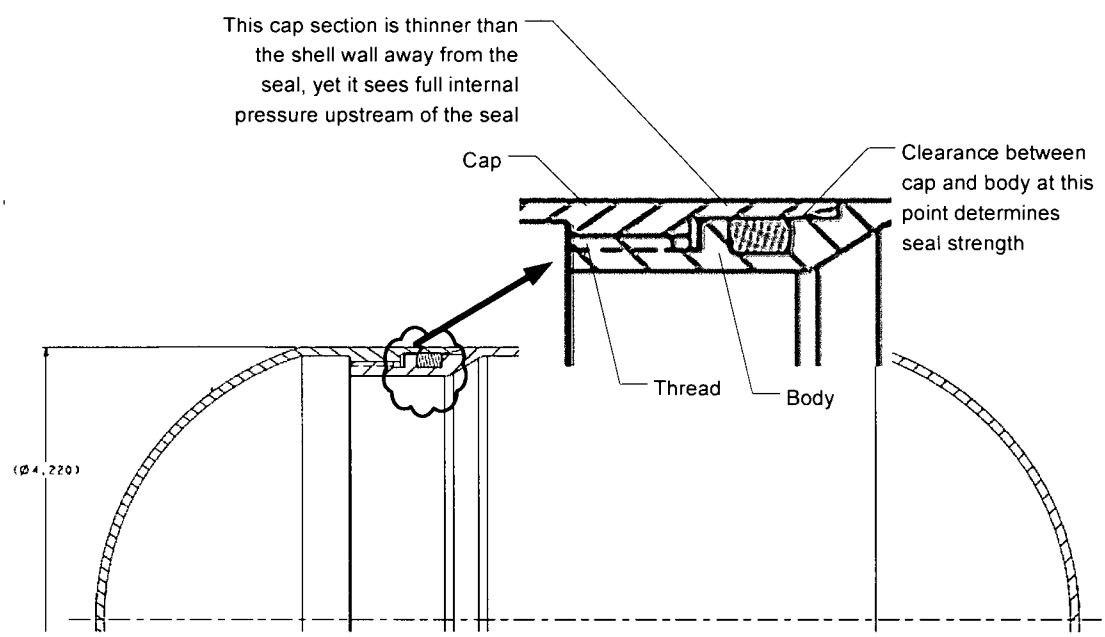

Figure 16: Blowup of Seal Area

The analysis is similar to that already completed for analysis area 1 with the dimensions, however, as specified in Figure 17. Allowable pressures in both the longitudinal and circumferential direction of the shell are based on the criteria set forth in Section UG-27 of Section VIII, and are summarized in equations 14 and 15.

The analyst should use data from the upper curve of Figure 11 for allowable stress, SA. Since the device in question is formed, joint efficiency, E, is 1.0.

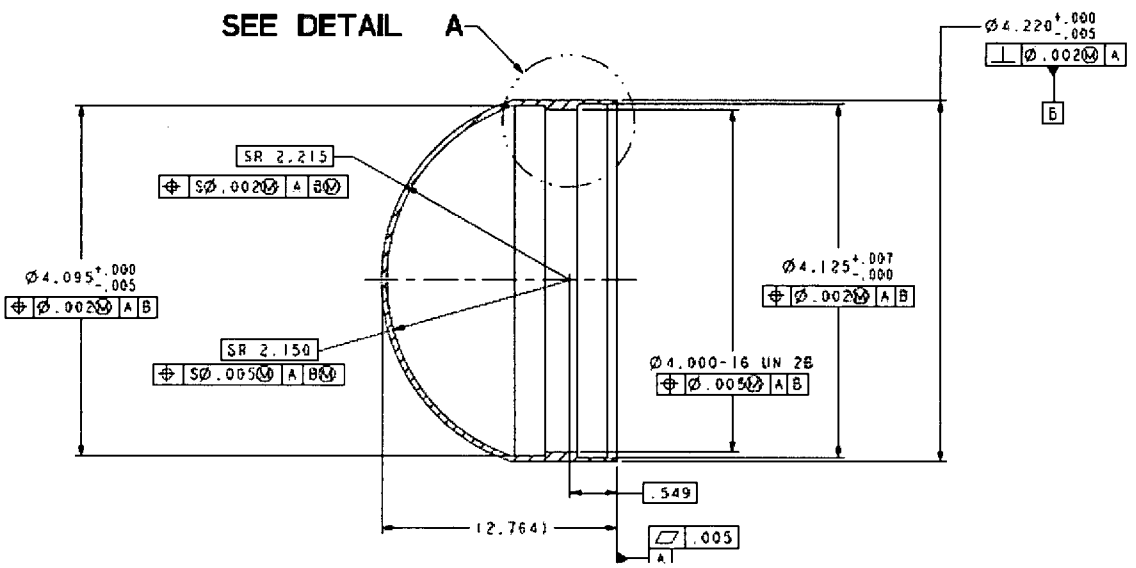

Figure 17: Dimensioned Sketch of T-Ampoule Lid

Table 14 contains both the input parameters to equations 14 and 15, as well as the final results. The allowable pressure for this analysis area is the pressure determined based on allowable circumferential stress with a value of 935 psig at room temperature.

Table 14: Parameters and Calculated Values Analysis Area 4

Parameter	Value	Units
d_i	4.132	in
d_o	4.22	in
R_i	2.066	in
R_o	2.11	in
t	0.0415	in
E	1	n/a
S_A	47100	psi
P_L	1910	psi
$P\phi$	935	psi

3.8 Analysis Area, 5, O-ring

While O-ring static seals are ubiquitous in industry and are well respected, their analysis is not part of the Boiler and Pressure Vessel Code. Neither does their analysis possess the rigor found in the Boiler and Pressure Vessel Code. This analysis that follows relies, instead on the vendor's recommendations and good engineering practice.

A static O-ring seal designed to the dimensional specifications of SAE standard AS5857 will hold pressure to 1500 psig [7] The T-Ampoule design follows this standard with two exceptions. Per the standard, the specified radial clearance in both directions, between the body and the cap should be 0.0015 to 0.003 inches. T-Ampoule clearances for both directions are relaxed for different reasons. Referring to Figure 18, the downstream clearance has been relaxed slightly to facilitate assembly in a glove box. The upstream clearance has relaxed even further to guard against excessive, external pressure. Sustainable pressures therefore require some adjustment.

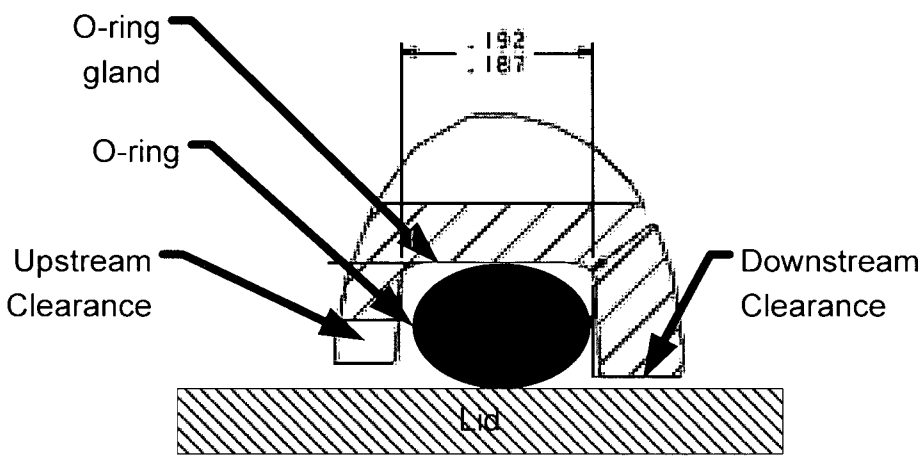

Figure 18: Pressure Containment for O-Ring Seals [7]

O-rings seal when pressure forces the relatively flexible elastomeric O-ring against the clearance between the cap and the body of the T-Ampoule. The downstream clearance supports the O-ring against internal pressure. The upstream O-ring supports the O-ring against external pressure.

Seal failure occurs when the O-ring extrudes into the clearance. As this clearance becomes tighter (smaller), the seal can sustain more pressure. Loosening (opening) the clearance causes the seal to hold less pressure. In addition, a seal's ability to withstand pressure depends on O-ring hardness, typically measured on the "Shore A" scale. Figure **19** contains a plot of information taken from an O-ring design manual [7] illustrating the relationship of an O-ring meeting the T-Ampoule seal's hardness specification

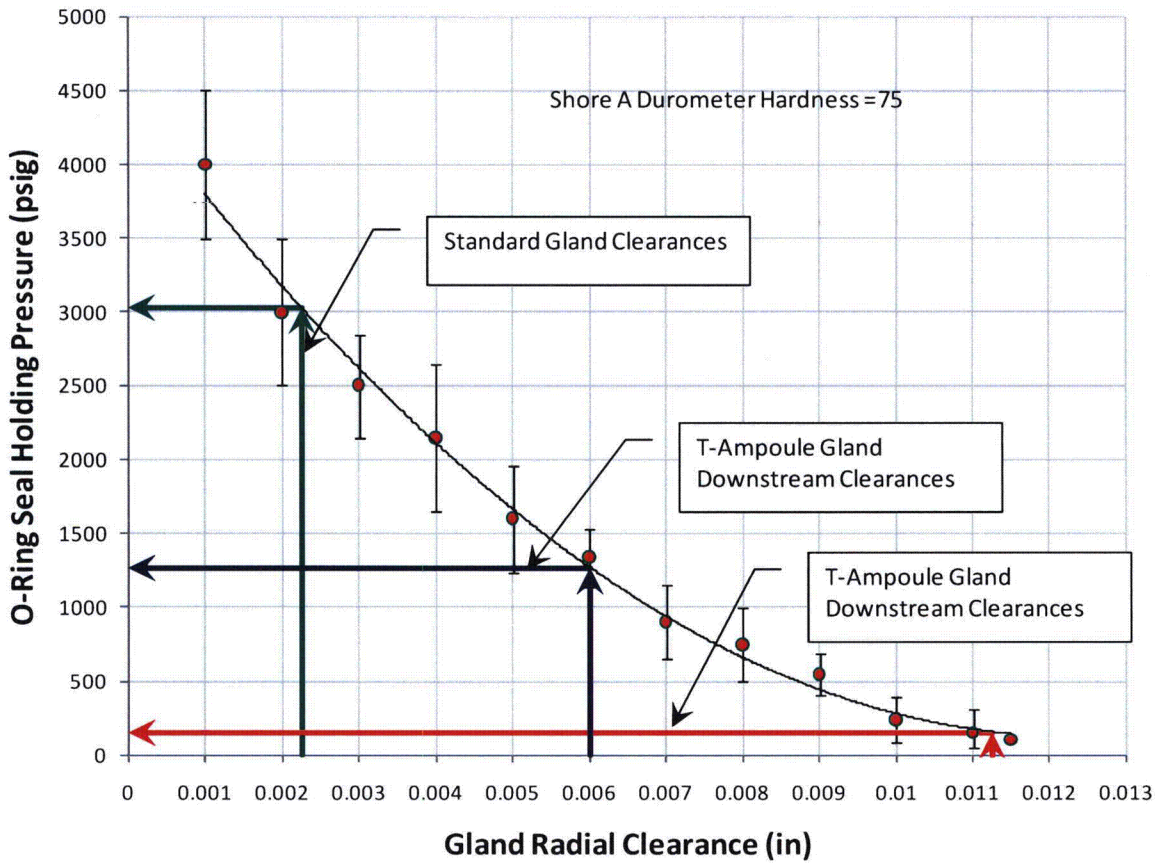

Figure 19: Internal Pressure Containment for O-Ring Seals [source: 8]

T-Ampoule design specifies an O-ring with a Shore A hardness of 75 over its useful temperature range (-15°F to 400°F). A standard O-ring gland specification would call for a radial clearance between 0.0015 and 0.003 inches. From Figure **19**, sustainable pressure is 3000 psig. The difference between this value and the value of 1500 psig quoted by the manufacturer represents factor of safety of 2.0 for a standard gland design.

The downstream clearance (radial) has been increased to 0006. From the figure, this level of clearance can sustain a pressure of 1270 psig. With the same factor of safety, the seal should be rated for internal pressure at 635 psig.

The upstream clearance (radial) has been relaxed at selected locations to an average radial value of 0.01125 inches. From Figure **19**, the seal can sustain a pressure of 160 psig. With the same factor of safety used above, the seal will be rated for a backpressure of 80 psig.

3.9 References

1. American Society of Mechanical Engineers (ASME); Boiler and Pressure Vessel Code, Section VIII Division 1, Rules for Construction of Pressure Vessels. 2007.

2. Rubin, J.B. "Thermal Decomposition of Viton® O-rings for the PAT-1 Packaging Accident Scenario." LA-UR-09-05112. Los Alamos National Laboratory. Los Alamos, NM.

3. Serban Moldoveanu: Analytical Pyrolysis of Synthetic Organic Polymers, Volume 25 (Techniques and Instrumentation in Analytical Chemistry) (Elsevier Science, 2005).

4. PAT-1040. Titanium and O-Ring Materials and Component Fabrication Specification.

5. DOT/FAA/AR-MMPDS-01 Metallic Materials Properties Development and Standardization: January 2003.

6. Society of Automotive Engineers; Standard AS5857; Gland Design, O-Ring and Other Elastomeric Seals, Static Applications; March 2005.

7. Parker Hannifin Corp document. "Parker O-Ring Handbook." ORD 5700.

8. Minnesota Rubber/Quadion Corporation, Elastomers and Thermoplastics Engineering Design Guide: copyright 2007.